THE IMPACT OF PROBIOTIC BACTERIA ON INTESTINAL BARRIER FUNCTION

Thesis submitted in fulfilment of the requirements

of the degree of Master of Philosophy

June 2023

Pascale Corinne Aeschlimann – Portner, BSc

College of Biomedical and Life Sciences

School of Dentistry

Cardiff University

DEDICATION

I would like to dedicate this work to my late mom,

who taught me that, no matter what,

if you put your mind (and hard work) into it,

the sky is the limit.

I miss you every day.

ACKNOWLEDGEMENTS

I would like to express my gratitude to my academic supervisors, Professor Ryan Moseley, and Professor Daniel Aeschlimann, for their excellent supervision, guidance, and encouragement throughout this research project. Prof. Aeschlimann has been my biggest inspiration in my scientific career as he is always so passionate about research, which has been a real driving force, but not only that, he has always been there come rain or shine.

I would like to thank KESS2 who have funded this project in partnership with Cultech Ltd., and convey my appreciation to my industry supervisor, Dr. Daryn Michael, and everyone at Cultech, for their support, and for offering me this great opportunity.

I would also like to convey my appreciation to Sue Wozniak from the Dental Pathology Laboratory and thank her for her excellent technical assistance, advice and friendship. She embedded all the membranes for me (a very fiddly job), and I would not have been able to do the immunostaining without her help and advice.

I would also like to thank Dr. Sharon Dewitt Parr for teaching me how to use the confocal microscope, helping me to find my little elusive caterpillars ;-) and for being supportive when I needed encouragement.

My appreciation and thanks also extend to my mentor, Professor Emma Kidd, who has given me excellent advice whenever I asked for it.

And, finally, a huge thank you to my husband and grown children, for their continuous and unparalleled love and support and for telling me ‘you can do this!’ when I struggled with the writing. I promise, I will turn back to my normal self when this is finished!

Knowledge Economy Skills Scholarships (KESS 2) is a pan-Wales higher level skills initiative led by Bangor University on behalf of the HE sector in Wales. It is part funded by the Welsh Government’s European Social Fund (ESF).

SUMMARY

It has been widely reported that probiotics have a variety of health benefits, however, the underlining mechanisms for these are mainly unknown. This KESS project was a collaboration with Cultech Ltd., a company that produces such a probiotic formulation, called Lab4, which has been shown in several clinical trials to have such benefits for gut health. Our hypothesis was that the health benefits reported, are related to augmentation of epithelial barrier integrity. To evaluate this, we established *in vitro* models of varying complexity to assess molecular responses of probiotic application to a mature epithelium. My results revealed, that conditioned medium (metabolites) from Lab4 improved barrier integrity and importantly, that this had a protective effect when a subsequent inflammatory stimulus (IL-22) was applied. Furthermore, I found, that inclusion of mucus producing cells altered the epithelial responses to the inflammatory challenge. The main probiotic-mediated change observed, was in the pattern of activation of the MAPK signalling pathway, which is known to control epithelial proliferation. Based on our findings we propose, that short-chain fatty acids (SCFA) are a key active constituent of Lab4 probiotic conditioned media, and that these modulate ERK1/2 activation, and thereby modulate the responses of the epithelial lining and ultimately control barrier integrity.

These novel findings provide important insights on actions in the host, driven by probiotic strains of *Bifidobacterium* and *Lactobacillus* on a mechanistic level, that significantly advance our current understanding, and may explain how probiotics mediate their health benefits.

TABLE OF CONTENTS

LIST OF ABBREVIATIONS

bp	Base-pair
BSA	Bovine serum albumin
CaSR	Calcium sensing receptor
CCK	Cholecystokinin
cDNA	Complementary deoxyribonucleid acid
CNS	Central nervous system
CFU	Colony forming units
DAPI	4′,6-Diamidino-2-phenylindole
DMEM	Dulbecco's modified Eagle medium
DMSO	Dimethylsulfoxide
DNA	Deoxyribonucleid acid
dNTPs	Deoxyribonucleotide triphosphate
DTT	Dithiothreitol
ECM	Extracellular matrix
EDTA	Ethylenediaminetetraacetic acid
ERK1/2	Extracellular signal-regulated kinase 1 and 2
FAO	Food and agriculture organization of the United Nations
FBS	Heat-inactivated fetal bovine serum
GALT	Gut-associated lymphoid tissue
GAPDH	Glyceraldehyde-3-phosphate dehydrogenase
GI	Gastrointestinal tract
GIP	Glucose-dependent insulinotropic peptide
GLP	Glucagon-like peptides
GPCR	G-protein-coupled receptor
H&E	Haematoxylin and Eosin
HBSS	Hank's balanced salt solution
HRP	Horseradish peroxidase
IBD	Irritable bowel disease
IELs	Intraepithelial lymphocytes
IgA	Immunoglobulin A

IgG	Immunoglobulin G
IL-22	Interleukin 22
ILC3	Type-3 innate lymphoid cells
JAK	Janus kinase
kDa	Kilo Dalton
Lab4 CM	Lab4 conditioned medium
Lab4 ET	Lab4 ethanol killed bacteria
LCFA	Long-chain fatty acids
LSD	Least significant difference
LY	Lucifer Yellow
M cells	Microfold cells
MAPK	Mitogen-activated protein kinase
MRD	Maximum recovery diluent
MRS	De Man, Rogosa, Sharpe broth
MTX	Methotrexate
NEAA	Non-essential amino acids
PAS	Periodic Acid Schiff
PBS	Phosphate-buffered saline
PCR	Polymerase chain reaction
PET	Polyethylene therephthalate
PFA	Paraformaldehyde
PYY	Peptide tyrosine tyrosine
QPCR	Quantitative polymerase chain reaction
REGγIII	Regenerating islet-derived protein gamma 3
RNA	Ribonucleid acid
S100A8	S100 calcium-binding protein A8
SAA1/2	Protein serum amyloid 1 and 2
SCFA	Short-chain fatty acids
SGLT1	Sodium dependent glucose transporter 1
SNAI2	Snail family transcriptional repressor 2
SOCS3	Suppressor of cytokine signalling-3
STAT	Signal Transducer and Activation of Transcription

TAE	Tris-acetate-EDTA buffer
TBS	Tris-buffered saline
TEER	Trans-epithelial electrical resistance
TNFα	Tumor necrosis factor α
Tyk2	Tyrosine kinase 2
v/v	Volume per unit volume
w/v	Weight per unit volume
WHO	World health organization
ZO-1	Zonula Occludens 1

1. INTRODUCTION

1.1. THE SMALL INTESTINE

The small intestine is part of the gastrointestinal tract (GI). It is responsible for the digestion of food and absorption of nutrients, and also for the excretion of molecules from the organism. Furthermore, it forms an important interface with the external environment and has a critical role in the development of immune responses (Pereira et al., 2016). In humans, the small intestine is about 3 meters long and contains three distinct sections: the duodenum, the jejunum and the ileum (Fanucci et al., 1988). In order to maximise nutrient absorption, the small intestine produces many infolds and small finger-like protrusions, called villi, with the net effect of vast expansion of the surface area. The surface of the small intestine is estimated to correspond to an area of $30m^2$ – $200m^2$ (Shimizu, 2010; Helander and Fändriks, 2014). The villi protrude into the intestinal lumen, with small invaginations at the base, called crypts, and are a site of the body subject to rapid cell turnover and extensive tissue remodelling, in parts to accommodate ever changing environmental conditions.

Of all the organ systems in the body, the gastrointestinal tract is the most complicated (apart from the brain) in terms of the numbers of structures involved, each with different functions. The outermost tissue layer facing the intestinal lumen is the mucosa, that consists of three principal layers, namely the epithelium, the lamina propria and the muscularis mucosae (Figure 1). The muscularis mucosae is, as the name suggests, a thin layer of smooth muscle supporting the lamina propria. The lamina propria is a gut region-specific layer of connective tissue made up of specialised stromal cells and extracellular matrix (ECM) proteins, harbouring blood vessels (capillaries and veins), a unique lymphatic system with specialised lymph nodes (Peyer's patches), and also aspects of the enteric nervous system. The enteric nervous system is part of the autonomous peripheral nervous system that orchestrates gastrointestinal behaviour independent of the central nervous system (CNS), consisting of sensory neurons, motor neurons, and interneurons (Figure 2). These

enteric neurons work together with enteric glial cells, macrophages, stromal cells, and enteroendocrine cells to integrate an array of cues to initiate outputs that are precisely regulated in space and time to control digestive functions and intestinal homeostasis (Talbot et al., 2020). The enteric nervous system interacts with the immune system, gut microbiota, and the epithelium to maintain mucosal defense and barrier function. However, increasing evidence also suggests that nerves that interconnect the enteric nervous system and the CNS can be conduits for disease spread (Rao and Gershon, 2016).

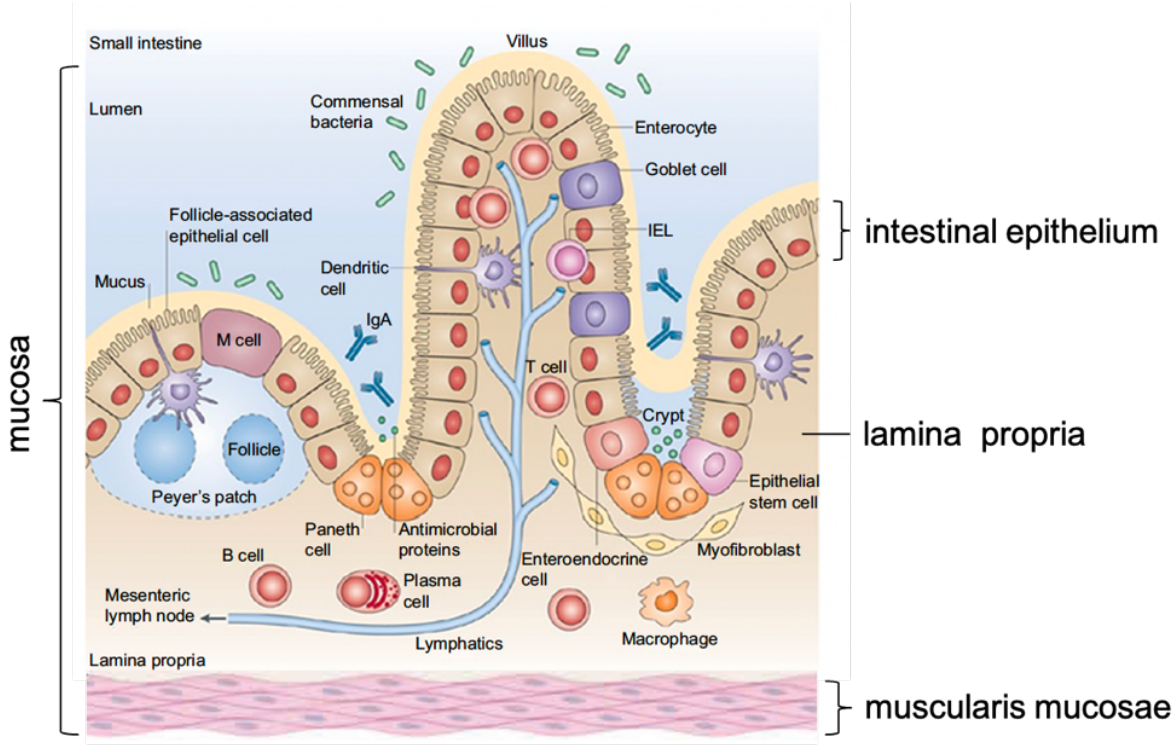

Figure 1 Schematic of the human small intestine. *The mucosa is the outermost tissue layer that directly surrounds the intestinal lumen and consists of the muscularis mucosae, lamina propria and the intestinal epithelium. The intestinal epithelium is made up of mostly enterocytes, but also contains goblet cells, entero-endocrine cells, M cells and Paneth cells. Newly differentiated cells migrate from the crypt along the villus before being shed at the villus apex. Goblet cells are responsible for producing a mucus layer that covers the epithelium (yellow). Commensal bacteria inhabit the lumen and interact with the epithelium. (Adapted from Abreu, 2012)*

The final layer is the intestinal epithelium, which is a monolayer of cells that covers the lamina propria and forms the lining of the small intestine (Abreu, 2012).

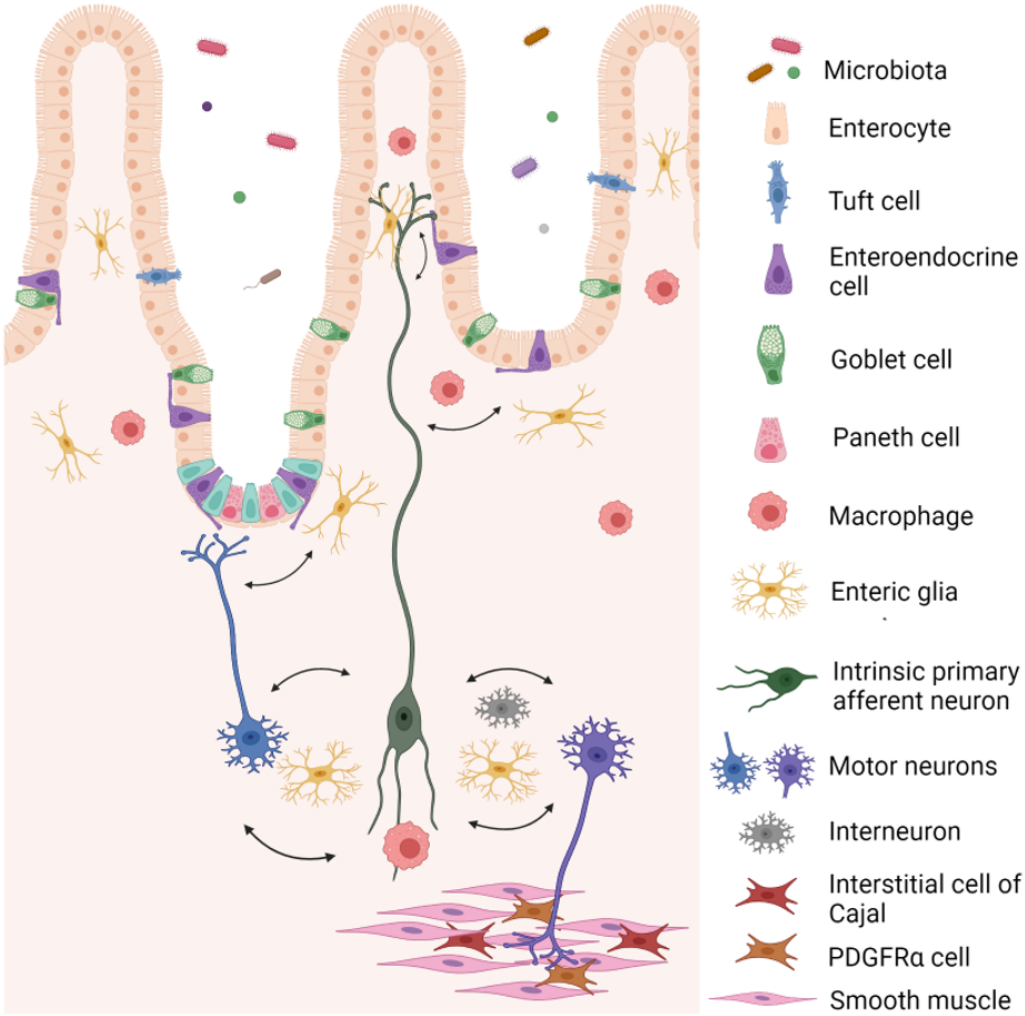

Figure 2 Schematic outlining the relationship between the architecture of the intestinal mucosa and enteric peripheral nervous system. *Read in comparison with Figure 1. (Taken from Sharkey and Mawe, 2023)*

1.2. INTESTINAL LINING

The two main cell types of the intestinal epithelium are absorptive (enterocyte) and mucus secreting (goblet) cells, and the relative percentage of those two main intestinal cell types varies in different gut regions. In the duodenum, the epithelium is formed by 90% absorptive cells and 10% goblet cells, while in the large intestine, the respective proportion changes to 76% and 24% (Hilgendorf et al., 1999; Mahler et al., 2009, Ferraretto et al., 2018).

The enterocytes are columnar and highly polarized cells with an apical brush border, which enables them to absorb nutrients from the intestinal lumen (Cheng et al., 1974).

As the epithelial cells are tightly connected through specialist adherens junctions, a separation is formed to the luminal content, enriched in nutrients and commensal bacteria residing in the gut, and hence, they also form a barrier against infection (Shimizu, 2010). The second most abundant cell type within the epithelium are goblet cells (Knoop and Newberry, 2018), which produce and secret a protective mucus, largely consisting of different mucins that are expressed and assembled in a gut region-specific manner (Johansson et al., 2011), which covers the intestinal epithelium and forms a chemical and mechanical protective layer.

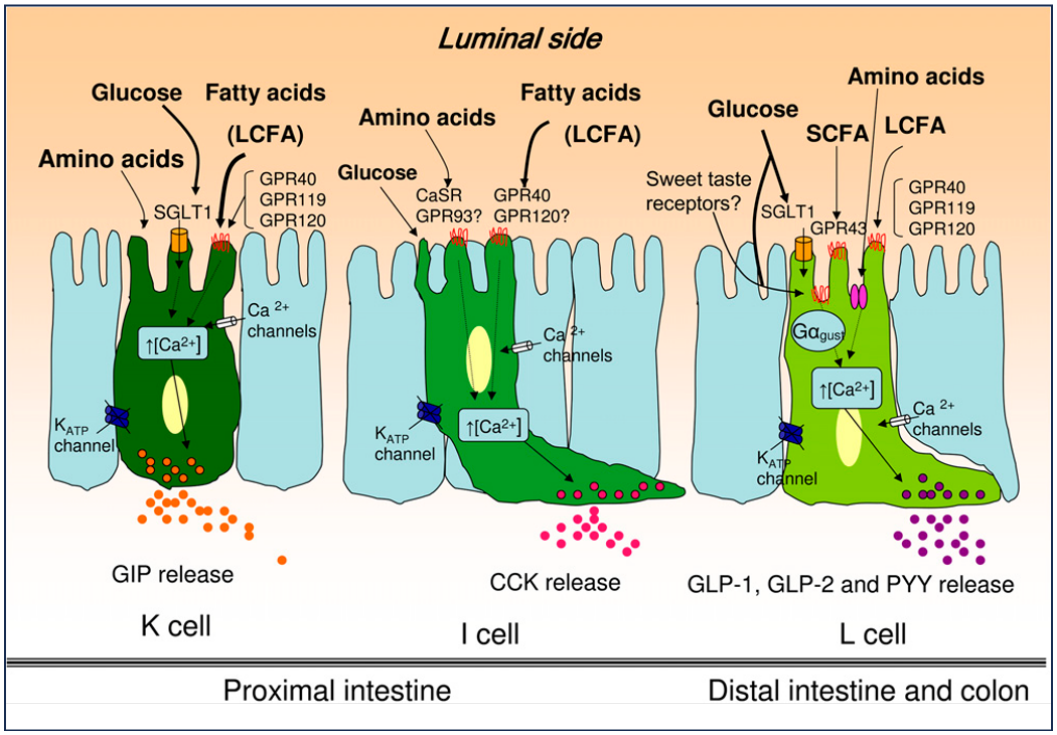

Figure 3 Sensing machinery of enteroendocrine cells. *K and I cells are primarily localized in the proximal intestine, whereas L cells are predominantly in the distal intestine and colon. K cells sectrete glucose-dependent insulinotropic peptide (GIP) to enhance insulin secretion and gastric acid release, I cells cholecystokinin (CKK) to regulate gall bladder and pancreas function and suppress food intake, and L cells glucagon-like peptides (GLP) and 36 amino acid peptide tyrosine tyrosine (PYY) to inhibit insulin secretion and gastric activity. CaSR, calcium sensing receptor; GPCR, G-protein-coupled receptor; LCFA, long -chain fatty acids; SCFA, short-chain fatty acids; SGLT1, sodium dependent glucose transporter 1. (Taken from Morán-Ramos et al., 2012)*

In both the small intestine and the colon, intestinal stem cells reside at the base of the crypts (Barker et al., 2007). These are the cells that divide and ultimately feed differentiated progeny into the villi. Other cell types present in the small intestinal lining are enteroendocrine cells, Paneth cells and M cells. Enteroendocrine cells contain specific sensory receptors (Figure 3), and can rapidly release hormones to the

basolateral side when stimulated. As such, they have a role in coordinating gut functions through specific hormonal secretions. Paneth cells reside at the crypts and constitute the interface with the immune system (Figure 1), by secreting proteins such as defensins and other antimicrobials (Bevins and Salzman, 2011; Pereira et al., 2016; Wang et al., 2018b).

The gut constitutes a complex host-environment interface. The immune system has to attack any harmful pathogens whilst maintaining tolerance to many other entities, including the commensal microbiota. Besides the mesenteric lymph nodes, the intestine harbours an abundance of specialist gut-associated lymphoid tissue, GALT, which includes Peyer's patches and isolated lymphoid follicles, which enable development of adaptive immunity at this interface. These lymphoid structures are the inductive sites at which T cells and B cells are primed with antigen before they migrate to effector sites via the blood stream, a complex process, the discussion of which is beyond the scope of this project. Microfold cells (M cells) form unique gateways where Peyer's patches or isolated lymphoid follicles make direct contact with the intestinal lumen to sample antigen (Figure 1) (Chang et al., 2019). In terms of effector function, two main sites need to be considered in the small intestine. The first being the lamina propria, where activated $CD4^+$ T cells and IgA class antibody producing plasma cells reside, and the second the intestinal epithelium itself, which is populated with intraepithelial lymphocytes (IELs).

As outlined above, intestinal epithelial cells, lining the inside surface of the intestinal tract, form an interconnected layer of cells, held together by tight junction proteins. Both, structural integrity of this lining and absorptive function of the epithelial cells are essential for a healthy intestine. Disruption to the integrity of the epithelial barrier has been observed in a number of inflammatory disorders and autoimmune conditions, including Irritable Bowel disease (IBD) - Ulcerative Colitis, Crohn's disease - and Coeliac disease (Cereijido et al., 2007; Shimizu, 2010). This is not surprising, given that the epithelial cell layer is exposed to pathogens entering the intestinal lumen from the stomach on a continuous basis, and exemplifies the connection between compromised barrier function and development of immune responses, that can ultimately drive tissue destruction (Cereijido et al., 2007). Indeed, pharmacologically

blocking tight junction disruption has been demonstrated beneficial for such patients (Leffler et al., 2015).

1.3. IN VITRO MODELS OF GUT LINING

Many complex *in vitro* systems for modelling of gut function have been developed over the last decades of research. Recent developments are based on organ-on-a-chip approaches, and such approaches are typically combined with the use of primary cells (Creff et al., 2021; Fedi et al., 2021; Shin and Kim, 2022). While such systems can often replicate *in vivo* tissue organisation and behaviour to an astonishing degree, the draw-back resides in the complexity of these systems and laboriousness of the respective experiments, variability in primary cell isolates (and sourcing of human cells), and scale, at which such experiments can be conducted, which makes them often unsuitable as a tool in discovery research. When attempting to decipher molecular mechanisms, simplicity of an experimental set-up, unlimited supply and stability of cell source materials, and tied to this, reproducibility of experimental outcomes, are paramount factors affecting likelihood of success.

Caco-2 is a cell line derived from a human colorectal adenocarcinoma. Caco-2 cells have been well characterized and have been widely used as a model to study absorption, metabolism and toxicity in the gut for over 40 years (Le Ferrec et al., 2001; Ferruzza et al., 2011). Caco-2 cells differentiate spontaneously in culture into polarized intestinal cells, with an apical brush border and with tight junctions between adjacent cells without the need of adding differentiation factors, making them a good model to study intestinal barrier integrity (Le Ferrec et al., 2001; Natoli et al., 2011).

In order to mimick the gut lining more closely, a co-culture model of Caco-2 and HT29-MTX cells has been developed, where the HT29-MTX cells develop into mucus producing goblet-like cells (Hilgendorf et al., 1999). This allows for establishment of a mucus layer under *in vitro* conditions, a key consideration, given the importance of this layer for tissue function (Johansson et al., 2015).

HT29 is a cell line established from a human colon adenocarcinoma. The HT29-MTX cell line was established by exposing HT29 cells to increasing concentrations of methotrexate (MTX), resulting in a stable cell line adopting a differentiated mucus-secreting phenotype (Martínez-Maqueda et al., 2015).

The fact that these models have been extensively validated, makes them an important tool for analysing mediators modulating absorptive and other functional properties in the intestine.

1.4. PROBIOTICS

It is now understood that the function and integrity of the epithelium is, at least in part, regulated by an interplay of the host with the trillions of microbes residing in the intestinal lumen (termed the gut microbiota). There is increasing evidence linking a low bacterial diversity of this gut microbiota – referred to as dysbiosis – to human disease (Sanders et al., 2018). Metabolic interplay between the microbiota, diet and the host have a critical role in regulation of organ homeostasis and host fitness (Zierer et al., 2018). Growing recognition of this has focused interest on the potential impact of probiotic bacteria on gut barrier function, and ultimately human health.

Probiotics are defined by the Food and Agriculture Organization of the United Nations and the World Health Organisation (FAO/WHO) as “live micro-organisms that, when administered in adequate amounts, confer a health benefit on the host” (Hill et al., 2014). There are a variety of probiotics commercially available, containing a multitude of strains of various bacterial species in different combinations, and research including well controlled clinical studies has contributed to an ever-increasing body of supporting evidence for a beneficial effect (Bron et al., 2017). Most studies use a disease setting to demonstrate a potential benefit of probiotic supplementation on gut related symptoms and quality of life (Williams et al., 2009; Staudacher et al., 2017), but more recently beneficial effects were also demonstrated for the “healthy” human population (Mullish et al., 2023).

The most common bacterial species supplied in commercially available probiotic products are strains of *Lactobacilli* and *Bifidobacteria* (Bron et al., 2017). Considering currently available literature based on well-designed clinical trials, and systematic reviews with meta-analysis, a consensus panel acknowledged that, especially for probiotic formulations containing strains of those 2 bacterial species, strong evidence exists for a beneficial effect on gut function (Hill et al., 2014). In fact, Health Canada has accepted that such probiotics, when delivered in food at a level of 1×10^9 colony forming units (CFU) per serving, can be called “probiotics”, with an implicit expectation of non-strain-specific benefits (Hill et al., 2014). Note: minimum number of viable probiotic bacteria, the effective dose, refers to the respective product at the end of its shelf-life, and although live bacteria constitute the active component of the formulation, there is no implicit connection of the associated health benefits to a physical colonization of the luminal surface. Furthermore, a recent review and meta-analysis found no significant difference between single-strain and multi-strain probiotic products (McFarland, 2021). Similarly, for the probiotic formulation investigated in my thesis called Lab4, increasing its complexity has not yielded any additional benefits in a recent clinical trial, but in fact reduced its efficacy (Mullish et al., 2023). This suggests, that certain bacterial strains have an overriding role in terms of delivering benefits for gut function, and the respective biological activity or activities / underpinning mechanism are shared across a number of bacterial species.

Probiotics travel through the gastrointestinal (GI) tract, interacting with the epithelium throughout the gut, as well as with immune cells, nutrients, and commensal bacteria to directly and indirectly deliver the respective health benefits. This is only possible if they can resist the harsh conditions encountered along the way, and ultimately reach the small intestine or colon in a viable state for any beneficial effects to occur. For example, the low pH and high concentration of conjugated and unconjugated bile acids found in the human digestive system can destroy bacteria, and due to strain-specific genetic differences, certain strains may be more resistant to this harsh environment than others (Ruiz et al., 2013). This may, perhaps, explain strain specific differences in efficacy. Not surprisingly, the respective probiotics have shown to be beneficial against GI tract-related diseases, such as IBD in preclinical and clinical studies (Ford et al., 2014). It is believed that this is achieved through competitive exclusion of

pathogenic microorganisms or secretion of metabolites that regulate host responses. These include inhibition of pathogen adhesion by increasing the expression of specific mucin genes, production of anti-microbial substances and modulation of the immune system (Pagnini et al., 2010; Hungin et al., 2018). Even mild gastrointestinal disturbances can be associated with profound effects on the organism as a whole, from gut symptoms and nutritional status to anxiety/depression (Vivier et al., 2020). It is therefore not surprising, that a broad range of benefits have been ascribed to probiotics in a wide range of conditions, including obesity, diabetes, hypertension, depression and anxiety. For example, probiotics may be lowering high blood cholesterol levels (Wang et al., 2018a), or improve the metabolic status of type 2 diabetes (Raygan et al., 2018), but discussing this is outside the scope of this document.

1.5. INFLAMMATION ALTERS GUT LINING: IL-22 SIGNALLING

Interleukin 22 (IL-22) is a cytokine that belongs to the IL-10 protein family, and has critical roles in regulating epithelial homeostasis and barrier function in the gut, as well as immune surveillance at the respective exposed luminal tissue surfaces (Sonnenberg et al., 2011; Parks et al., 2016). In fact, this signalling mediator is a double-edged sword, in that it can be tissue protective, promoting innate immunity and wound healing following acute intestinal injury, for example, but it can also act as a pro-inflammatory mediator driving pathological inflammatory responses and epithelial proliferation in the gut. IL-22 is produced by innate (ILC3) and adaptive (Th1, Th17, Th22) immune cells (Sonnenberg et al., 2011; Dudakov et al., 2015; Parks et al., 2016). Unlike most other cytokines, it does not target hematopoietic cells, but the primary target are tissue resident epithelial (and stromal) cells in a diverse variety of organs and tissues, including gut, lung, liver, pancreas, kidney, skin, oral mucosa and others (Dudakov et al., 2015). In the intestine, its major function is the stimulation of epithelial cells to produce a wide variety of antibacterial proteins, maintain tight junction stability, and reinforce the mucus barrier through stimulation of mucin production (e.g. MUC-1, MUC-3A/B) (Figure 4). Specifically, IL-22 has an essential

role in mediating immunity to specific pathogens, when controlling effector functions of ILC3-mediated innate immunity (Zheng et al., 2008; Leupold and Wirtz, 2022). ILCs also regulate adaptive immunity ($CD4^+$ T cell responses to microbials), and this has a protective role against intestinal inflammatory conditions, such as IBD (Parks et al., 2016). Both mice deficient in ILC3s and mice deficient in IL-22 are highly susceptible to develop severe colitis in experimental models (Sawa et al., 2011; Sonnenberg et al. 2011). In colitis, IL-22 enhances the epithelial regeneration and goblet cell restitution in particular, to re-establish the protective mucus layer (Sugimoto et al., 2008). Notably, IL-22 mediated JAK-STAT3 pathway activation also promotes proliferation of Lgr5+ stem cells in the small intestine, thus promoting in ileal regeneration (Lindemans et al., 2015). A more detailed description of specific aspects of IL-22 biology will be given in context of experimentation in later Sections of this document.

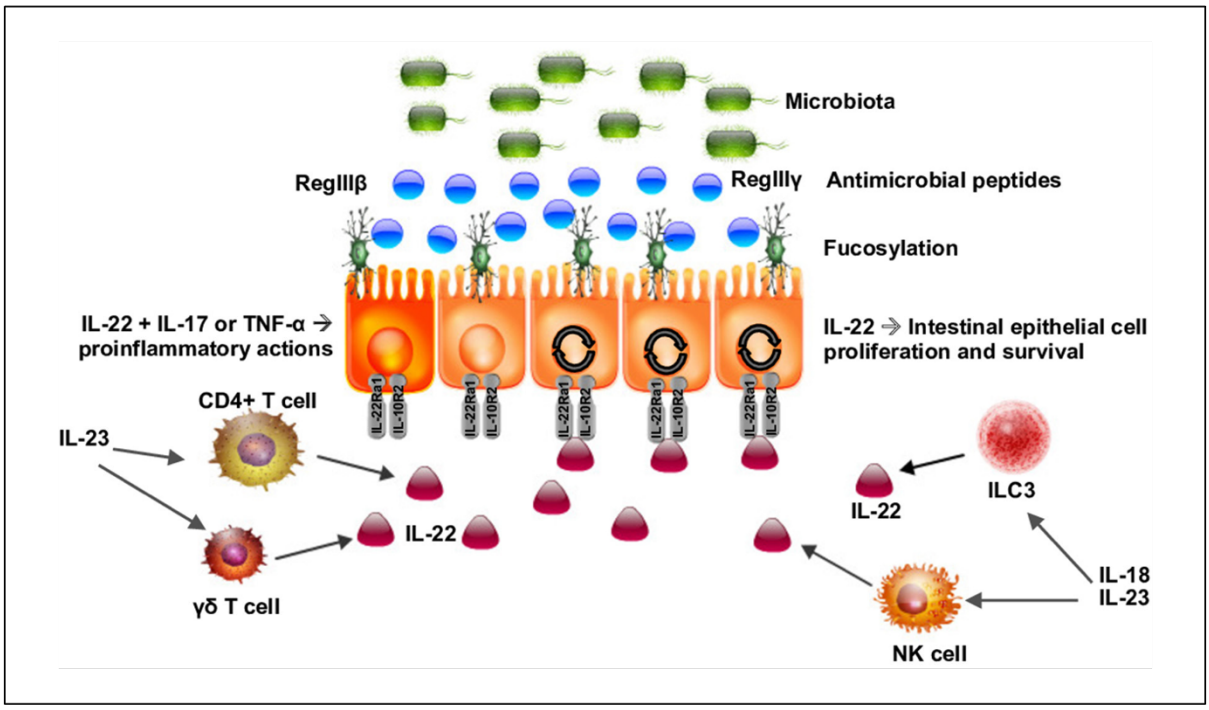

Figure 4 Schematic outlining the role of IL-22 as key regulator of the interaction of the microbiota with the intestinal epithelium. *IL-22 is produced by $DC4^+$ and $\gamma\delta$ T cells as well as type-3 innate lymphoid cells (ILC3s). IL-22 acts on intestinal epithelial cells inducing release of antimicrobial peptides, regulating the microbiota, and maintaining gut barrier homeostasis. IL-22 can act synergistically with IL-17 and TNFα to activate proinflammatory response to certain pathogens. (Taken from Parks et al., 2016)*

In terms of the associated molecular events, IL-22 signals through a heterodimeric class 2 receptor (IL-22R), composed of the IL-22R1 (IL-22Rα1) subunit, and the IL-

10R2 (IL-10Rβ2), the latter being shared with receptors binding other cytokines in the same protein family (Sonnenberg et al., 2010 and 2011). IL-22 initially interacts with IL-22R1, and the IL-22 - IL-22R1 complex then associates with the IL-10R2 chain to initiate downstream signalling. IL-22 propagates signals predominantly through the Jak-STAT pathway (Figure 5). Briefly, binding of IL-22 to its receptor activates the receptor-associated Janus kinase 1 (Jak1) and tyrosine kinase 2 (Tyk2), which in turn phosphorylate Signal Transducer and Activation of Transcription (STAT) proteins. The main target is STAT3, but in some instances STAT1 and STAT5 can also be activated (Sonnenberg et al., 2010; Dudakov et al., 2015).

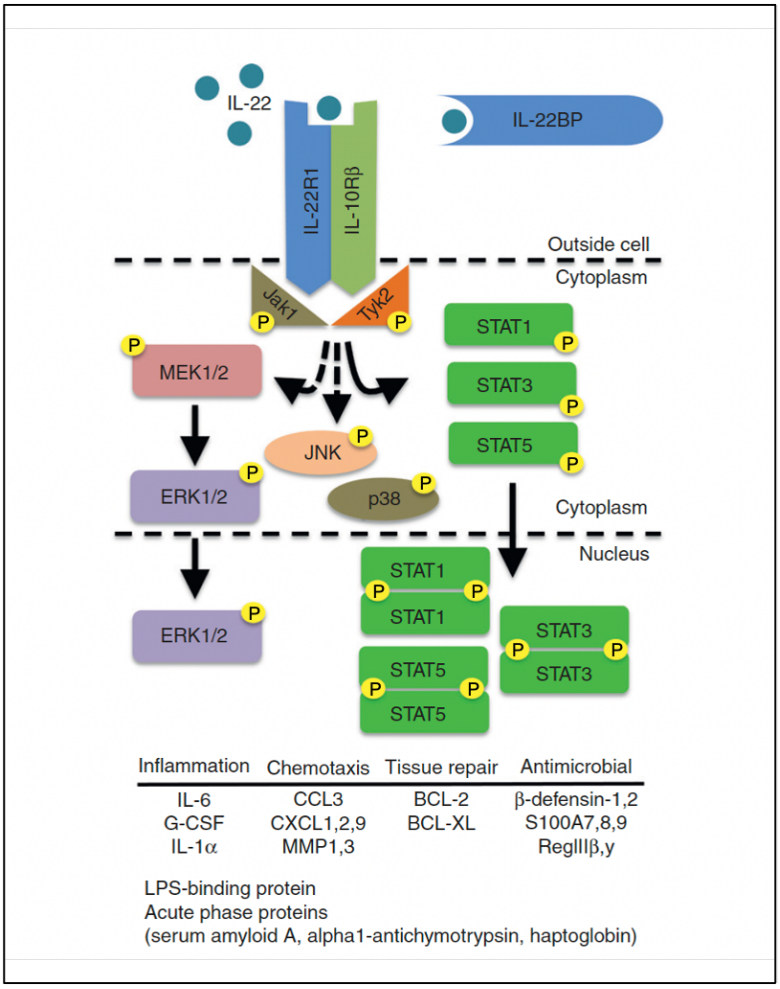

Figure 5 Signal transduction pathways downstream of IL-22 receptor. *IL-22 can be bound by a soluble decoy receptor (IL-22BP, also called IL-22Rα2) or a heterodimeric surface-bound receptor composed of IL-22Rα1 and IL-10Rβ2. Ligation of IL-22 by the functional IL-22R activates a number of signalling pathways, including the STAT pathway and the MAPK pathways as indicated. This controls a broad range of tissue responses including i. host defense, ii. tissue protection iii. inflammation and iv. tissue repair, with some of the respective target genes stated at the bottom of the schematic. Soluble IL-22 binding protein is competing with the cell surface receptor for IL-22, and is only expressed following robust persistent IL-22 signalling, suggesting that its function is as a negative regulator of this pathway.* P*, phosphorylation site. (Adapted from Sonnenberg et al., 2010)*

Several members of the IL-10 family propagate signals via STAT3. However, there are important differences. IL-22 not only leads to Tyr phosphorylation of STAT3, but also phosphorylates Ser^{727}, and this enables unique downstream outcomes (Sonnenberg et al., 2010). IL-22 binding also activates the mitogen activated protein kinase (MAPK) pathways (MEK1/2, p38 pathways), which has a differential role in regulation of epithelial cell proliferation and inhibition of cell death (Moniruzzuman et al., 2019).

1.6. WORK LEADING UP TO THIS PROJECT

This KESS project is based on a collaboration with Cultech Ltd. Cultech produces a probiotic supplement that is termed 'Lab4 probiotic consortium', which comprises of 2 strains of *Lactobacilli* (*L. Acidophilus CUL21 and L. Acidophilus CUL60*) and 2 strains of *Bifidobacteria* (*B. animalis subs. Lactis CUL34 and B. Bifidum CUL20*). Previous work by Cultech with various collaborators has revealed that in healthy Wistar rats, daily supplementation with Lab4 resulted in elevated blood glucose levels (in the absence of changes in food consumption rates). Glucose uptake by intestinal epithelial cells is an active process and therefore, provides a proxy measure of the intestinal epithelium integrity/functional activity (Michael et al., 2017). Additionally, increased rates of carbohydrate oxidation were observed in the Lab4 group of a placebo-controlled study in endurance athletes, which could be consistent with increased glucose absorption (Pugh et al., 2019). Note, endurance exercise has a detrimental impact upon the intestinal epithelium, manifesting in inefficient absorption of dietary carbohydrates. This result, therefore, indicates a protective effect of probiotic supplementation on the intestinal lining under conditions of stress. Although the previous animal model and endurance athlete *in vivo* findings provide promising evidence suggesting that Lab4 probiotic supplementation possesses beneficial properties to help maintain intestinal epithelial integrity, to date, no *in vitro* studies have been performed into the potential mechanisms by which Lab4 induces such desirable effects in the intestinal epithelium.

1.7. AIMS AND OBJECTIVES

Therefore, this study aimed to utilise appropriate *in vitro* culture models mimicking gut epithelium to:

(1) Confirm the beneficial 'protective' effects of Lab4 probiotics on intestinal epithelial cell functionality and responses to a challenge;

and

(2) Identify potential mechanisms by which Lab4 probiotics facilitates these cellular effects, leading to improved epithelial integrity.

Objective 1: To establish *in vitro* models of differentiated epithelia for the assessment of barrier function using Caco-2 and HT29-MTX cells. Confirm epithelial integrity using transepithelial electrical resistance (TEER) measurement and lucifer yellow permeation, and use immunolocalization of differentiation markers to demonstrate establishment of a mature enterocyte phenotype with a brush border membrane.

Objective 2: To demonstrate that a physiologically relevant inflammatory challenge causes damage to the gut lining that is of a reproducible magnitude and completely reversible, as determined by epithelial integrity (TEER) and immunolocalization of appropriate markers.

Objective 3: To investigate a potential 'protective' effect of Lab4 probiotic on intestinal integrity and function when applied either prior to an inflammatory challenge or during recovery of the epithelium following an inflammatory challenge. Gene expression patterns characterizing different epithelial phenotypes will be used as a proxy for functional activity of enterocytes and determined alongside direct assessment of barrier integrity (TEER) to evaluate impact of probiotics on epithelial lining.

Ultimately, the data obtained by this project will provide a set of model systems that provide a controlled environment and are amenable to experimentation, and hence will enable mechanistic questions to be addressed. The previously proposed potential of Lab4 to make the epithelium more tolerant to stress (and thereby enabling protection from damage) will be validated, and if so, further delineated to understand exactly in what specific context this holds true. A reproducible model system combined with an accessible read-out will furnish us with the means to design an experiment to elucidate the underpinning mechanism of action. Although executing the latter may be beyond this short project, the body of experimentation undertaken here is providing the tools and scientific foundation for advancing our current understanding of how Lab4 affects gut responses.

2. METHODS

2.1. CELL CULTURE

The human colon carcinoma Caco-2 cell line (Fogh et al., 1977; Lea, 2015b) was kindly provided by Professor A.T. Jones, School of Pharmacy and Pharmaceutical Sciences, Cardiff University, and unless indicated otherwise, cultured in high glucose Dulbecco's modified Eagle medium (DMEM; biosera, France, LM-D1110/500) supplemented with 10% heat-inactivated fetal bovine serum (FBS; Gibco, 10500-064), 100 units/ml penicillin, 100 μg/ml streptomycin (Gibco, 15140-122) and 1% non-essential amino acids (NEAA; Gibco, 11140-035) at 37^0C / 5% CO_2 in a humidified atmosphere. Caco-2 cells were used for the experiments between passages 30 and 41.

The HT29-MTX/E12 cell line (Lesuffleur et al., 1990; Behrens et al., 2001) was obtained from Merck (#12040401), and unless indicated otherwise, cultured in the same medium as Caco-2 cells. From here on onwards these cells will be referred to as HT29-MTX cells. HT29-MTX cells were used for the experiments between passages 53 and 68.

Cells were passaged when reaching 80% to 90% confluence. 1.2ml of pre-warmed 1:3 diluted 0.5% trypsin / ethylenediaminetetraacetic acid (Trypsin/EDTA; Gibco, 15400-054) in phosphate-buffered saline (PBS) was added to the washed cells in a T75 flask, incubated for 5min at 37^0C / 5% CO_2 before checking under the microscope that the cells had detached. The reaction was stopped by adding 10ml of pre-warmed DMEM (containing FBS), then the cell suspension was transferred to a 15ml Falcon tube and centrifuged 5min at 1500rpm to collect the cells. They were taken up in fresh pre-warmed supplemented DMEM and new plates were seeded - 1:10 dilution for Caco-2 cells, 1:12 dilution for HT29-MTX cells.

To create cryostocks, cells were detached from a T75 flask as described above. The resulting cell pellet was taken up in 1800μl (for 2 stocks) cryomedium (high glucose DMEM, 20% FBS, 1% NEAA), and 900μl cell suspension was transferred to a cryotube

containing 100µl dimethylsulfoxide (DMSO). The tubes were slowly frozen in a Mr Frosty at -80^{0}C before being transferred to liquid nitrogen for longer term storage.

All cells were regularly checked for the presence of mycoplasma (VenorGem Mycoplasma Detection kit; Cambio) and tested negative at all times.

2.2. SURFACE COATING

Human collagen type I (Collagen Corp.; 44µg/ml) or human collagen type IV (Sigma, C7521; 44µg/ml), respectively were reconstituted under sterile conditions in 0.1M acetic acid to make a 3mg/ml stock solution. The required amount was diluted in sterile distilled water, then 1/10th volume of 0.2M Tris/HCl, pH 7.4 was added to fibrillize the collagen and to reach a final concentration of 44µg/ml. Each chamber slide well or transwell was coated with 70µl of this solution, sealed and incubated over night at 4^{0}C. When needed, the collagen solution was aspirated off and the wells were dried in the cell culture hood at room temperature for 1h. After extensive washing with PBS, they were ready to be seeded.

2.3. CHAMBER SLIDE CULTURES

Caco-2 cells (passage 32 and 35 respectively) were seeded onto chamber slides (BD Falcon, #354118) i. either coated with human collagen type I, ii. human collagen type IV (as described in Chapter 2.2.) or iii. uncoated at a cell density of 1.2 x 10^5 cells/cm^2. Cells were grown in high glucose DMEM medium, supplemented as described in Section 2.1. Cells were maintained in a 37^{0}C incubator / 5% CO_2 for up to 21 days, and medium was changed every 2 to 3 days.

At the desired day, cells were washed with PBS (137mM NaCl, 3mM KCl, 8mM Na_2HPO_4, 1.5mM NaH_2PO_4, pH 7.3), then fixed by incubating with 4% paraformaldehyde in PBS, pH 7.4 (PFA, Sigma Aldrich) for 15min, before washing twice in PBS.

Chamber slides with fixed epithelia were kept sealed in PBS at 4^0C until further processing.

Fixed cells were washed twice in Tris-buffered saline (TBS; 20mM Tris/HCl, pH 7.4, 150mM NaCl), then permeabilized by incubating 15 minutes in 0.5% Triton X-100 in TBS. Non-specific protein binding was blocked by incubating the cells for 30min in 1% (w/v) bovine serum albumin (BSA; Crohn's fraction V, Sigma A9647) in TBS at room temperature. All primary and secondary antibodies used were diluted in 1% BSA/TBS to the appropriate working concentration (see Table 1), and centrifuged for 5min at 10'000 x g prior to application to remove any aggregated antibodies / carrier protein.

Table 1 *Antibodies used for staining of chamber slide cultures*

Antibody	**Dilution factor**	**Source**
ZO-1, rabbit polyclonal antibodies	1:200	ThermoFisher, 61-7300
Cubilin, rabbit polyclonal antibodies	1:100	Prof Daniel Aeschlimann, Cardiff University (Lindblom et al., 1999)
Donkey αrabbit IgG, AlexaFluor 488	1:200	Invitrogen, A21206

Incubation time of cells with primary antibodies was 1h, then the chamber slides were washed three times for 5min in TBS, before the secondary antibody was applied; donkey anti-rabbit IgG, AlexaFluor 488 conjugated, followed by incubation for 1h in the dark. Chamber slides were again washed three times 5 minutes in TBS, then taken apart, air dried briefly, and mounted using Vectashield antifade mounting medium with 4',6-diamidino-2-phenylindole (DAPI) (VectaLabs H-1200).

Pictures were taken on an Axiovert 100 Zeiss Microscope using epifluorescence illumination and 20x or 40x Plan Neofluar objectives. For more detailed analysis of specific features, pictures were taken on a Leica SP5 confocal microscope with a 40x or 63x objective and a 488nm laser for excitation.

2.4. TRANSWELL CULTURES

For generation of differentiated polarized epithelia, cells were cultured in transwells (Figure 6). In order to establish which transwells are best to use, 3 different types of transwells with different membranes were evaluated in an initial set of experiments:

- ThinCert PET membrane (Greiner #662641)
- PET membrane (Sarstedt, #83.3932.040)
- Polycarbonate membrane (Corning, #CLS3413)

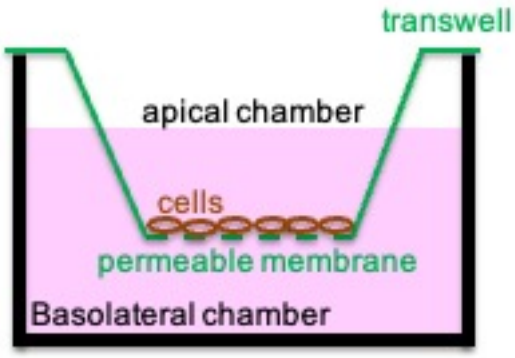

Figure 6 Schematic of transwell insert in 24-well plate

All had a surface area of 0.33cm^2, and membrane pore size 0.4μm. Some transwells were coated with human collagen type I or human collagen type IV using the same procedure as the chamber slides (see Section 2.2), and some were left uncoated. For the pilot experiment, Caco-2 cells (passage 32) were seeded at a density of 1.7 x 10^5 cells/well and were grown in high glucose DMEM medium, supplemented as described in Section 2.1. on both apical and basolateral side in a 24-well plate in a 37^{0}C incubator, 5% CO_2. All conditions were run in duplicate and medium was changed every 2 to 3 days. The amount of medium applied to the individual transwells (upper/apical chamber) and the bottom (basolateral) chamber is shown in Table 2.

Table 2 *Volume of medium applied to transwells in initial experiments*

Transwell type	Upper (apical) chamber	Bottom chamber
ThinCert PET (Greiner)	300μl	1200μl
Polycarbonate (Corning)	250μl	1000μl
PET (Sarstedt)	400μl	1500μl

To protect the membrane and cell layer from damage during medium exchanges, the medium in the transwell (upper chamber) was carefully poured out by inverting the transwell rather than by pipetting. The medium in the bottom chamber was removed at the same time. Then, fresh medium was added to the bottom chamber first, before replenishing the medium in the upper chamber.

At the indicated time point, a Lucifer Yellow (LY) assay was performed (see Section 2.5.) to assess the barrier integrity before fixing the cells with 4% PFA for subsequent histological analysis. For the repeat of this experiment, the seeding density of Caco-2 cells (passage 35) was adjusted to 0.84 x 10^5 cells/well.

The final seeding density decided upon following pilot experiments (data not shown) was 0.4 x 10^5 cells/well, in order for cells to reach confluency within 3 days. This was applied to all subsequent experiments where responses to inflammatory mediator (IL-22) or probiotic treatment were evaluated, as well as all Caco-2 / HT29-MTX co-culture experiments. For these latter experiments, Sarstedt PET transwells were used and the volumes in top and bottom compartment were 400µl and 1200µl, respectively. These volumes equate to a small positive hydrostatic pressure.

2.5. LUCIFER YELLOW PERMEABILITY ASSAY

Lucifer Yellow permeability assay was performed essentially as previously described (Kermanizadeh et al., 2018). Briefly, a sterile stock solution of 0.4mg/ml Lucifer Yellow (Merck, L0259) in Hank's balanced salt solution (HBSS; Merck, #6648) was made. Transwells were carefully washed with HBSS buffer before placing into a new 24-well plate containing 1ml pre-warmed HBSS buffer on the basolateral side. 250µl of LY stock solution was added to the apical side (Figure 7), and the transwells were incubated at 37^0C / 5% CO_2 for 2h, before collecting both apical and basolateral conditioned solutions for further assessment. Included in this assay were empty transwells (no coating, no seeded cells) as controls (= maximum permeability). For analysis of the impact of this procedure on epithelial integrity, some transwells were

washed extensively in PBS, before fixing them with 4% PFA, washing with PBS again, and finally keeping them sealed in PBS at 4^0C until further processing.

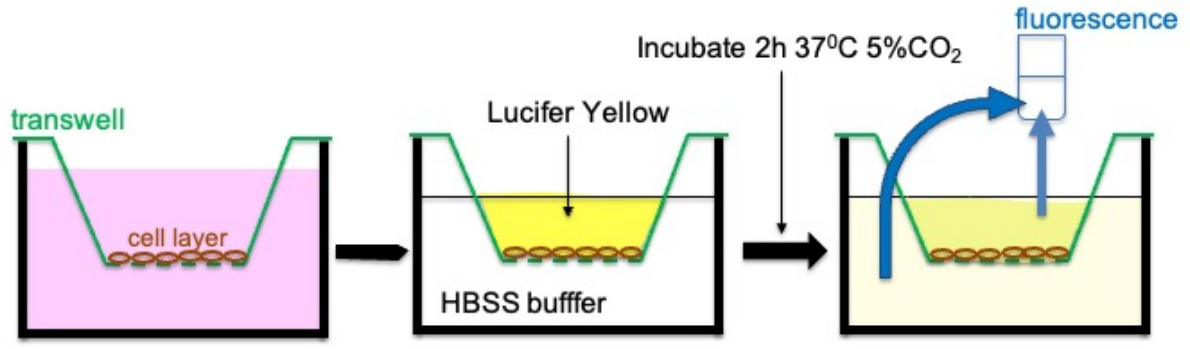

Figure 7 Schematic of LY assay

To evaluate permeability of the barrier, 100μl of collected conditioned solution containing LY was pipetted into a 96-well optical Polymer Base black plate (ThermoFisher, #165305), either neat or 1:50 diluted in HBSS and fluorescence was measured on a BMG Optima Plate Reader using a 420-10nm excitation filter and 550-10nm emission filter. The fluorescent signal was assessed against a standard curve made up of a dilution series of the initial LY stock solution ranging from 0.01μg/ml to 0.1mg/ml. The LY concentration in both upper and lower chamber of each experimental condition was determined by linear regression analysis (r^2 for standard curve was > 0.99). To see how much LY had passed from the apex to the basolateral side, the data was volume corrected and expressed as a percentage of the starting concentration.

2.6. TEER MEASUREMENTS

Trans Epithelial Electrical Resistance (TEER) was used to determine tight junction functionality (barrier integrity). TEER was measured using an EVOM2 Epithelial Voltohmmeter (World Precision Instruments) when changing the medium on the transwells. The medium was removed from both the apical and basolateral side, and the cells were washed once with pre-warmed HBSS buffer (apical and basolateral

compartment). TEER measurements were then performed in HBSS buffer using the 2-prongued chopstick electrode (Figure 8).

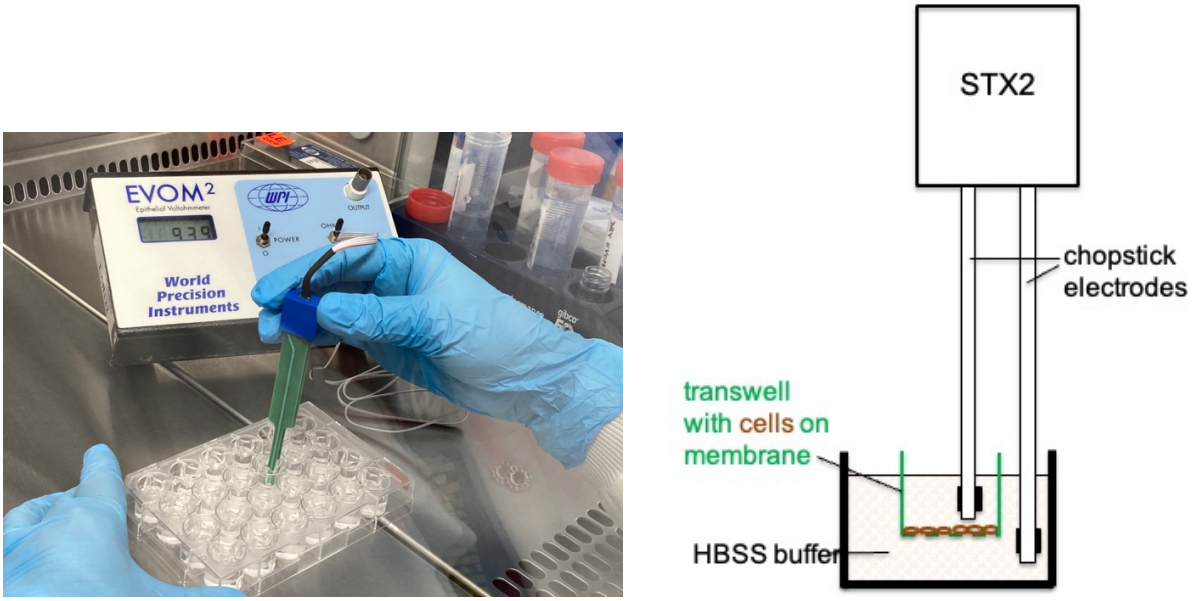

Figure 8 Schematic of EVOM for TEER measurements

The 2 electrodes were placed on either side of the wall of a transwell insert with a confluent cell layer as illustrated in Figure 8, and a small AC current was passed from one electrode to the other. TEER measures how much of this electrical signal is blocked by the cellular layer, thereby quantifying barrier integrity. Because this is non-invasive and label-free, the barrier can be monitored frequently without disturbing the cells. Particular attention was paid to holding the electrodes at a 90 degree angle relative to the bottom plate, and not to touch or move the transwells during reading as this appeared to influence the measurements.

The HBSS buffer was then removed from both the apical and basolateral side and replaced with fresh pre-warmed high glucose DMEM with supplements, and the cells were returned to the incubator as soon as possible, typically within 10 to 15 minutes. Included in these measurements were empty transwells (transwells with no coating and no seeded cells) to determine background readings (typical measurement value was 90 - 120Ω). HBSS buffer was removed and the empty transwells stored under sterile conditions at 4^0C for repeated use. For calculations, the average background

reading was deducted from the measurements and the surface area of the transwells taken into account.

Briefly, the measurement reflects the resistance across the cell layer on the semipermeable membrane (R_{TOTAL}). The cell specific resistance (R_{TISSUE}) in units of Ω, can be obtained as:

$$R_{TISSUE} = R_{TOTAL} - R_{BLANK}$$

whereby the blank resistance (R_{BLANK}) of the system corresponds to the semi-permeable membrane on its own (without cells).

The measured resistance is inversely proportional to the effective area of the semi-permeable membrane (A) which is typically reported in units of cm^2 (Srinivasan et al., 2015).

$$R_{TISSUE} \propto \frac{1}{A}$$

TEER values ($TEER_{REPORTED}$) are therefore given in units of Ω x cm^2 and calculated as:

$$TEER_{REPORTED} = R_{TISSUE} \times A$$

2.7. Sectioning and Immunostaining of epithelia / transwell membranes

Transwell membranes harbouring fixed epithelia were cut out of polystyrene carcasses using a scalpel, cut in half and handed over to the Pathology service laboratory at UHW School of Dentistry for paraffin embedding and cutting into 4μm thick transverse sections.

Sections were deparaffinized in xylene (2 x 10min) and rehydrated with a series of decreasing ethanol concentrations for 5min (90%, 70%, 60%, 40% (v/v)), ending with 15min in TBS). Staining with Haematoxylin and Eosin (H&E) was performed using a

Leica Autostaining Machine (Pathology Laboratory, UHW). Haematoxylin and Eosin staining is commonly used to assess the tissue and cell morphology, and was used here to assess epithelial morphology. Haematoxylin stains nuclei blue to purple and Eosin stains cytoplasmic structures pink to red.

Table 3 *Antibodies used for staining epithelium grown on transwell membranes*

Antibody	Dilution factor	Source
ZO-1, rabbit polyclonal antibodies (0.25mg/ml)	1:100	ThermoFisher, 61-7300
Cubilin, rabbit polyclonal antibodies (serum)	1:100 or 1:300	Prof Daniel Aeschlimann, Cardiff University
Villin-1 (CWWB1), mouse monoclonal antibody	1:50	Cell Signalling, 55883
MUC-5AC (45M1), mouse monoclonal antibody (0.2mg/ml)	1:100	Invitrogen, MA5-12178
Donkey αrabbit IgG, AlexaFluor 488 (2mg/ml)	1:200	Invitrogen, A21206
Donkey αmouse IgG, AlexaFluor 488 (2mg/ml)	1:200	Invitrogen, A21202

For cubilin and MUC-5AC staining, sections were deparaffinized as above, before non-specific protein binding was blocked with 1% (w/v) BSA in TBS for 30min. Primary antibodies were diluted in 1% (w/v) BSA in TBS as indicated in Table 3. The diluted antibodies were centrifuged at 10'000 x g for 5min to remove any protein aggregates prior to application to the sections, and were then incubated with sections in a humid chamber for 1h. After washing extensively (3 x 5min TBS), the appropriate diluted and centrifuged secondary antibody solution was applied, and the sections incubated in the dark in a humid chamber for 1h. After further washing (3 x 5min TBS), the sections were briefly air-dried in the dark, before mounting using Vectashield antifade mounting medium with DAPI. Sections were subsequently kept at 4^0C in the dark, until pictures were taken. Images were acquired on an Axiovert 100 Zeiss Microscope as detailed in Section 2.2.

For villin-1 staining, sections were deparaffinized as above, and antigen-retrieval was performed prior to blocking non-specific protein binding, as follows: 1 litre of 0.01M

citric acid, pH 6.0 was heated to boiling point in a microwave. The deparaffinized sections were added, and boiled submerged in citric acid for a further 10min, before cooling down gently by adding tap water for 10min. The sections were then incubated in TBS for 10min, before continuing with the protocol outlined above. The anti villin-1 antibody was diluted in signal stain ab diluent (Cell Signalling, 8112S) instead of 1% BSA in TBS in accordance with the manufacturer's instructions. Note, villin-1 was not detectable without antigen retrieval.

For ZO-1 staining of epithelia grown on transwells, fixed, but not embedded tissue was immunolabeled according to the chamberslide protocol (Section 2.3.), and the membrane containing cells cut out before mounting as normal.

Periodic Acid Schiff (PAS) staining was done using the PAS stain kit (TCS biosciences, HS462). Briefly, PAS is a staining method used to detect polysaccharides including mucins in tissues. The periodic acid reaction oxidizes vicinal diols in polysaccharides to aldehydes, typically without breaking glycosidic linkages connecting sugar units. These aldehydes then react with the Schiff reagent to yield a purple-magenta coloured compound. After dewaxing and rehydrating through a descending series of ethanol, the sections were incubated in periodic acid solution for 5min, then rinsed under running tap water. The sections were then immersed in Feulgen stain for 13min, before rinsing extensively (5min) with lukewarm tap water. The nuclei were stained using Haemtatoxylin Gill 3 for 5-10 seconds, and differentiated and "blued" in tap water (5-10s). Sections were dehydrated by immersing twice in 100% ethanol (10s each), and 2 x 10min in xylene, before mounting in DPX.

2.8. PROBIOTIC SAMPLE PREPARATION

Probiotic sample preparation was performed at Cultech Ltd. in Port Talbot, UK, and the prepared Lab4 CM and Lab ET fractions transported on ice back to Cardiff University. Lyophilized probiotic preparations were provided by Cultech Ltd. 1g of lyophilized *Acidophilus premix* (*L. Acidophilus CUL21 and L. Acidophilus CUL60*) and *Bifidum premix* (*B. animalis subs. Lactis CUL34 and B. Bifidum CUL20*) were

suspended in 9ml of Maximal Recovery Diluent (MRD, ThermoFisher, #CM0733) and incubated for 15min at room temperature with agitation. Flow cytometry was performed on a BD Accuri C6 Plus (live/dead staining with SYTO24/propidium iodide) (Tracey et al., 2023) to assess the amount of live bacteria, and based on that the bacterial suspensions were diluted in MRD to achieve 10^9 live bacteria per ml. Suspensions of the *Acidophilus premix* and the *Bifidum premix* were mixed at a ratio of 3:1 to create the Lab4 premix (containing 10^9 live bacteria per ml).

To create the Lab4 conditioned medium (Lab4 CM), 1ml of the Lab4 premix was added to 9ml MRD, bacteria collected by centrifugation for 10min at 2000 x g, and washed twice with 10ml MRD. After the final wash, the bacterial pellet was resuspended in 10ml DMEM (Gibco, #41966-029) to give 10^8 live bacteria per ml, and incubated anaerobically (10% carbon dioxide, 5% hydrogen and 85% nitrogen) for 5h at 37^0C without agitation. Flow cytometry was performed to confirm the viability of the bacteria at the end of the incubation (losses were less than 15%). The bacteria were removed by centrifugation (10min, 2000 x g), the conditioned media collected, sterile filtered (0.22μm), adjusted to pH 7.4 with sodium hydroxide and aliquoted to be stored at -80^0C until used. When needed, the conditioned medium was defrosted, and supplemented with 10% FBS, 100 units/ml penicillin, and 100 μg/ml streptomycin.

To create the ethanol killed bacteria (Lab4 ET), 4ml of the Lab4 premix was centrifuged 10min at 2000 x g, the bacterial pellet suspended in 4ml of 70% ethanol and incubated for 30min at room temperature. The bacterial pellet was harvested by centrifuging for 10min at 2000 x g, and washed 3 times with 4ml MRD. Bacterial killing was confirmed by flow cytometry (typically >99%), and the bacterial pellet was resuspended in De Man, Rogosa, Sharpe broth (MRS, ThermoFisher #CM0359) containing 20% glycerol, to achieve 10^8 dead bacteria per ml. The suspension of dead bacteria was divided into 1ml aliquots and stored at -80^0C until use. When needed, the aliquots were defrosted, centrifuged for 10min at 2000 x g, and washed 3 times with 1ml DMEM containing 10% FBS, 100 units/ml penicillin, 100 μg/ml streptomycin.

The respective fractions were applied to epithelia on the apical side only, without further dilution, unless otherwise indicated. Matched DMEM was used as a control treatment.

2.9. GENE EXPRESSION

2.9.1 RNA ISOLATION

The appropriate amount of wells of a 24 well plate (Sartstedt, 81.3922.30) or transwells (Sarstedt, 83.3932.040) were coated with collagen IV as described in Section 2.3, and each well was seeded with 1.21 x 10^5 cells/cm^2 (2.206 x 10^5 cells/well or 0.4 x 10^5 cells/transwell), either Caco-2 cells only, or a 9:1 mixture of Caco-2 and HT29-MTX cells. Cells were maintained at 37^0C, 5% CO_2 for 16 days with media changes every 2-3 days. On day 16, a third of the wells received probiotics in the form of conditioned media (Lab 4 CM), another third probiotics in the form of ethanol killed bacteria (Lab4 ET), and the remaining third supplemented Gibco DMEM medium (mock treatment ct) (Figure 9). On transwells, probiotics were only applied to the apex, supplemented Gibco DMEM was added to all basolateral compartments. On day 18, recombinant human IL-22 (PeproTech, #200-22; 10ng/ml) was added apically and basolaterally. RNA was extracted on the following days:

- Day 16 ct (before probiotic treatment)
- Day 18 ct, Lab4 CM, Lab4 ET
- Day 19 ct, Lab4 CM, Lab4 ET after IL-22 application for 24h
- Day 19 ct without IL-22 exposure

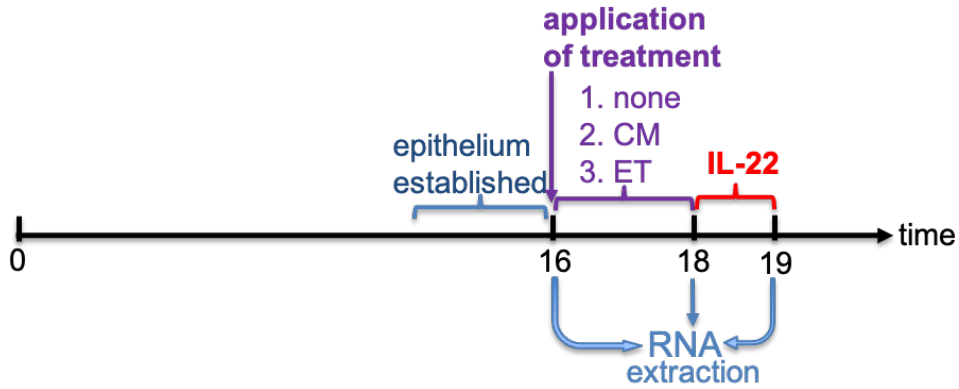

Figure 9 Schematic outlining experimental approach

For total RNA extraction, QIAshredder kit (Qiagen #79654) and RNeasy Mini Kit (Qiagen #74104) were used as follows: the cells were washed three times with pre-warmed PBS. 150µl RLT buffer from the RNeasy Mini Kit was added to each well and

the cells disrupted by scraping with the pipette tip. The cell suspension from 2 duplicate wells were pooled together and pipetted into the QIAshredder spin column to homogenize the lysate by centrifugation for 2min at 16'000 x g. 1 volume of 70% ethanol was added to the lysate, and the mixed solution transferred to a RNeasy spin column harbouring the nucleic acid binding resin. The column was centrifuged 15s at 10'000 x g to apply the lysate, and then washed first with 700µl, and then 500µl RW1 buffer. After washing with 500µl buffer RPE to eliminate contaminating DNA, the RNA was eluted in 2 steps in a total volume of 60µl RNase-free water. RNA was stored at -80^{0}C until further use.

On transwells, RNA extraction was done using 70µl RLT buffer instead of 150µl RLT buffer to accommodate for the smaller surface area. An additional step was introduced after the first (reduced) wash with buffer RW1. 10µl DNAse I stock solution (Promega #79254) was mixed with 70µl RDD buffer, applied to the RNeasy column and incubated for 15min at room temperature, before adding the remaining 350µl RW1 buffer, and continuing with the purification steps of the protocol. This step was added to ensure no genomic DNA was transferred into the RNA elution fraction, as not all primer pairs could be designed to include an intron/exon boundary (SOCS3 and claudin 2 genes have no introns).

2.9.2. cDNA SYNTHESIS

First-strand cDNA synthesis was performed in a 2-step protocol using SuperScript II reverse transcriptase (Invitrogen #18064-022). 11.5µl RNA was added to 1µl oligo(dT)$_{12\text{-}18}$ primer (0.5mg/ml) and 1µl 10mM dNTP's, incubated for 5min at 65^{0}C, and then rapidly chilled on ice to denature the RNA. 4µl 5x First Strand Buffer (final concentration 50 mM Tris-HCl, pH 8.3, 75 mM KCl, 3 mM $MgCl_2$) was added, as well as 2µl 0.1M Dithiothreitol (10mM DTT). The mixture was pre-warmed 2min at 42^{0}C before 0.5µl SuperScript II reverse transctiptase was added. The mixture was incubated for 50min at 42^{0}C for cDNA synthesis. For higher cDNA yield, a second cycle was performed: the mixture was heated to 95^{0}C for 2min, before immediate chilling on ice. Another 0.5µl SuperScript II reverse transcriptase was added after pre-

warming for 2min at 42^{0}C, and the reaction was continued by incubating at 42^{0}C for another 50min, before termination by inactivating the enzyme (70°C for 15min). The obtained cDNA was stored at -20^{0}C until further use.

2.9.3. PCR ASSAYS FOR GENES OF INTEREST

Primers used for PCR and QPCR reactions (Table 4) were designed using Oligo 4.0 software, and were commercially synthesised by Eurofins Genomics UK. The amplicon size was kept below 300bp to achieve efficient amplification, and whenever possible, the amplicon was designed to span at least one exon–intron boundary to ensure that any product was derived from poly(A)$^+$RNA. Quenched fluorescently–labelled probes harboured 5'-6-carboxylfluorescein as reporter and 3'-6-carboxytetramethylrhodamine as quencher.

Table 4 *Primers used for PCR and QPCR reactions*

Gene	Sequence of forward (F) and reverse (R) primer and probe (P)	final conc. QPCR	Amlicon size
TNFα	F: 5'- GAACCCCGAGTGACAAGCCTG	600nM	189bp
	P: 5'- CCAATGGCGTGGAGCTGAGAGATAACCA	175nM	
	R: 5'- CAGCCTTGGCCCTTGAAGAG	600nM	
hIL-6	F: 5'- GAGTAACATGTGTGAAAGCAGC	300nM	219bp
	R: 5'- TGTACTCATCTGCACAGCTCTG	300nM	
S100A8	F: 5'- GCTAGAGACCGAGTGTCCTCAG	-	126bp
	R: 5'- GCCCATCTTTATCACCAGAATG	-	
SAA1/2	F: 5'- CATCGGCTCAGACAAATACTTCC	300nM	219bp
	R: 5'- CTCAGGCAGGCCAGCAGGTCG	300nM	
REGγIII	F: 5'- GCTGTCCCAAAGGCTCCAAGG	-	243bp
	R: 5'- CATCCATCTCCATCAGGCTCAG	-	
SNAI2	F: 5'- GGACACATTAGAACTCACACGG	300nM	183bp
	R: 5'- CAGATTCCTCATGTTTGTGCAG	300nM	
claudin 2	F: 5'- CAGCATTGTGACAGCAGTTGG	300nM	245bp
	R: 5'- GCTACCGCCACTCTGTCTTTG	300nM	
MUC-3A	F: 5'- GCAGAACGCCAGCCAGGATGT	300nM	269bp
	R: 5'- CACGTGGGACCGCTCGTCTCC	300nM	
SOCS3	F: 5'- GCTCCAAGAGCGAGTACCAGC	300nM	202bp
	R: 5'- CAGGTTCTTGGTCCCAGACTG	300nM	
h36B4	F: 5'- CAGCATTGTGACAGCAGTTGG	300nM	129bp
	P: 5'- AGGCTGTGGTGCTGATGGGCAAGAAC	150nM	
	R: 5'- ATATGAGGCAGCAGTTTCTCCAG	300nM	

New primers (S100A8, SAA1/2, REGγIII, claudin 2, MUC-3A, SOCS3) were tested using cDNA obtained from day 19 Caco-2 IL-22 ct. PCR reactions were set up as follows: 10μl 2x SybrGreen Master Mix (Applied Biosystems, #4367659), 1μl cDNA, 7.8μl RNase free water and 0.6μl forward and reverse primer (10μM) each for a total of 20μl. The PCR was run on a GeneAmp PCR System 9700 (Applied Biosystems). Running conditions were as follows: 10min at 95^0C (to activate the polymerase), [15s at 95^0C (denature), 1min at 60^0C (anneal and extend)] x 50; and finally 7min at 72^0C (to ensure full extension).

To visualize the PCR products, 10μl of PCR reaction was mixed with 2μl 6x sample buffer (60mM EDTA, 0.25% (w/v) bromphenol blue, 30% (v/v) glycerol) and separated by agarose gel electrophoresis on a 1% (w/v) agarose gel containing 1.25μM ethidium bromide, alongside 5μl 1kb plus ladder (0.5μg/μl; Invitrogen, #10787018). The agarose electorphoresis was performed under constant voltage (100V) using TAE running buffer (40 mM Tris/acetate, pH 8.5, 2 mM EDTA), containing 0.5μM ethidium bromide and DNA visualised under UV light. A photograph was taken on the iBright 2000 Gel Documentation System (Invitrogen).

2.9.4. QPCR ASSAYS

QPCR assays were performed according to the manufacturer's protocol using either TaqMan Fast Advanced Master Mix (Applied Biosystems, #4444556) or Power SybrGreen PCR Master Mix (Applied Biosystems, #4367659). Briefly, master mixes were created using the respective master mix, the appropriate amount of primers (Table 4) and making up the volume with RNase free water. cDNA (1μl or 2μl) were pipetted in duplicate wells, and 19ul or 18ul of master mix added (for a total reaction volume of 20μl). After sealing the plate, it was centrifuged for 1min at 1000 x g to ensure all content was at the bottom of the plate before running on the QuantStudio™ 6 Flex System equipped with a 96-well fast block (Applied Biosystems). All SybrGreen assays were validated by assessing the melting (dissociation) curve to ensure that only one product was amplified. Selected reactions were also run on a 1% (w/v) agarose gel to confirm that the amplified product had the expected size. For

normalization, h36B4 was used as the housekeeping gene, based on its well-established robust constitutive expression (Wagener et al., 2001), and relative gene of interest expression determined using the ΔΔCt method. Fold changes in gene expression were calculated as the respective $2^{-\Delta\Delta Ct}$ value in relation to the day 16 control.

2.10. Analysis of intracellular signalling

2.10.1. Protein extraction for western blots

The approach for investigating intracellular signalling mediators is given in Figure 10. Briefly, the appropriate amount of wells of a 24 well plate (Sartstedt, 81.3922.30) or transwells (Sarstedt, 83.3932.040) were coated with collagen IV as described in Section 2.3., and each well was seeded with 1.21 x 10^5 cells/cm^2 (2.206 x 10^5 cells/well or 0.4 x 10^5 cells/transwell), either Caco-2 cells only, or a 9:1 mixture of Caco-2 and HT29-MTX cells. Cells were maintained at 37^0C, 5% CO_2 for 16 days with a media change every 2-3 days. On day 16, half the wells received probiotics in the form of conditioned media (Lab4 CM) for 48h, the other half matched Gibco DMEM (ct). On day 18, IL-22 (10ng/ml) was added to all wells, and the cells were extracted at various time points: 0h (no IL-22), 15min, 30min, 1h, 4h, 8h and 24h.

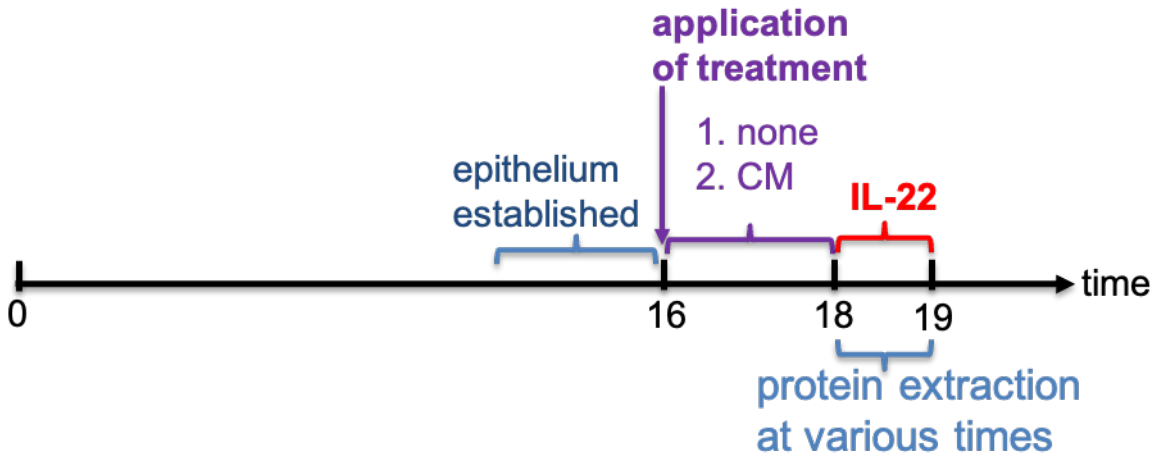

Figure 10 Schematic outlining experimental approach

Intracellular proteins regulated through phosphorylation were extracted as previously described in the presence of phosphatase inhibitors (Stephens et al., 2004). The epithelia were briefly washed in PBS, then scraped into 150µl ice cold lysis buffer (20mM Hepes/NaOH, pH 7.4, 150mM NaCl, 1% NP40, 1mM Na_3VO_4, 20mM β-glycerophosphate, 20mM *p*-nitrophenyl phosphate, 2mM NaF, 0.25% sodium deoxycholate, 1mM EGTA, 1mM PMSF, 10mg/ml leupeptin, 10mg/ml aprotinin, 10% glycerol), transferred to an Eppendorf tube and lysed by sonication (Branson Sonifier Cell Disruptor SLPe with a 3/32" micro probe) (2 short bursts of 5s with icing in-between bursts to avoid heat denaturation of proteins). The cell extract was centrifuged at 15'000 x g for 10min at 4^0C, and the soluble cytosolic fraction collected. The pellet was re-extracted in 150µl ice cold lysis buffer supplemented with 0.5% Triton X-100, yielding the membrane fraction. The resulting protein fractions were stored at -20^0C until further use.

2.10.2. PROTEIN CONCENTRATION DETERMINATION

The protein concentration in extracts was determined by performing a BCA assay (Pierce BCA Protein Assay Kit #23225) according to the protocol provided by the manufacturer. The BCA method is based on Cu^{+2} to Cu^{+1} reduction in an alkaline solution in the presence of protein (the biuret reaction), leading to purple colour development, and has a sensitivity reaching 5µg/ml. Briefly, Bovine Serum Albumin (BSA) was used as the protein standard, and a dilution series thereof was made (12.5 – 2000µg/ml). 10µl of each standard and sample, as well as appropriate buffer blanks were pipetted into a 96-well plate and 190µl of working solution (Reagent A with Reagent B at a ratio of 50:1) was added to each well. The plate was sealed, and incubated at 37 °C for 30 min. After equilibrating the plate to room temperature (5min), the absorbance was read at 562nm using a Fluostar Omega plate reader (BMG). Absorbance values were blank corrected. The standard curve for BSA was derived by linear regression and protein concentrations were calculated from the standard curve.

2.10.3. PROTEIN SEPARATION BY SDS-PAGE

Proteins were separated in 4-20% Tris-Glycine mini protein gels (Invitrogen Novex WedgeWell 1.0mm, XP040205BOX) under reducing conditions. Protein samples were mixed with an equal volume of 2x sample buffer (200mM Tris/HCl, pH 6.8, 4% (w/v) SDS, 11mM EDTA, 30% (v/v) glycerol, 0.3% (w/v) bromophenolblue) containing 2% β-mercaptoethanol (Sigma, M3148) and boiled for 2min prior to loading. A set amount of protein (5μg) from extracts was loaded into each lane, alongside 5μl of molecular weight standards (Amersham Low Molecular Weight Calibration Kit for SDS Electrophoresis, GE Healthcare, #17044601). Electrophoresis was run for 1h 40min at constant voltage (125V, ~40mA), with the gel tank packed in ice to dissipate any developing heat. The electrophoresis was performed in 24mM Tris (Fisher, T/3710/60) / 192mM glycine (Fisher, G/0800/60), and 0.1% (w/v) sodium dodecyl sulfate (SDS, Sigma, L4509).

2.10.4. WESTERN BLOTTING

Conventional wet blotting method was used to transfer proteins onto nitrocellulose membrane. For this, the sponges, blotting paper (Whatman) and Whatman Protran BA83 nitrocellulose membrane (WHA 10401403) were pre-soaked in the transfer buffer (24mM Tris / 192mM glycine, 20% (v/v) methanol). Then the “blotting sandwich” containing sponge, blotting paper, Tris-glycine gel with adhered nitrocellulose membrane, blotting paper and sponge was assembled in transfer buffer, and placed into the transfer chamber. Proteins were transferred onto the nitrocellulose membrane by electrophoresis for 1h 36min in ice cold transfer buffer, using 125 mA constant current (~25 V). The transfer chamber was placed in ice to dissipate heat. After transfer, the nitrocellulose membrane was stained with Ponceau S solution (0.1% (w/v) ponceau S, 5% (v/v) acetic acid), and developed with H_2O to confirm protein transfer had been efficient, and to mark the protein Mr marker positions with a pencil. After extensive washing in TBS to destain proteins, non-specific binding sites on the

membrane were blocked by incubating in either 5% (w/v) skimmed milk in TBS or 5% (w/v) BSA in TBS for 1 hour while agitating.

Primary antibodies were diluted in either 5% milk/TBS or 5% BSA/TBS (see Table 5), and the membranes were incubated with the antibodies for 90min at room temperature under agitation, or alternatively over night at 4^0C. After washing extensively in TBS containing 0.005% Tween 20 (TBS/Tween) (3 x 5min), the membranes were incubated with the appropriate secondary antibody (Table 5) for 90min at room temperature under agitation. Following extensive washing with TBS/Tween, the protein bands were visualized by chemiluminescence using Amersham ECL Plus Western blotting Detection Reagents (GE Healthcare, RPN21322133) according to the manufacturer's instructions and images acquired on the iBright 2000 Gel Documentation System (Invitrogen). The built in features of the iBright Analysis Software were used to derive densitometric data from images captured in chemiluminescence mode.

Table 5 *Antibodies used for Western Blots*

Antibody	**Dilution used**	**Source**
Phospho p44/42 Map Kinase (Thr202/Tyr204), rabbit polyclonal antibodies	1:250 in 5% milk/TBS	Cell Signalling, #9101
ERK1 (K-23) sc-94, rabbit polyclonal antibodies (100μg/ml)	1:1000 in 5% milk/TBS	Santa Cruz
Phospho STAT3, rabbit polyclonal antibodies	1:1000 in 5% BSA/TBS	Cell Signalling, #9131
STAT3 (79D7) rabbit monoclonal antibody	1:1000 in 5% BSA/TBS	Cell Signalling, #4904
GAPDH, mouse monoclonal antibody	1:5000 in 5% milk/TBS	Sigma, G8795
Swine αrabbit IgG/HRP (0.26mg/ml)	1:1000 in same as 1^0AB	Dako P0399
Rabbit αmouse IgG/HRP (1.3mg/ml)	1:1000 in 5% milk/TBS	Dako P0260

2.11. STATISTICAL ANALYSIS

Statistical analysis of data was carried out using GraphPad PRSIM version 9. One-way ANOVA (comparison of multiple groups) and t-test (comparison of 2 groups) was used as appropriate, whereby $p < 0.05$ was considered significant. When significant differences between multiple distributions were identified through ANOVA, a Fisher least significance difference test was conducted to investigate whether means of predetermined pairs of groups were significantly different from each other.

3. RESULTS

3.1. MODEL ESTABLISHMENT

3.1.1. TIGHT JUNCTION FORMATION BY CACO-2 CELLS ON DIFFERENT SUBSTRATES

It has previously been shown that coating of membranes with collagen type I can facilitate formation of differentiated epithelia by Caco-2 cells (Sambuy et al., 2005). However, epithelia are in contact with a basement membrane, and the major collagen forming its framework is type IV collagen (Sekiguchi et al., 2018). Collagen type IV is not only an essential component for basement membrane formation but likely supports more rapid establishment of the desired cell – ECM adhesion complexes. Indeed, the intestinal type I collagen promoted rapid migration of Caco-2 cells, whereas collagen type IV was shown to be more potent in enhancing the expression of brush border enzymes, a marker for establishment of a differentiated epithelial phenotype (Basson et al., 1996). Hence, to establish a relevant model, we initially assessed the behaviour of Caco-2 cells on different substrates.

Cell culture treated glass chamber slides were used to assess whether different coatings had an effect on how quickly cells became confluent, established cell junctions and ultimately polarized. Some wells were coated with human fibrillar collagen type I or human fibrillar collagen type IV as described in Chapter 2.2., and some were left untreated. After coating and drying, the wells were washed extensively with PBS before seeding with Caco-2 cells. The cells were grown in supplemented DMEM as described, and media was changed every 2 to 3 days. For analysis, cell layers were washed and fixed at day 3, day 7, day 14 and day 21.

Staining for ZO-1 shows the development of tight junctions between the Caco-2 cells on day 3 (Figure 11) for all conditions tested. ZO-1, or Zonula Occludens 1, is a tight junction protein assembled at cell-cell contacts, so can be used as a marker for establishment of a continuous epithelial cell sheet. This data shows that an intact epithelium is formed within 3 days under our conditions. Figure A in the Appendix shows the data obtained for day 7, day 14 and day 21 respectively.

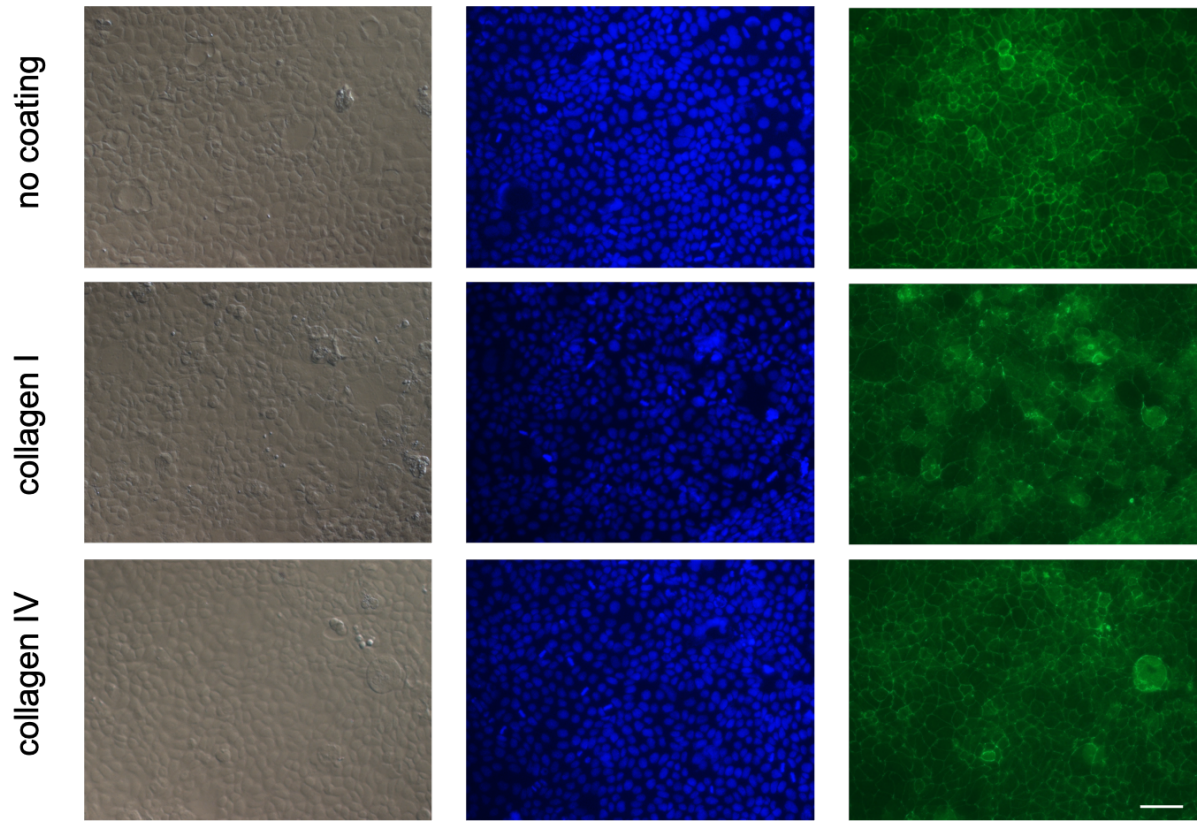

***Figure 11 ZO-1 immunolabeling of Caco-2 cells on different substrates**. Caco-2 cells (1.2 x 10^5 cells/cm^2) were seeded on uncoated chamber slides or following coating with 44ug/ml collagen type I or collagen type IV. On day 3, cells were fixed with paraformaldehyde, permeabilized and immunolabeled with polyclonal antibodies to ZO-1, Alexa Fluor 488 secondary antibodies (green), and counterstained with DAPI (blue). DIC images (left), as well as epifluorescence images for DAPI (middle) and ZO-1 (right) were captured, and are given to illustrate cell boundaries, nuclei and associated ZO-1 localization. Representative images from 1 of 2 independent experiments with replicates. Bar = 50μm*

Comparing the ZO-1 staining from day 3 to day 21 on all 3 substrates reveals the differences between the 3 types of coating conditions (Figure 12).

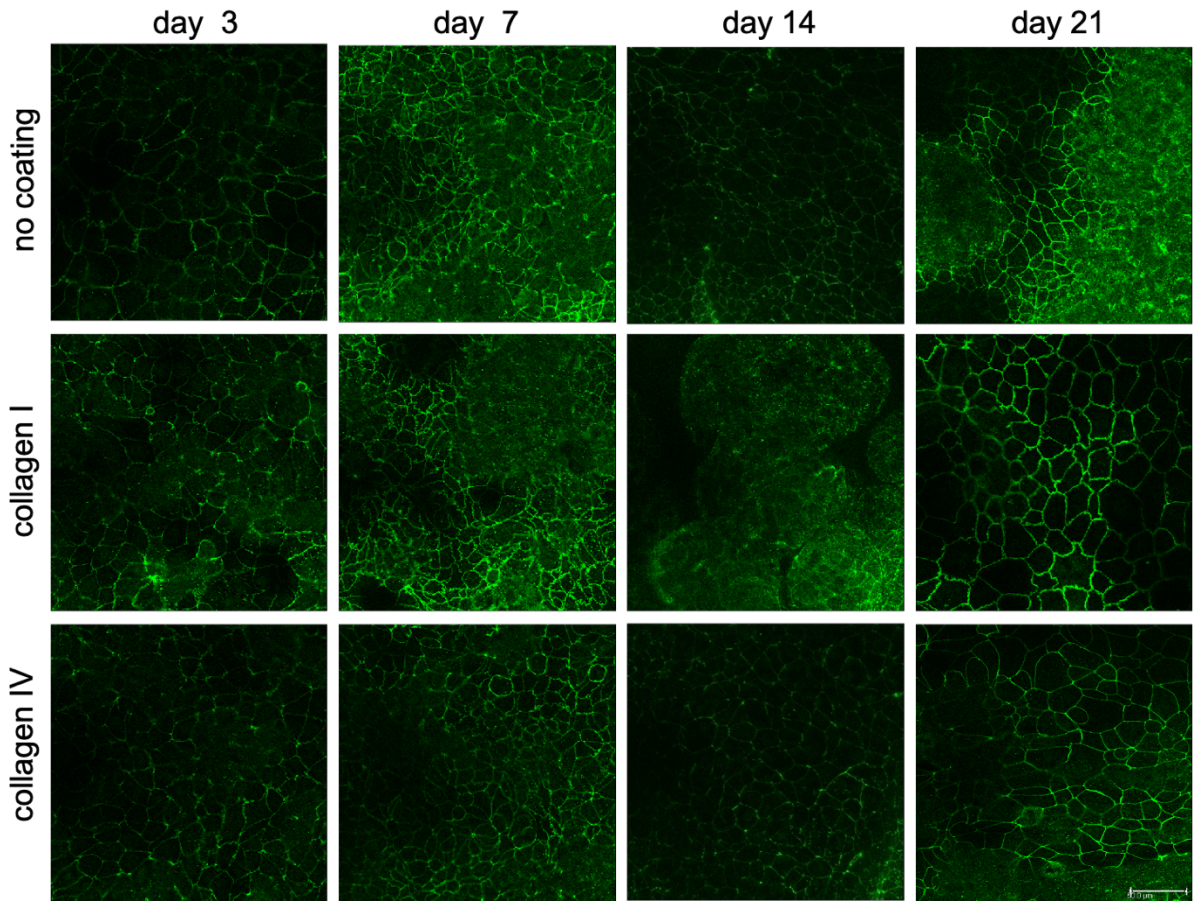

Figure 12 Confocal microscopy overview of ZO-1 immunolabeling of Caco-2 cells on different substrates. *Caco-2 cells (1.2 x 10^5 cells/cm^2) were seeded on uncoated chamber slides or following coating with 44ug/ml collagen type I or collagen type IV. On day 3, day 7, day 14 and day 21 cells were fixed with paraformaldehyde, permeabilized and immunolabeled with polyclonal antibodies to ZO-1, Alexa Fluor 488 secondary antibodies (green). Images reflect an optical section through the epithelial cell layer acquired by confocal microscopy. ZO-1 staining shows the formation of tight junctions. Note, prominent variability in staining intensity at later time (day 14 and day 21) is due to epithelial folding (see also Figure 7 & 8). Representative images from 1 of 2 independent experiments with replicates. Bar = 50 μm*

Higher magnification images of ZO-1 staining on day 21 show that the ZO-1 not only stains the tight junctions between the Caco-2 cells, but there was abundant cytoplasmic staining visible within the cells on uncoated chamber slides (Figure 13, top row). Either collagen type I (Figure 13, middle row) or collagen type IV (Figure 13, bottom row) coated chamber slides show a lot less of this cytoplasmic protein pool, presumably constituting unassembled protein, suggesting that a more mature state of cell junctions has been reached. Cells on collagen type IV-coated chamber slides in particular show very distinct and clearly defined localization of ZO-1 at cell boundaries, versus the more diffuse and wider appearing cell boundary on collagen type I or uncoated chamber slides. Although we are unable to ascertain the exact differences

at the cell junction on a molecular level by this methodology, the data confirms that cells on collagen type IV reach a state of maturity not seen under the other conditions.

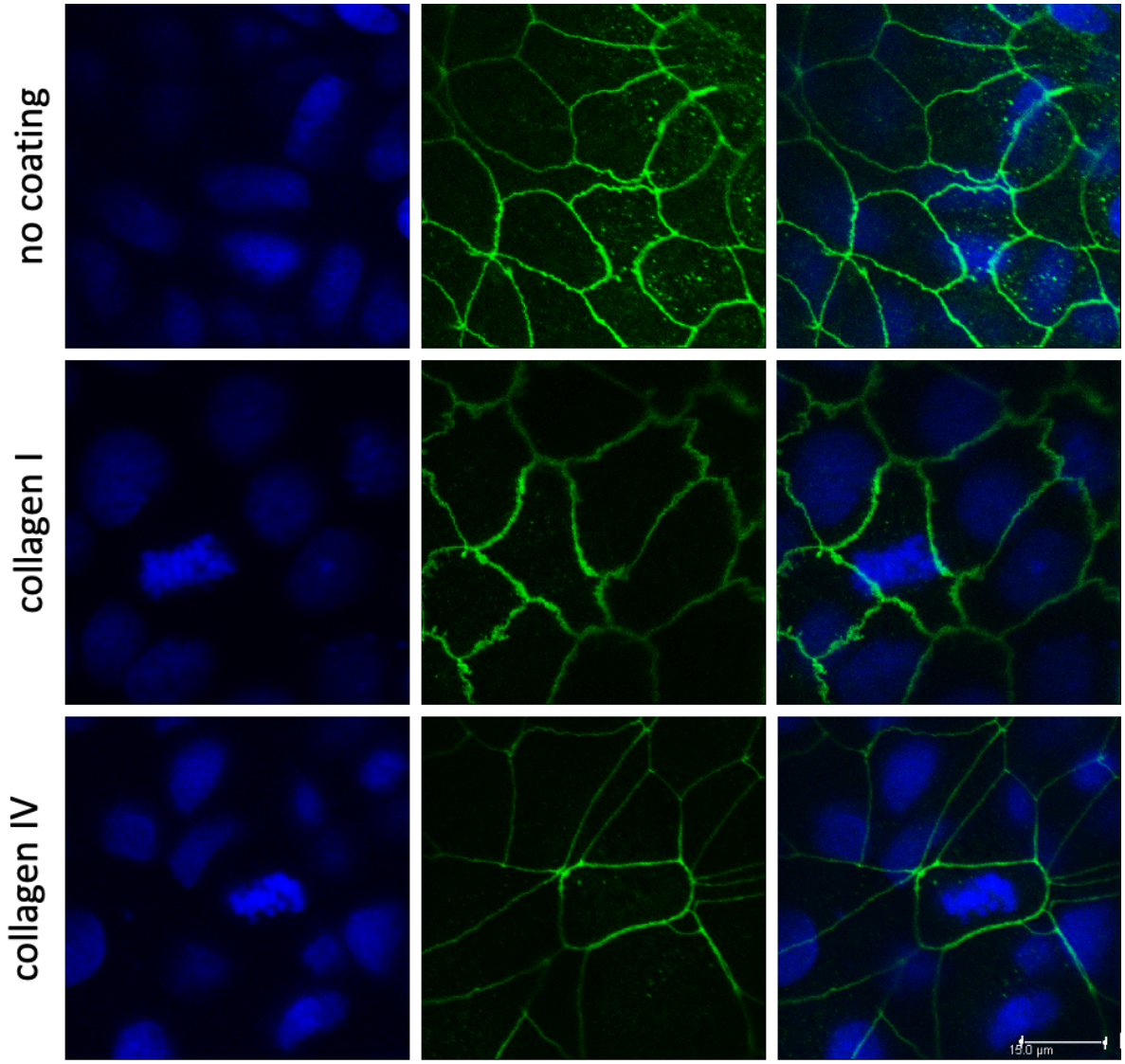

Figure 13 Confocal microscopy high magnification images of ZO-1 immunolabeled Caco-2 cells on different substrates. *Caco-2 cells (1.2 x 10^5 cells/cm^2) were seeded on uncoated chamber slides or following coating with 44ug/ml collagen type I or collagen type IV. On day 21, cells were fixed with paraformaldehyde, permeabilized and immunolabeled with polyclonal antibodies to ZO-1, Alexa Fluor 488 secondary antibodies (green), and counterstained with DAPI (blue). DAPI fluorescence is shown on the left, ZO-1 staining in the middle, and merged images on the right. Bar = 15 µm*

Looking at a z-stack of optical sections, one could see that the Caco-2 cells grown on collagen type IV-coated chamber slides in particular, had started to lift off and form domes (Figure 14 and 15). This phenomenon has been widely described in the literature (Pinto et al., 1983) and ascribed to a state of maturity of the epithelium.

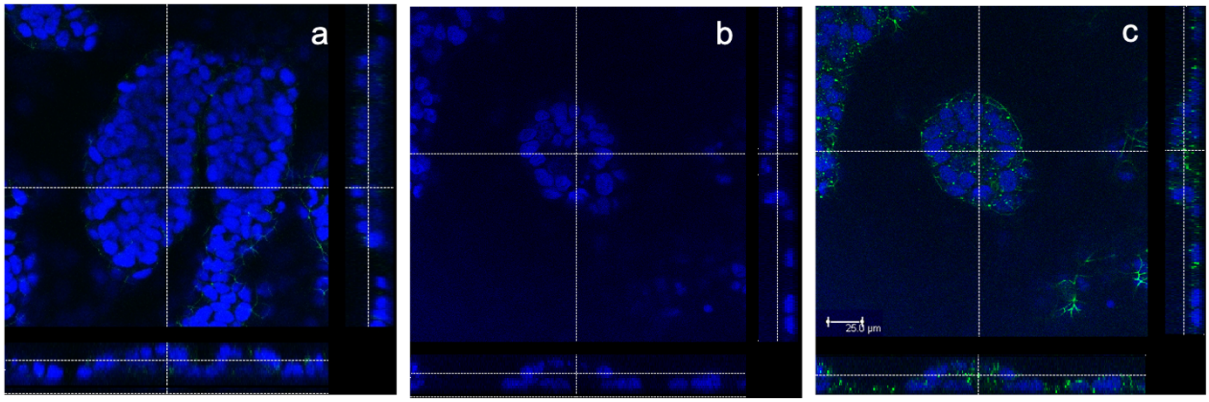

Figure 14 Confocal microscopy z-stack of optical sections of ZO-1 immunolabeled Caco-2 cells on collagen IV reveals epithelial folding. *Caco-2 cells (1.2 x 10^5 cells/cm^2) were seeded on chamber slides following coating with 44ug/ml collagen type IV. On day 21, cells were fixed with paraformaldehyde, permeabilized and immunolabeled with polyclonal antibodies to ZO-1, Alexa Fluor 488 secondary antibodies (green), and counterstained with DAPI (blue). A z-stack over a distance of 37.5μm (a), and 29.64μm (b, c), respectively, from the top of the dome to the glass slide surface was acquired at steps of 1.98μm. Image stacks reflect two representative areas (a, b: DAPI only), with merged DAPI/Alexa Fluor image for b given in c. Dotted lines show position for front (x-direction) and side (y-direction) views which are given to the right and bottom in each image. Front and side view of the z-stack highlight the dome shape of the Caco-2 epithelium. Bar = 25μm*

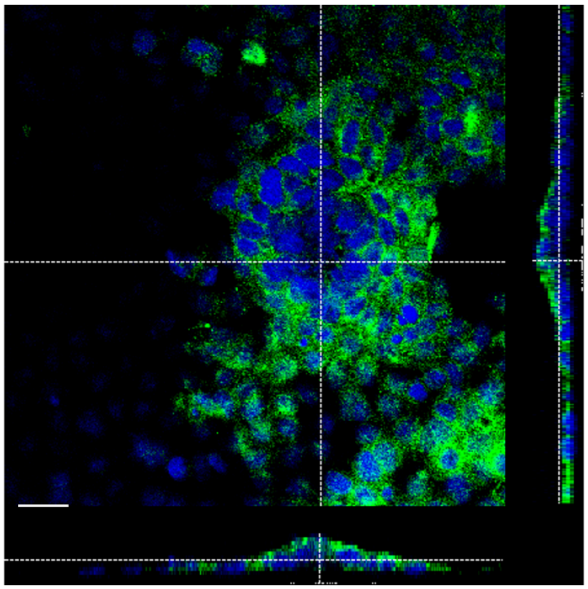

Figure 15 Confocal microscopy z-stack of Cubilin immunolabeled Caco-2 cells on collagen IV*. Caco-2 cells (1.2 x 10^5 cells/cm^2) were seeded on chamber slides following coating with 44ug/ml collagen type IV. On day 21, cells were fixed with paraformaldehyde, permeabilized and immunolabeled with polyclonal antibodies to cubilin, Alexa Fluor 488 secondary antibodies (green), and counterstained with DAPI (blue) (n = 2). A z-stack over a distance of 25.7μm from the top of the dome to the glass slide surface was acquired at steps of 1.98μm. Front and side view of the z-stack shows the dome shaped Caco-2 epithelium, with cubilin localizing to the apical brush border membrane. Bar = 25μm*

3.1.2. Evaluation of different membrane supports for establishment of intact epithelium

Both shape and membrane material have a profound impact on cell behaviour and differentiation (communication with D. Aeschlimann). Therefore, 3 different transwells were assessed in parallel as described in Chapter 2.4. All had the same surface area and same pore size. A literature search was performed to identify what transwells were

used for Caco-2 cells by other research groups. While this revealed that a wide variety of different transwells were employed, most frequently these had either polycarbonate or PET membranes (Hilgendorf et al., 1999; Sambuy et al., 2005; Natoli et al., 2010; Ferruzza et al., 2012; Lea, 2015b). Based on this and the laboratory's prior experience, a transwell from Sarstedt with PET membrane and one from Corning with a polycarbonate membrane were selected. In addition, a third type of transwell previously used by Cultech (personal communication with D. Michael) was included for comparison. This latter transwell has a transparent PET type membrane, thus making it ideal for visualization of cells during culture.

A third of the transwells were coated with human collagen type I, another third with human collagen type IV, and the remaining third left uncoated as described in Chapter 2.3. After coating, the transwells were washed extensively with PBS before seeding Caco-2 cells. The cells were grown in supplemented DMEM as described, and media was changed every 2 to 3 days. After growing for 21 days, a Lucifer Yellow permeability assay was performed to determine the barrier integrity before fixing the cells with 4% PFA. The small hydrophilic compound Lucifer Yellow (LY) can pass paracellularly from the apex to the basolateral side. The tighter the tight junctions, the less LY can pass through, making this assay a useful tool to assess barrier integrity of an epithelium (Lea, 2015a).

Figure 16 clearly shows the different performance of the 3 different types of transwells used, despite the same surface area, pore size, coating and seeding density of Caco-2 cells. The polycarbonate transwells from Corning and the PET transwells from Sarstedt performed equally well and vastly superior to the ThinCert PET transwells from Greiner. Most notably, very little diffusion was observed in an empty transwell (no coating, no cells), indicating that either the pore size stated by the manufacturer is not correct, or that LY interacts with the membrane material. The data for both the Sarstedt PET and Corning polycarbonate transwells demonstrated good epithelial integrity.

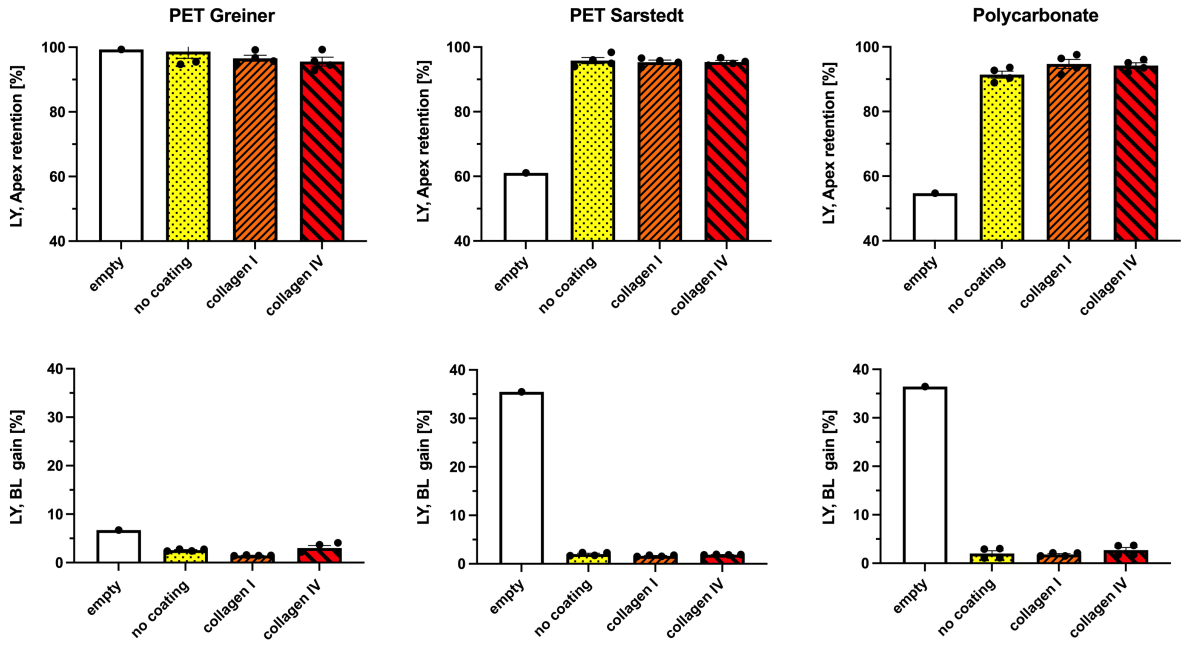

Figure 16 Determination of epithelial barrier integrity with Lucifer Yellow permeability assay. *Caco-2 cells (1.7 x 10^5 cells/well) were seeded on uncoated transwells or following coating with 44ug/ml human collagen type I or human collagen type IV and grown for 21 days. Lucifer Yellow Assay was performed and the fluorescent signal measured and LY concentration determined from a standard series. HBSS background signal was deducted from the measurements. Fluorescence is given as a percentage of starting concentration added to the top chamber (apex) at the start of the experiment, for both top chamber (upper panels) and bottom (basolateral, BL) chamber (lower panels) for the different types of transwells following 2 hours of diffusion Figure shows representative data for one out of 2 experiments conducted. For each of two experiments, all transwell types and coating conditions were analysed in parallel using the same batch of cells.*

H&E staining of the fixed and transversally cut Caco-2 epithelia on day 21 (Figure 17) showed a clear difference in appearance with respect to the type of transwell used. Figure 17a and 17b show the epithelia grown on the polycarbonate membrane, either uncoated (a) or collagen type IV-coated (b), and reveal a cuboidal cell shape typical of simple epithelia. Figure 17c shows epithelial cells grown on collagen type IV-coated ThinCert PET membrane from Greiner, revealing a largely undifferentiated cell layer. In contrast, Figure 17d to 17f show the epithelia grown on the PET membrane from Sarstedt with varying coating, where clear evidence of cell polarization is apparent despite technically imperfect preservation of cell morphology.

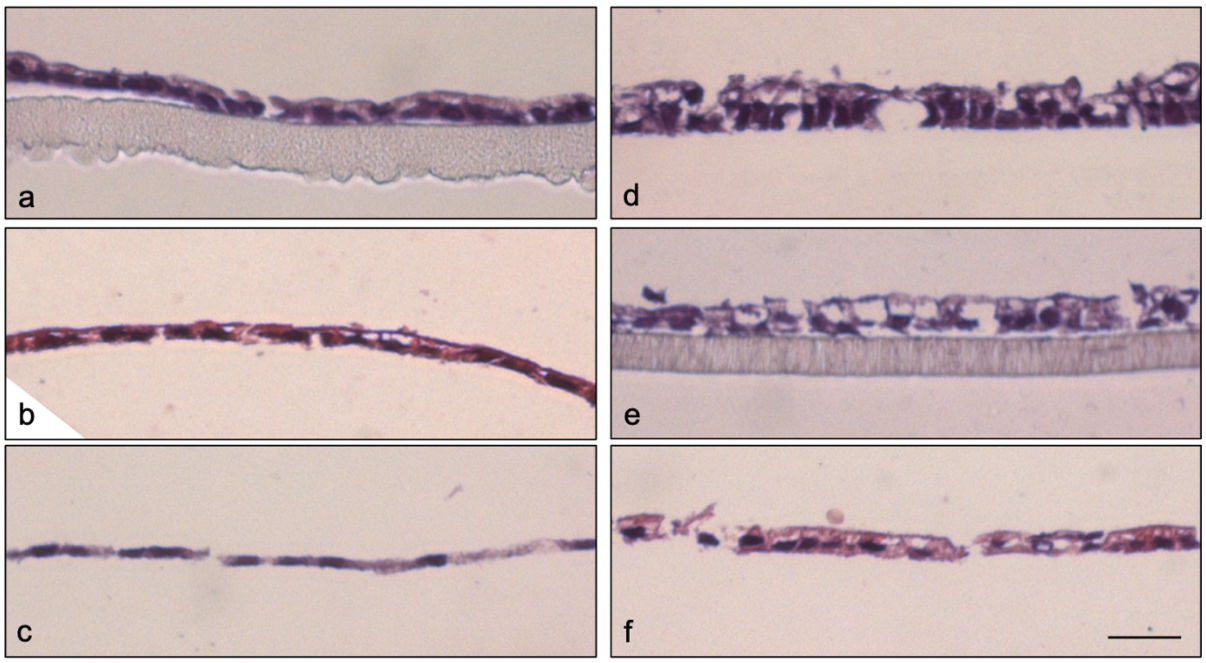

Figure 17 H&E stained sections of Caco-2 epithelium grown for 21 days on various types of transwells. *Caco-2 cells (1.7 x 10^5 cells/well) were seeded on uncoated (a, d) transwells or following coating with 44ug/ml human collagen type I (e) or human collagen type IV (b, c, f) and grown for 21 days. Cells were fixed with PFA, membranes cut out, paraffin embedded, cut into 4μm sections and H&E stained.* ***a,b*** *Corning polycarbonate transwells ,* ***c*** *PET transwell from Greiner,* ***d, e, f*** *PET transwells from Sarstedt. Data from 1 out of 2 experiments. Bar = 25μm*

Cubilin (vitamin B_{12} receptor) is an integral transmembrane protein expressed on the intestinal brush border membrane (Lindblom et al., 1999). It has been shown to be primarily and abundantly expressed in the small intestine and the kidney, but it was unclear to what extent it is present in the colon.

To test if cubilin could be used as marker for polarization of colonic epithelia, some of the paraffin embedded sections from day 21 were stained as per Chapter 2.7. with the antibodies for cubilin. Staining restricted to the apical side of the epthelia on collagen type IV coated polycarbonate and Sarstedt PET membranes could be observed, demonstrating that the cells had undergone polarization, and that cubilin was expressed at the brush border membrane, although at lower levels compared to the upper gut (Lindblom et al., 1999).

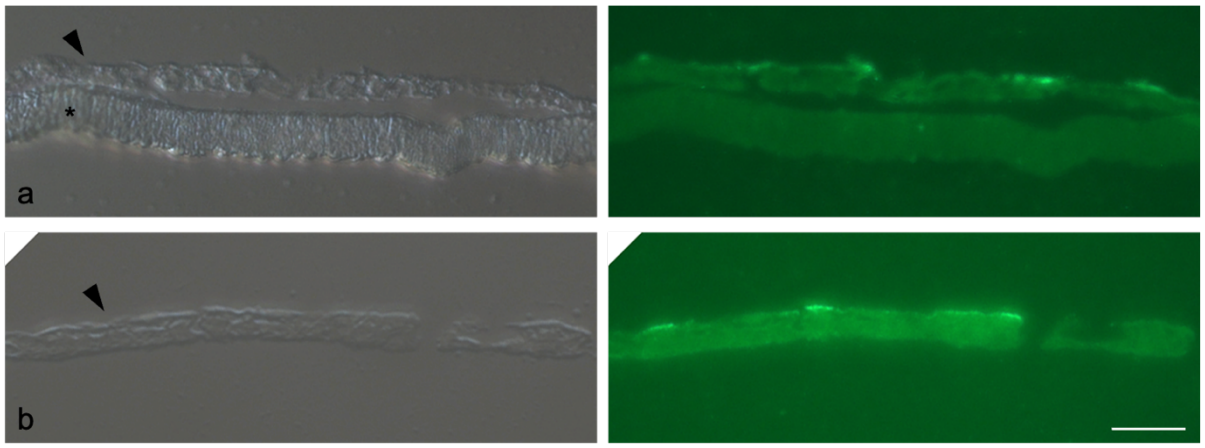

Figure 18 Cubilin immunostaining of Caco-2 cells grown on different types of transwell membranes on day 21 reveals cell polarization. *Caco-2 cells were seeded (1.7 x 10^5 cells/well) onto collagen type IV-coated Corning polycarbonate transwells (a) or PET transwells from Sarstedt (b). After blocking non-specific binding with BSA, cells were immunolabeled with polyclonal anti-cubilin antibodies (1:300), and antibody binding revealed with AlexaFluor 488-conjugated secondary antibodies. DIC images (left) and corresponding epifluorescence images for cubilin (right) are given. Arrowheads point to epithelium, asterisk indicates the transwell membrane. Bar = 25μm*

Based on these initial results, the decision was made to use human collagen type IV coating for the gut model. Both zona occludens-1 and cubilin localization indicated that a mature, polarized epithelium developed readily on this substratum (Figures 13, 15, and 18). Furthermore, based on the histological analysis (Figures 17 and 18), combined with the results from the LY permeability assay (Figure 16), the decision was made to use the PET transwells from Sarstedt for our model, as they performed similar to the polycarbonate transwells but at a fraction of the costs.

3.1.3. *Determination of epithelial integrity and cell polarization*

Having decided on the transwell and coating type, more PET transwells from Sarstedt were set up, seeded with Caco-2 cells (0.4 x 10^5 cells/well) and grown as previously described for up to 21 days. The aim of this experiment was to more precisely delineate at what point during the culture a continuous epithelium was reached and at what point cells polarize and develop a brush border, features associated with a mature epithelial interface. TEER measurements were employed to assess epithelial integrity and were taken every time a medium change was made.

TEER appears to continuously increase over the duration of the experiment (Figure 19, left). An initial rapid increase up to day 5 or 7 was followed by a more gently slope, which we interpreted as cells reaching confluency. This is followed by phase 3 reflected by a steeper slope, starting around day 10 or 12 and presumably reflects maturation of the epithelia. Some transwells were fixed at days 7, 9, 14, 16 and 20 to assess the development of the epithelium. The membranes were cut out, paraffin embedded and 4μm sections cut, before immunostaining was performed, as described in Chapter 2.7.

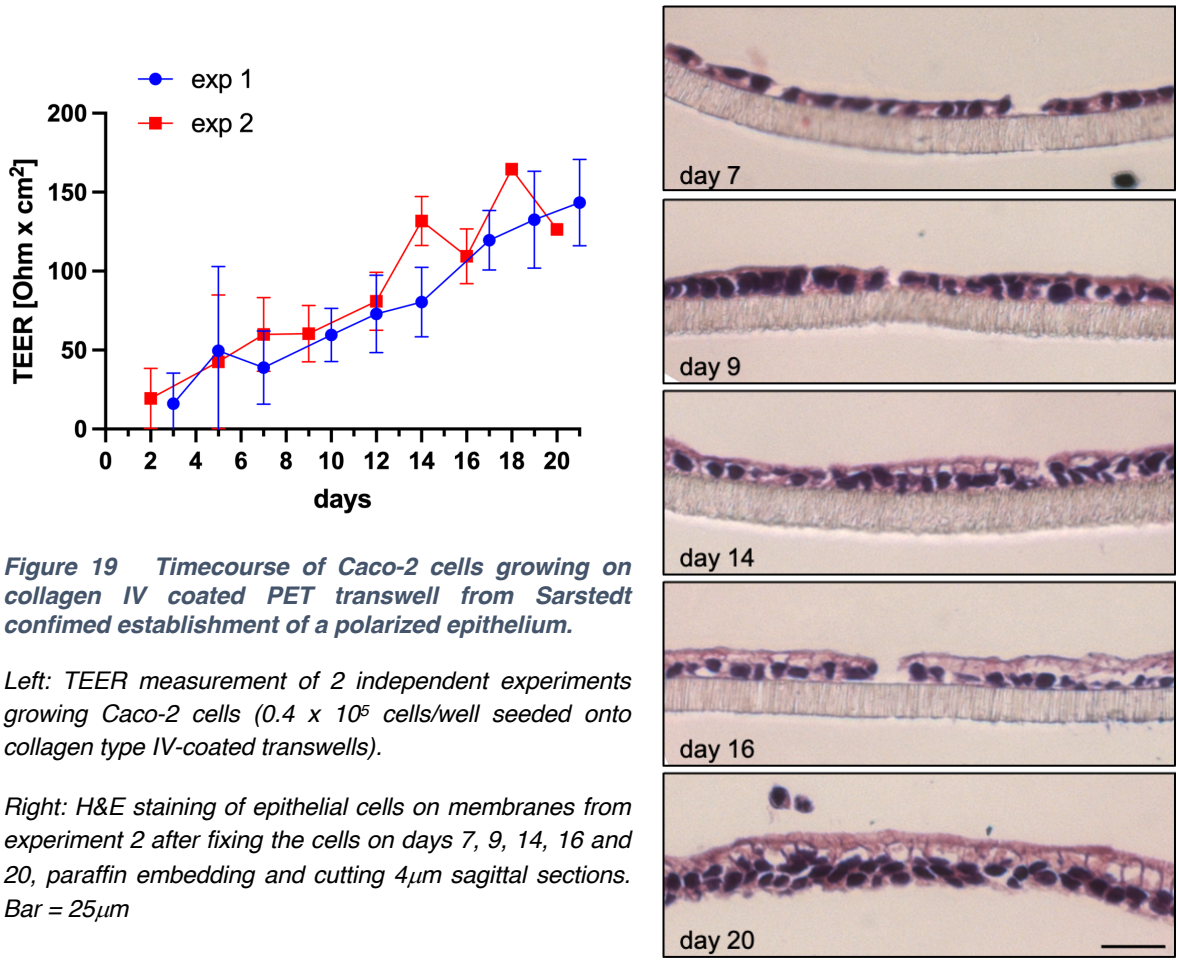

Figure 19 Timecourse of Caco-2 cells growing on collagen IV coated PET transwell from Sarstedt confimed establishment of a polarized epithelium.

Left: TEER measurement of 2 independent experiments growing Caco-2 cells (0.4 x 10^5 cells/well seeded onto collagen type IV-coated transwells).

Right: H&E staining of epithelial cells on membranes from experiment 2 after fixing the cells on days 7, 9, 14, 16 and 20, paraffin embedding and cutting 4μm sagittal sections. Bar = 25μm

Figure 19 (right) shows the H&E stained epithelia on days 7, 9, 14, 16, and 20, respectively. Note that a continuous monolayer is established by day 7, and cell polarization seems to be happening between day 9 and day 14, as the nuclei move towards the basolateral side; fully polarized epithelium is established by day 16. By day 20, the cells seem to have formed multilayers. The reason for this is unclear at

present, but this phenomenon has been observed by others and is described in publications (Ferraretto et al., 2018).

Looking at the cubilin immunolocalization (brush border membrane marker) on the same sections, no specific staining was observed at day 7 (Figure 20a), with some focal faint staining appearing on day 14 (Figure 20b), and intense and near continuous staining of the apical edge on days 16 and 20 evident (Figure 20c-e). This confirms that cell polarization had occurred and a brush border membrane been established by day 16, much earlier than previously reported on uncoated or collagen type I coated transwells (Sambuy et al., 2005; Lea, 2015b). This was further confirmed by detecting another protein associated with epithelial brush border formation, villin-1 (Figure 20f). A confocal microscopy image is given in Appendix B.

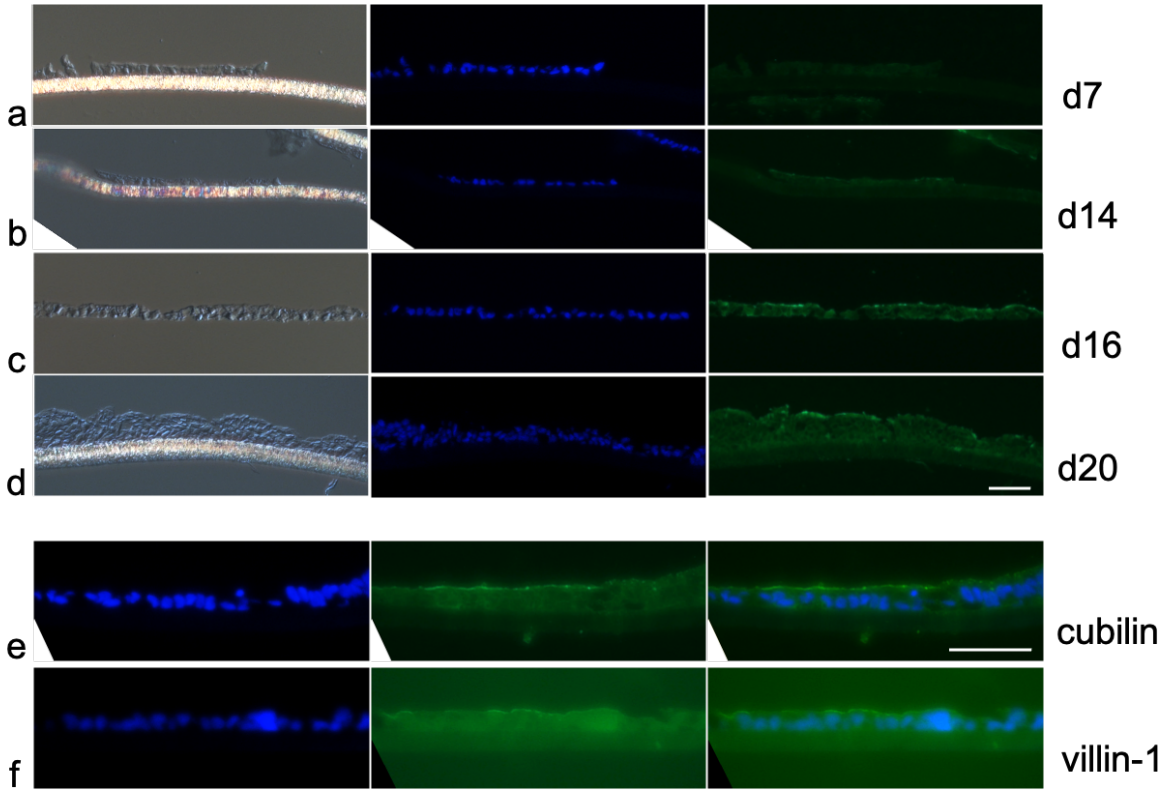

Figure 20 Cubilin and villin-1 localization to apical membrane on Caco-2 epithelium is indicative of organotypic cell differentiation. *Caco-2 cells were seeded (0.4 x 10^5 cells/well) onto human collagen type IV-coated PET transwells from Sarstedt and grown for 7 (a), 14 (b), 16 (c) or 20 days (d). Fixed, paraffin embedded transwell membranes harbouring epithelia were sectioned and stained with cubilin-specific polyclonal antibodies (1:100) and detected with AlexaFluor 488 secondary antibodies. DIC (left), DAPI (middle) and AlexaFluor 488 (right) images were acquired using a 20x Plan Neofluar objective. Panel (e) shows a higher magnification (40x) of a section stained for cubilin at day 16. Panel (f) shows a representative section of an epithelium at day 14, stained with monoclonal antibody to villin-1 (1:50, after antigen retrieval) and detected with AlexaFluor 488 secondary antibodies at 40x magnification. Bars = 50μm*

[Cell junctions were visualized through ZO-1 staining as discussed in Section 3.1.1. and an example is shown for comparison in Appendix C.]

3.1.4. EPITHELIA WITH MUCUS-SECRETING EXOCRINE CELLS

For an improved, more realistic gut model, mucus producing cells were included. Mucin-secreting goblet cells are interspersed into the epithelium, and provide the mucosal surfaces with a thick mucus lining, which acts as a barrier and limits interaction with luminal microbes (Knoop and Newberry, 2018). As this mucin lining may impact on sensing of probiotic-derived components, it appeared essential to consider this within our experimental design. To achieve this HT29-MTX cells were incorporated with Caco-2 cells. The HT29-MTX cells are a stable cell line that can differentiate into mucus-secreting "Goblet-like" cells under appropriate conditions (Hildgendorf et al., 1999), a sublineage of a human colon-derived cell line (HT29).

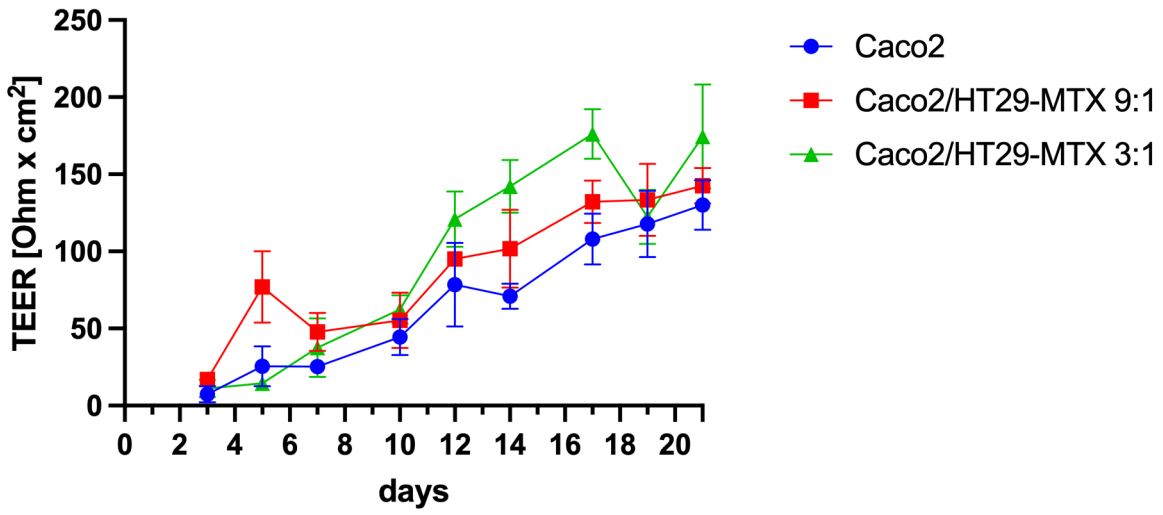

Figure 21 TEER measurements of Caco-2 cells alone versus co-cultures with mucus producing cells. *Cells were seeded onto collagen type IV-coated transwells at a density of 0.4 x 10^5 cells/well, either (a) Caco-2 only, (b) Caco-2 / HT29-MTX 9:1 mix, or (c) Caco-2 / HT29-MTX 3:1 mix and grown for 21 days. Transwells for the three conditions were cultured in parallel (n = 3).*

In an initial experiment, transwells were coated with collagen type IV as previously described, and seeded with either Caco-2 cells (0.4 x 10^5 cells/well) alone, a 9:1

mixture of Caco-2 and HT29-MTX cells (total of 0.4 x 10^5 cells/well), or a 3:1 mixture of Caco-2 and HT29-MTX cells (total of 0.4 x 10^5 cells/well) and grown in supplemented DMEM medium as previously described, to determine the most appropriate ratio of mucus cells to be included. TEER measurements and media change were conducted every 2 to 3 days (Figure 21).

TEER measurements for Caco-2 cells alone were in line with previous experiments (compare to Figure 19), and revealed an increase for Caco-2 / HT29-MTX co-cultures at 3:1 ratio, when compared to Caco-2 cells alone from day 12 onwards (Figure 21). This could be consistent with establishment of a mucus layer, as previous studies have shown that TEER increases with the formation a mucus layer (Mahler et al., 2009). By contrast, TEER measurements for the co-cultures at the lower 9:1 ratio were comparable to those of Caco-2 cells alone. Sectioning of the epithelia further confirmed the presence of differentiated mucus producing cells interspersed among the epithelial cells (Figures 22, Appendix D).

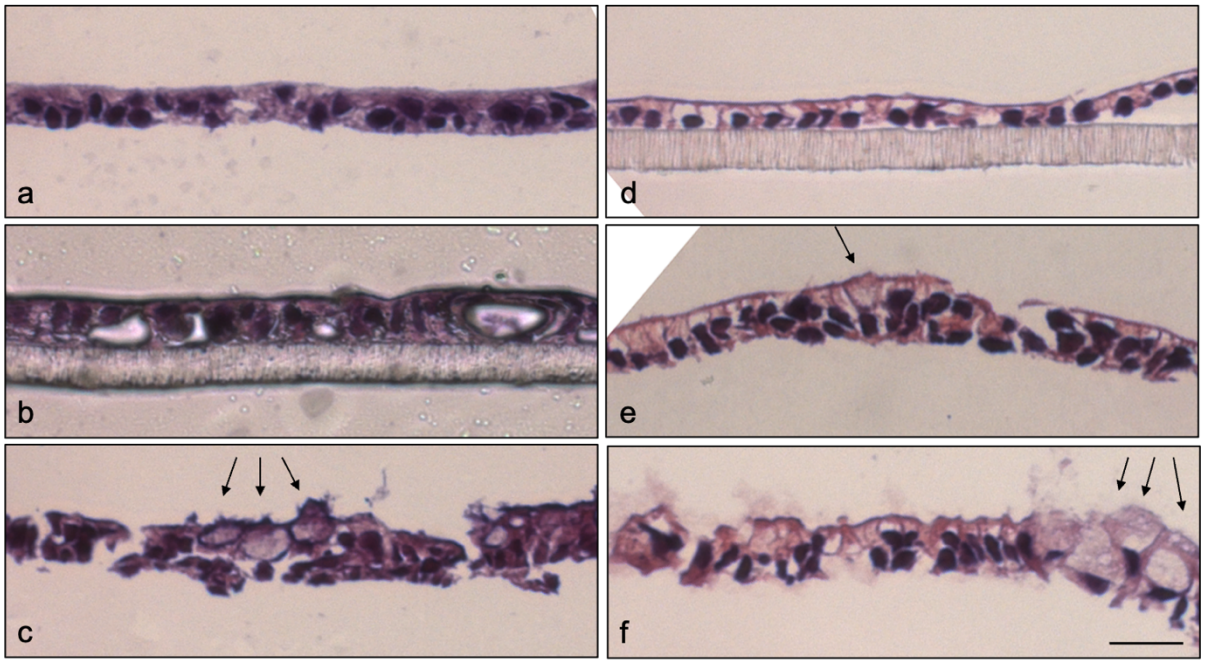

Figure 22 H&E stained sections of epithelia grown on collagen type IV coated transwells with and without mucus producing cells on day 12 and day 21. *Cells were seeded onto collagen type IV-coated transwells at a density of 0.4 x 10^5 cells/well, either (a/d) Caco-2 only, (b/e) Caco-2 / HT29-MTX 9:1 mixture, or (c/f) Caco-2 / HT29-MTX 3:1 mixture and grown for up to 21 days (n = 2). (a/b/c) were fixed, paraffin embedded and H&E stained on day 12, (d/e/f) on day 21. Arrows indicate mucus producing cells (c/e/f). Bar = 25μm*

Different gel-forming mucins are secreted by goblet cells lining mucosal surfaces in different parts of the body, and the pattern of mucin expression also changes along the digestive tract (Knoop and Newberry, 2018). In the upper intestine and colon, and unlike the stomach, MUC2 is the predominant mucin produced (Johansson et al., 2011). However, MUC-5AC which lines the gastric mucosal surfaces can also be produced in the intestine where it plays a critical role in immune defense (Forgue-Lafitte et al., 2007; Hasnain et al., 2011). Mucus production in our model was initially confirmed in two ways: periodic acid schiff (PAS) staining and immunolabeling of MUC-5AC. PAS staining is a histochemical method to detect the mucin-linked carbohydrates in the mucus layer. Both approaches confirmed the presence of mucus secreting cells interspersed in the epithelium (Figure 23), with the epithelia formed by Caco-2 / HT29-MTX cells seeded at the 3:1 ratio forming expansive mucus producing islands (Figure 23b,d; arrows).

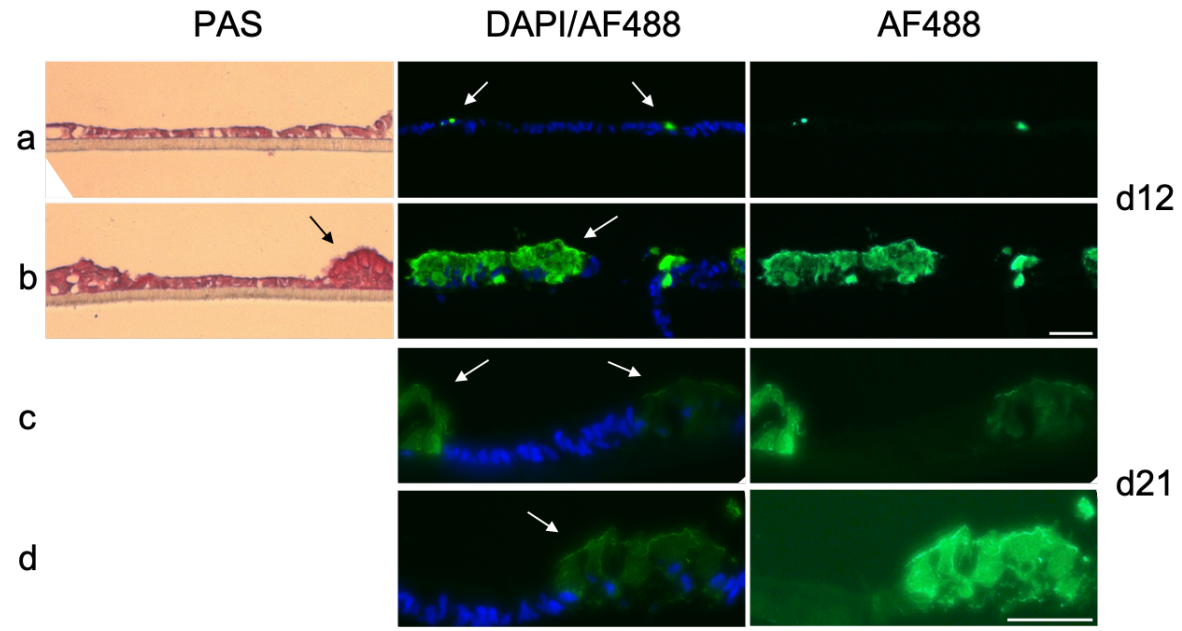

Figure 23 PAS staining and MUC-5AC immunolabeling of epithelia grown on collagen type IV coated transwells to visualise mucus producing cells on day 12 and day 21. *Cells were seeded onto collagen type IV-coated transwells at a density of 0.4 x 10^5 cells/well, either (a,c) Caco-2 / HT29-MTX 9:1 mixture, or (b,d) Caco-2 / HT29-MTX 3:1 mixture, and grown for 12 (a,b) or 21 days (c,d). Cells were fixed, membranes cut out, paraffin embedded, cut into 4μm sections and PAS stained (left; red stain), or stained with monoclonal antibody to MUC-5AC (1:100) and detected with AlexaFluor 488 secondary antibodies. DAPI and FITC overlay (middle) and AlexaFluor 488 (right) images were acquired using a 20x (a,b) or 40x (c,d) Plan Neofluar objective, respectively. Mucus producing cells are indicated by arrows. Bars = 50μm*

Published data suggests that a 90% to 10% mixture of Caco-2 cells to HT29/MTX cells represent the epithelium in the small intestine, whereas a 75% to 25% mixture is more akin to what is seen in the distal colon (Mahler et al., 2009). Given that we think the probiotics are more likely to act at the level of the upper gut, a 9:1 ratio is more likely to be a representative model and was therefore chosen as our enhanced gut model.

For detailed characterization of our model incorporating the mucus producing cells, transwells coated with collagen type IV were seeded with a 9:1 mixture of Caco-2 and HT29-MTX cells (total of 0.4 x 10^5 cells/well) and grown for up to 20 days. Transwells were fixed at days 7, 9, 12, 14, 16, 18 and 20 respectively, membranes cut out and embedded in paraffin, and sections were stained for the two brush border membrane markers cubilin and villin-1 as before (Figure 24).

Looking at the detection of cubilin (Figure 24a), no membrane-specific staining was apparent at day 7, whereas some focal faint staining appeared by day 9, and intense and near continuous staining of the apical enterocyte edge was evident by day 12. This is in line with what we observed previously for epithelia formed by Caco-2 cells in isolation (Figure 20). Villin-1, a cytoskeletal protein associated with brush border development, was detected even earlier, starting on day 7, with almost continuous apical membrane staining observed by day 9 (Figure 23b). Note the staining is restricted to epithelial cells.

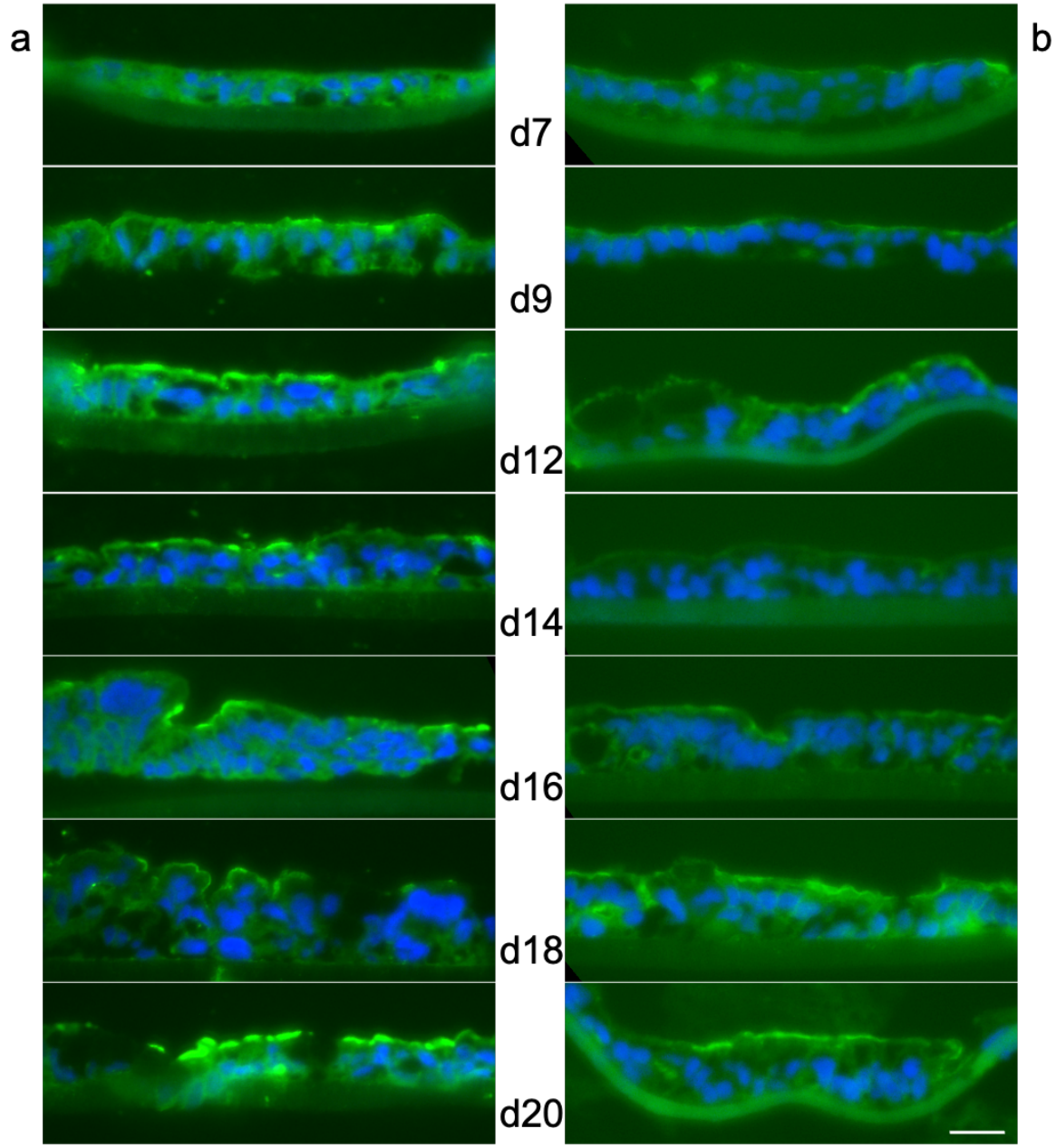

Figure 24 Timecourse of brush border development as detected by cubilin and villin-1 staining on mixed model (Caco-2 / HT29-MTX 9:1 mixture). *A 9:1 mixture of Caco-2 and HT29-MTX cells were seeded onto collagen type IV-coated transwells at a density of 0.4 x 10^5 cells/well and grown for up to 20 days. Fixed, paraffin embedded transwell membranes harbouring epithelia were sectioned and stained with (a) polyclonal antibodies to cubilin (1:100), or (b) with monoclonal anti-villin-1 antibody (1:50 after antigen retrieval), detected with AlexaFluor 488 secondary antibodies. DAPI / AlexaFluor 488 overlay images were acquired using a 20x Plan Neofluar objective. Note: dark areas (e.g. panel at day 20 are not gaps in the epithelium but reflect areas occupied by mucus producing cells. Bar = 50μm*

Mucus production was assessed either with PAS or MUC-5AC staining as described in Chapter 2.7. (Figure 25). On day 9, intense staining of the differentiated mucus producing Goblet-like cells can be observed. By day 14, a mucus layer that has started to spread across the enterocytes (Caco-2 cells) is apparent (Figure 25, arrowheads).

A close-up picture on day 16 clearly shows the green mucus layer above the Caco-2 cells (Figure 25, bottom panel). The mucus layer formed in the small intestine is discontinuous, and less well defined than in the stomach or colon proper (Johansson et al., 2011). It moves upwards from the crypts along the villi towards the tip where enterocytes are shed, with often only partial coverage of the villi in the outer aspect. Hence, variable coverage of enterocytes as observed in our model is in line with the physiological situation in the native tissue.

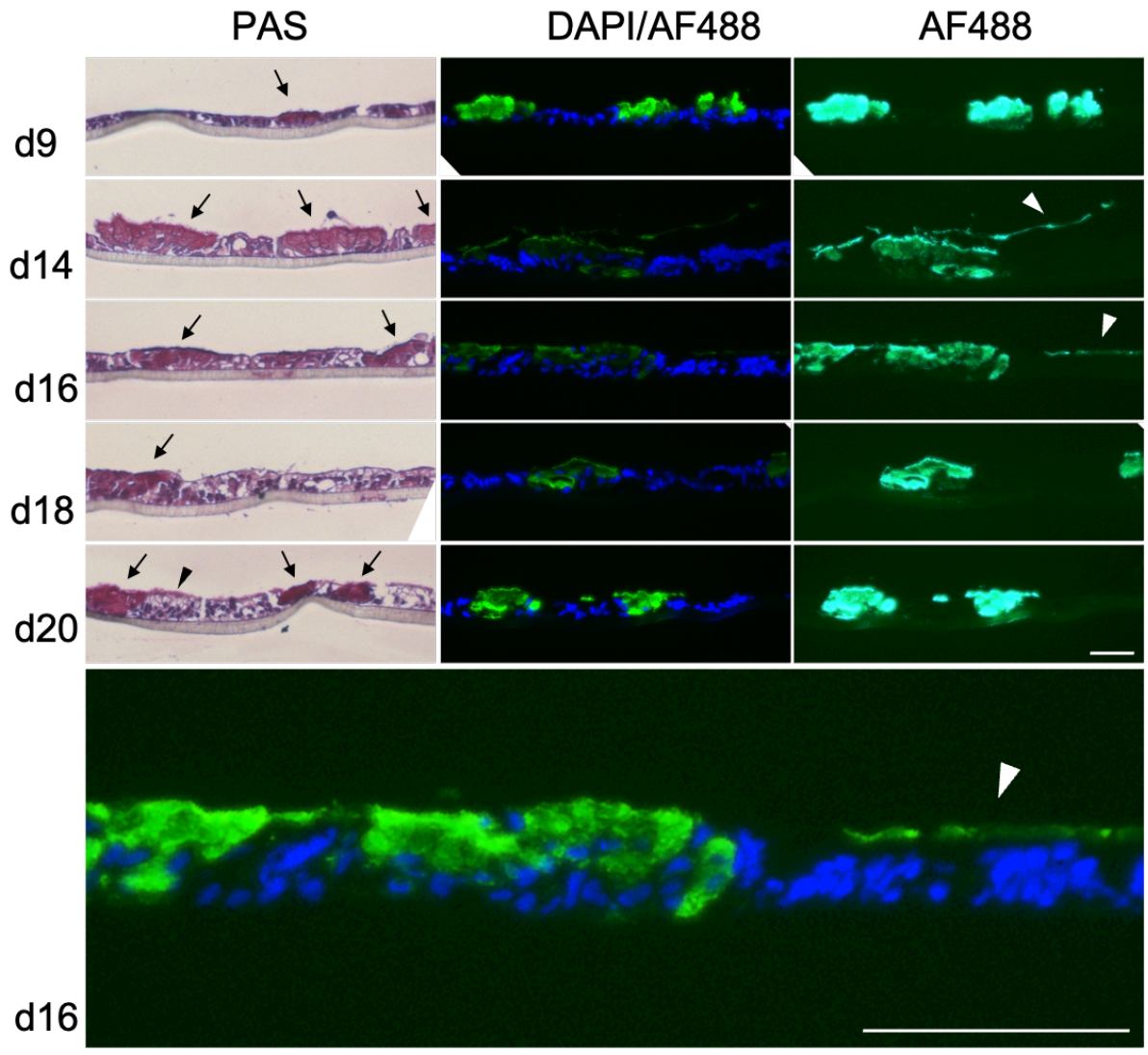

Figure 25 Timecourse for mucus layer formation as detected by PAS staining and MUC-5AC detection on mixed model (Caco-2 / HT29-MTX 9:1 mixture). *A 9:1 mixture of Caco-2 and HT29-MTX cells were seeded onto collagen type IV-coated transwells at a density of 0.4 x 10^5 cells/well and grown for up to 20 days. Fixed, paraffin embedded transwell membranes harbouring epithelia were sectioned and PAS stained (left; red stain), or immunolabeled with monoclonal antibody to MUC-5AC (1:100), detected with AlexaFluor 488 secondary antibodies (green). DAPI / AlexaFluor 488 overlay (middle) and AlexaFluor 488 (right) images were acquired using a 20x Plan Neofluar objective. Bottom panel shows a higher magnification (40x) of day 16 section. Arrows point to the mucus producing cells, arrowheads to the mucus layer stretching over the epithelium beyond the mucus producing cells. Bars = 50μm*

Taken together, these results have shown that we have developed a mature, fully polarized and functioning (barrier) epithelium by day 16 in both models. This will consequently be the starting point for my analysis of the impact of probiotic application which will be described in the following chapters (3.2. and 3.3.).

3.1.5. Lucifer Yellow compromises epithelial cells

As Lucifer Yellow assay (LY) is an alternative way of measuring epithelium integrity, we wanted to assess whether repeated Lucifer Yellow assays could be performed without having a negative effect on cell growth. This would allow us to confirm the TEER data by an independent method. Therefore, transwells were set up and seeded with Caco-2 cells as before.

Before every media change, TEER measurements were taken, before putting half of the transwells back into supplemented DMEM as normal. A LY permeability assay was performed with the other half of the transwells, before putting those back into supplemented DMEM after extensive washing in HBSS buffer to remove any traces of LY. This experiment was stopped after 9 days, as the TEER measurements (Figure 26) clearly showed that repeated exposure to LY has a detrimental effect on epithelial integrity.

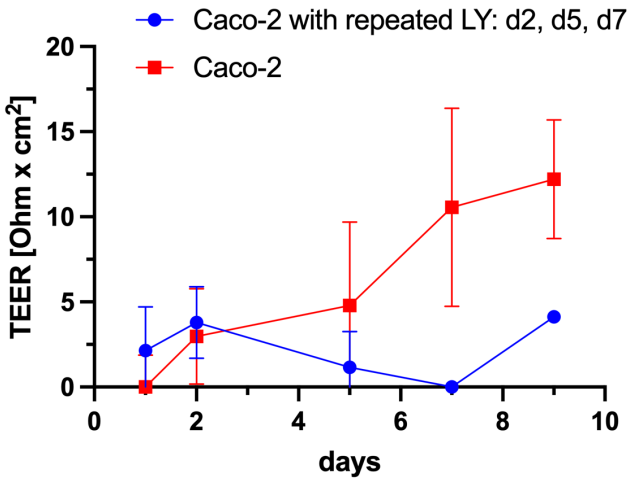

Figure 26 TEER measurements of Caco-2 cells with and without undergoing repeated LY assays. *Caco-2 cells (0.4 x 10^5 cells/well) were seeded onto collagen type IV coated transwells and grown for 9 days. During the media change, TEER was performed on days 2, 5, 7 and 9. One half of transwells also underwent LY assay after TEER measurement on days 2, 5 and 7 (blue data points), whereas the other half did not (red data points) (n = 2).*

Some of the transwells seeded for the pilot co-culture experiments (Figure 21) underwent LY permeability assay on day 21, prior to being fixed and paraffin embedded. H&E staining of sections provided further evidence for a detrimental effect of LY exposure, even when applied to fully mature and polarized epithelia (Figure 27; compare a-c with d-f). It was not possible to establish the exact reason for this observation, but these findings precluded using the LY assay in its current form as a second tool for monitoring epithelial integrity.

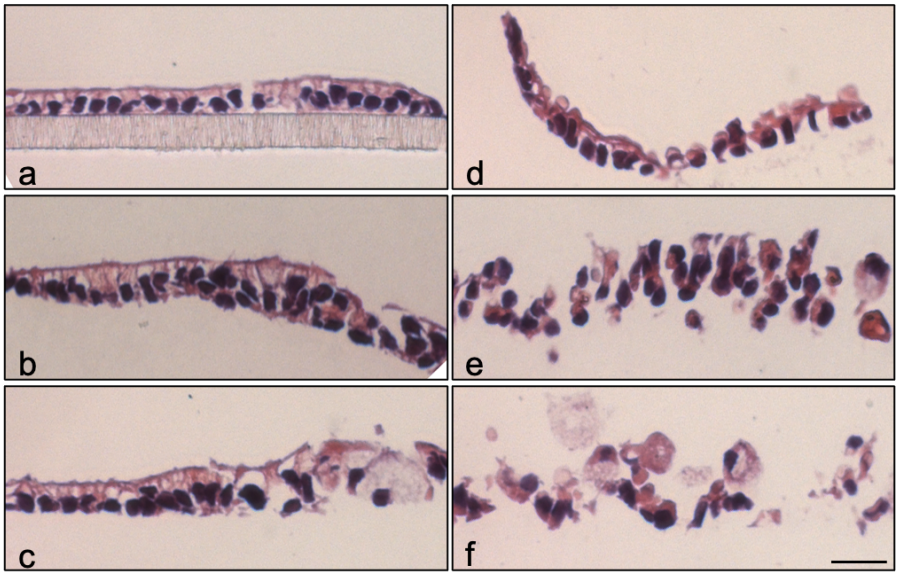

Figure 27 H&E stained sections of epithelia grown on collagen type IV coated transwells with or without LY exposure on day 21. *Cells were seeded onto collagen type IV-coated transwells at a density of 0.4 x 10^5 cells/well, either (a/d) Caco-2 only, (b/e) Caco-2 / HT29-MTX 9:1 mixture, or (c/f) Caco-2 / HT29-MTX 3:1 mixture, and grown for 21 days. Panels a-c: fixed, paraffin embedded, sectioned and H&E stained without LY assay; panels d-f: fixed, paraffin embedded, sectioned and H&E stained after LY assay. Bar = 25μm*

3.2. DISRUPTION OF EPITHELIAL INTEGRITY WITH IL-22

The intestinal mucosa plays a role in both uptake of food-derived nutrients and microbiome-derived metabolites, and as a barrier that prevents tissue invasion by pathogens and dampens inflammatory reactions to luminal contents. How these processes are regulated remains incompletely understood. IL-22 is a key cytokine that is produced by type-3 innate lymphoid cells (ILC3). ILC3 have a central role in regulation of gut immune responses essentially acting as a central conduit for

regulation of immune homeostasis through integrating signals from inflammatory mediators and enteric nervous system and conveying messages to intestinal epithelial and other cells in the lamina propria (Sonnenberg et al., 2011; Talbot et al., 2020). These cells are the only source of IL-22 in the non-inflamed gut, and under homeostatic conditions. ILC3-derived IL-22 has been suggested to have a protective role on the epithelial barrier (Leupold and Wirtz, 2022). IL-22 promotes innate immunity to fungal and bacterial pathogens at this barrier, both in human and mice, in parts through induction of expression of antimicrobial peptides by epithelial cells (Zheng et al., 2008; Sano et al., 2015). However, there is dichotomy in this control as dysregulation of IL-22 signalling contributes to pathology in certain human inflammatory conditions (e.g. IBD, Crohn's disease) as IL-22 contributes to the expression of a range of pro-inflammatory mediators including IL-2, IL-1α, G-CSF and serum amyloid A protein (Sonnenberg et al., 2011; Sano et al., 2015). On the other hand, IL-22 has been reported to promote epithelial regeneration and barrier restoration by modulating mucus layer formation (Sugimoto et al., 2008). Hence, although ILC3 mediated IL-22 signalling has principally a protective function, it can be pathogenic in certain contexts. Local or systemic delivery of exogenous IL-22 has been shown to promote an inflammatory state, and recent data shows that IL-22 signalling can result in enhanced epithelial permeability (Wang et al., 2017; Delbue et al., 2021). Therefore, the aim of this section of my work was to investigate whether exogenous IL-22 application could lead to a reversible "epithelial injury" in my gut models.

To assess whether we could disrupt the epithelial layer by exposure to IL-22 we set up transwell cultures as described before with Caco-2 cells (0.4 x 10^5 cells/well) and grew them for 21 days. TEER measurements were taken before every media change to confirm establishment of a mature epithelium. On day 21, IL-22 was applied to both the apex and basolateral side (10ng/ml IL-22 in supplemented DMEM) for 48h, and IL-22 application was repeated on day 23 for another 48h. The IL-22 concentration was selected based on previous published work (Delbue et al., 2021). On day 25 half the transwell were fixed for histological analysis, and the other half put back onto supplemented DMEM to see if any disruption to the epithelial barrier can recover. The experiment was stopped on day 35, 10 days after termination of the IL-22 insult.

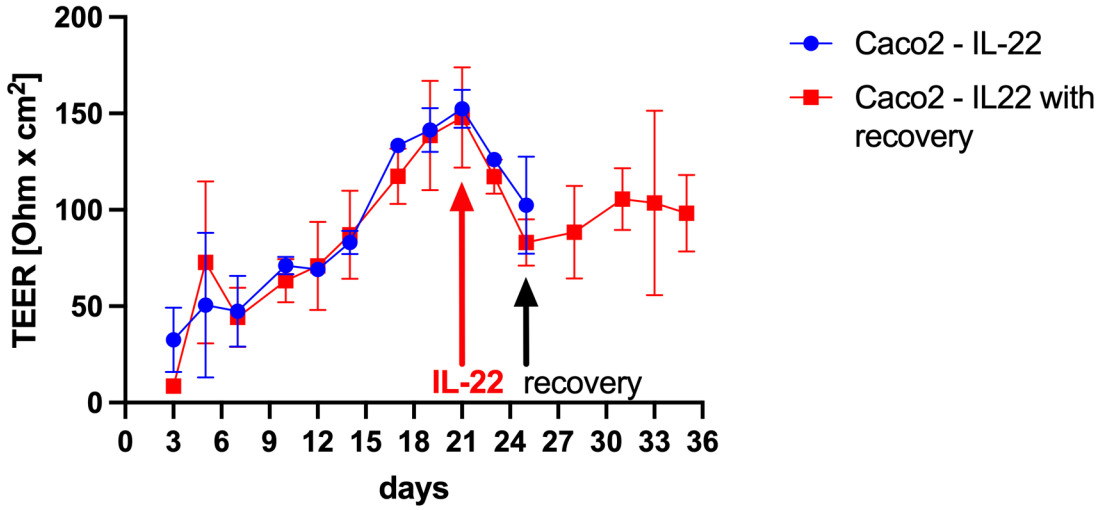

Figure 28 TEER measurements of Caco-2 cells growing on collagen IV-coated PET transwell. *0.4 x 10^5 cells/well were seeded onto collagen type IV-coated transwells and grown to day 21, to establish mature epithelia. IL-22 (10ng/ml) was applied for 4 days (2 x 2 days), and followed by a recovery period for which cells were put back into normal growth medium (n = 3).*

As expected, TEER values increased over the first 21 days, reaching 150 ± 12 Ohm.cm^2 (Figure 28), comparable to previous experiments (Figure 19). IL-22 application reduced the TEER values by an average of 17% after 2 days, and 37% after 4 days incubation. The epithelia were able to partially recover, following cytokine withdrawal, though only reaching 106 ± 11 Ohm.cm^2, equating to 70% of the 21 day peak value. One needs to keep in mind, however, that differentiated epithelia have a finite live span and cell loss may lead to increased permeability over time (Pinto et al., 1983), hence the TEER values might naturally decrease from their peak after such a long time. Histological analysis of sections revealed morphological changes in the epithelia in response to IL-22 treatment, mirroring the enhanced permeability. This data will be discussed as part of the definitive experiments investigating probiotic application in the final Results Chapter (see Figures 31-34).

In an attempt to minimize the overall culture period, a repeat of this experiment was conducted, where I moved the IL-22 application forward to day 18, and applied it only for 3 days with one media change., i.e. on day 18 for 42h and on day 20 for 30h. Figure 29A shows the reduction of TEER values achieved (24% after 2 days, 37% after 3 days). In fact, an average TEER value of 202 ± 2 Ohm.cm^2 at day 18 confirmed that a mature epithelium had been established, that IL-22 application resulted in a

significant reduction in permeability compared to a matched control, and that the Caco-2 epithelium was able to recover in 7 days yielding TEER values at the same level as unstimulated Caco-2 epithelia grown in parallel (Figure 29B). Note, the TEER values decrease after day 28 which may indicate that a plateau has been reached.

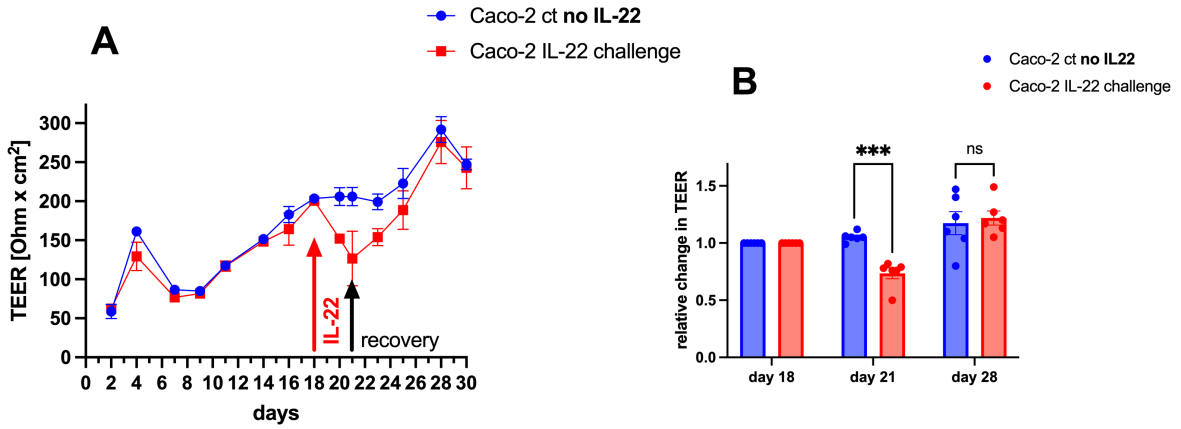

Figure 29 IL-22 treatment reduces epithelial permeability in Caco-2 epithelia in a reversible manner. *TEER measurements of Caco-2 cells growing on collagen IV-coated PET transwells were conducted on indicated days (A). 0.4 x 10^5 cells/well were seeded onto collagen type IV coated transwells and grown to day 18. Then IL-22 was applied for a total of 3 days (red group), and followed by a recovery period for which cells were put back into normal growth medium to recover. Representative graph for 1 out of 3 experiments conducted, with experimental points representing data from duplicates. Summary data from all three experiments for day 18 (mature), day 21 (disrupted) and day 28 (recovered)(B). Data is given as relative change in TEER as absolute values vary from experiment to experiment. Analysis was done using unpaired t-test, p = 0.000187 (n = 6).*

As IL-22 signalling has been shown to directly impact on goblet cell function and consequently the mucus layer covering the epithelium (Sugimoto et al., 2008), it was necessary to investigate whether the epithelial barrier was affected to a similar extent in the presence of mucus producing cells. Hence, the same experiment was performed using the mixed model (Figure 30). IL-22 reduced the TEER values (13 % after 2 days, 20% after 3 days), though to a lesser extent compared to the enterocyte only model. This could be due to the mucus forming a protective layer over the epithelium, specifically Muc-2 and Muc-3, which counteracts epithelial junction disassembly. Alternatively, IL-22 may regulate other molecules involved in cross-talk between enterocytes and mucus-producing cells.

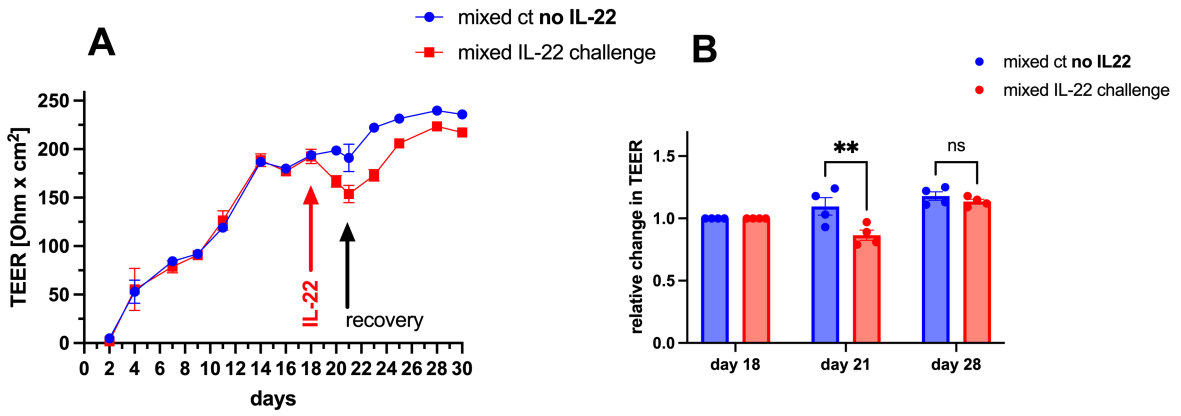

Figure 30 Mixed model epithelium is less sensitive to disruption by Il-22. *TEER measurements of Caco-2 / HT29-MTX mixed epithelia growing on collagen IV-coated PET transwells were conducted on indicated days (A). 0.4 x 10^5 cells/well Caco-2 / HT29-MTX 9:1 mix were seeded onto collagen type IV coated transwells and grown to day 18. Then, IL-22 was applied for a total of 3 days (red group), and followed by a recovery period for which cells were put back into normal growth medium to recover. Representative graph for 1 out of 2 experiments conducted, with experimental points presenting data from duplicates. Summary data from two experiments for day 18 (mature), day 21 (disrupted) and day 28 (recovered)(B). Data is given as relative change in TEER as absolute values vary from experiment to experiment. Analysis was done using unpaired t-test, p = 0.000346 (n = 4).*

Taken together, the data show that a recoverable "inflammatory" state can be induced in the epithelium by IL-22 application which constitutes a physiologically relevant model of gut "injury".

3.3. Effect of probiotics on intestinal barrier

As outlined in the Introduction section, gut microbiota-derived metabolites can have a profound influence on gut health in terms of promoting intestinal barrier integrity and also mucus production, and in protecting against intestinal inflammation (Koh et al., 2016; Torres-Fuentes et al., 2017). These findings have focused interest on the potential use of probiotic bacteria as a means of improving gut health (Staudacher et al., 2017). Species most commonly used as probiotics belong to *Bifidobacterium* spp. and *Lactobacillus* spp. strains. One such formulation that gave encouraging results in human trials is Lab4 produced by Cultech (Pugh et al., 2019). However, the active components of the probiotic formulation and mechanism through which they act, remain to be identified. In order to investigate what effect this Lab4 probiotic formulation has on intestinal barrier integrity and function, Lab4 probiotics were

prepared and fractions generated that are suitable for application in cell culture and may harbour bioactive compounds. A set amount of bacteria constituting an 'effective dose' based on previous investigations (Hill et al., 2014) were grown anaerobically for 5 hours in an appropriate cell culture medium (DMEM), and conditioned media harvested to be applied to our models. This fraction will harbour bacteria derived metabolites. In parallel, another batch of the same bacteria were killed through exposure to 70% ethanol, and the resulting bacteria collected, washed and resuspended in cell culture medium (see Chapter 2.8. for details). This fraction is expected to harbour the dead bacteria, but at the same time to be largely devoid of lipids and other lipophilic organic compounds (metabolites) that are soluble in ethanol. The resulting Lab4 probiotic fractions were applied to the apex of the transwells only, either in the form of conditioned media (Lab4 CM), or ethanol killed bacteria (Lab4 ET), with matching DMEM medium (referred to as DMEM ct) on the basolateral side, and also used for the mock treatment control.

3.3.1. PROBIOTIC APPLICATION PRE IL-22 INSULT

An initial set of experiments evaluated whether application of probiotic fractions had an impact on subsequent pro-inflammatory insult (IL-22). For this, collagen IV-coated PET transwells were seeded with either Caco-2 cells (0.4 x 10^5 cells/well) or a 9:1 mixture of Caco-2 and HT29-MTX cells (total 0.4 x 10^5 cells/well) and grown to day 16 as before. TEER measurements were taken before each media change. As we showed that our epithelium is established by day 16, we applied a single dose of the probiotic treatments on day 16 apically. After 2 days of probiotic treatment, IL-22 (10ng/ml) was applied both apically and basolaterally for 3 days with a media change halfway through. Following inflammatory stimulation, the transwells were put back into the regular supplemented DMEM and grown until day 30 to see if they could recover from the IL-22 insult. Besides the mock treatment control for probiotic application, an additional control group was included, that was not exposed to the IL-22 insult, to account for any spontaneous epithelium deterioration. This later control confirmed that it was feasible to maintain epithelia to at least day 30 (Figure 31 A&D).

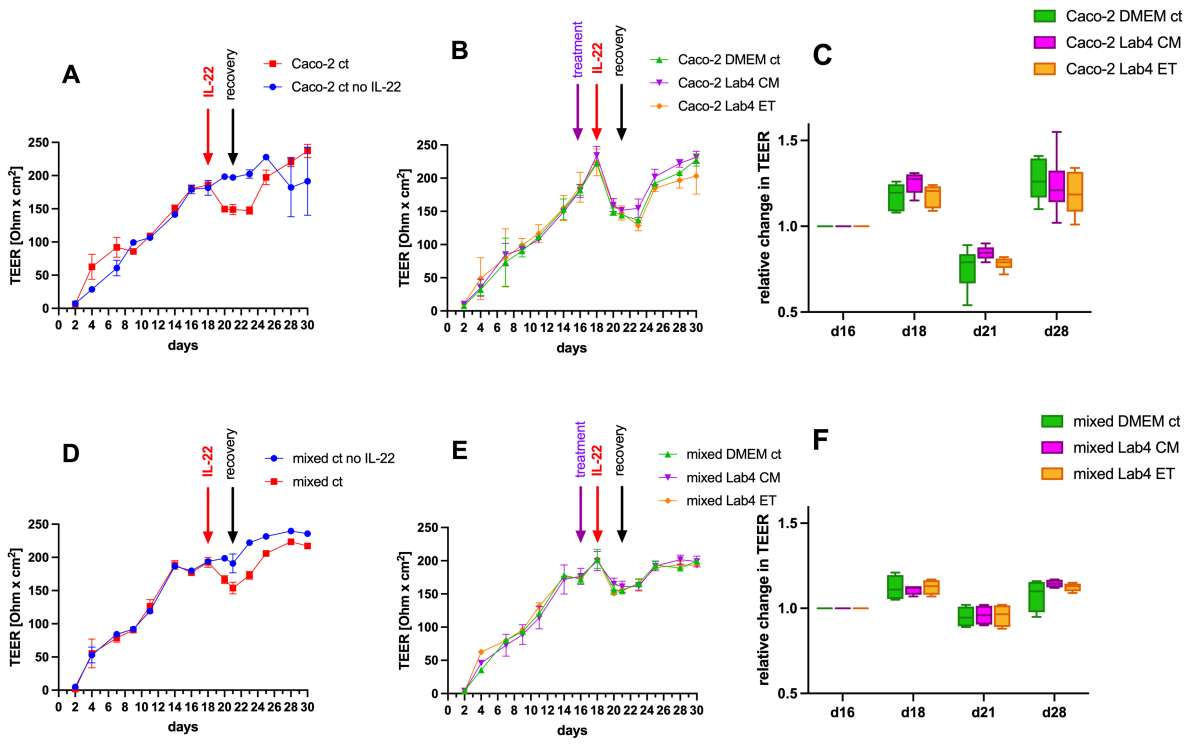

Figure 31 TEER measurements of epithelia undergoing probiotic treatment and IL-22 disruption. *Cells were seeded on collagen IV-coated transwells and epithelia developed as before. Top row: TEER measurements of 3 independent experiments using Caco-2 cells with probiotic treatment on day 16, followed by IL-22 disruption for 3 days and recovery for 9 days. Panel A,B show data from transwells grown in parallel for one representative experiment, with controls (A) and probiotic treatment (B) seprated for clarity. Panel C shows summary data for the 3 experiments at critical points as follows: day 18 – probiotic treated, day 21 – IL-22 stimulated and day 28 – following recovery period. For each transwell, TEER is given relative to its value at day 16 at which point treatment regimen was started. Averaged data is shown in box and whisker format with minimum and maximum indicated. Bottom row: TEER measurements of 2 independent experiments using a 9:1 mixture of Caco-2 and HT29-MTX cells with probiotic treatment on day 16, followed by IL-22 disruption for 3 days and recovery for 9 days. Panels D,E show data for one representative experiment and Panel F the summary data from both experiments as above.*

A small, but consistent improvement in TEER following Lab4 CM application could be observed on day 18 (Figure 31C). Importantly, this difference was even more pronounced on day 21, after 3 days of IL-22 disruption (Figure 31C). Unfortunately, the data did not reach statistical significance (two-way Anova, Lab4 CM vs DMEM control) due to the limited number of replicate data points in each experiment. However, the fact that although small in magnitude, similar differences were consistently observed in all 3 independent experiments, combined with the reduction of data spread for the treated group, suggests, that there is nonetheless likely to be a biologically relevant difference. Clearly, further experimentation with more replicates

will be required to substantiate this notion, but this was not possible within the confines of this project for both time and cost reasons.

Furthermore, we also tested different batches of Lab4 CM to see whether it would affect the apparent but small response we see in TEER (Figure 32A). The data consistently replicated across three independent conditioned media. We also investigated a dilution series of our reference Lab4 CM (Figure 32B). However, no clear dose response could be established, likely due to the fact that any small differences present would be hidden within the experimental variability.

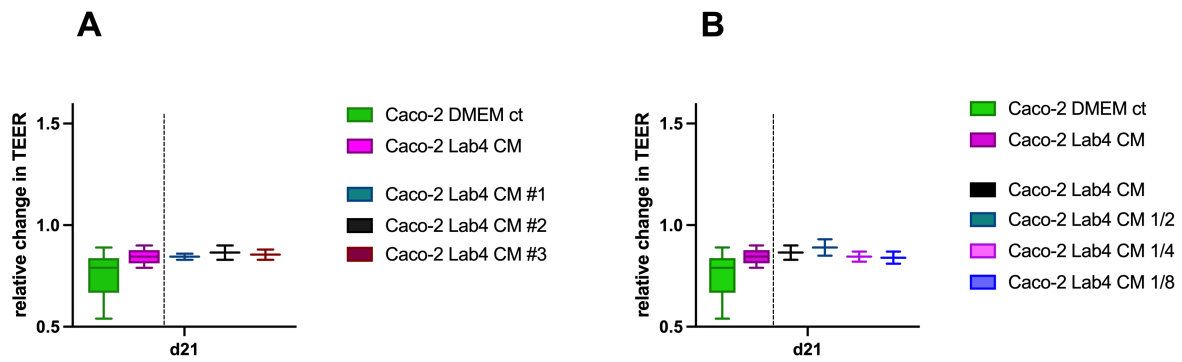

Figure 32 Testing different batches of Lab4 CM confirms protective effect on epithelial integrity. *The experiment outlined in Figure 31 (top row) was repeated but with three independently generated batches of Lab4 CM (A) or with our reference Lab4 CM at different dilutions (B). For simplicity only data for day 21 is shown. The summary data from Figure 31C is shown (left of dotted line) vis-à-vis the additional data from different batches of Lab4 CM (A) or different dilutions of reference Lab4 CM as indicated (B).*

Finally, at the end of the experiment, the transwells were processed for histology. We stained sections from the day 30 transwells for H&E (Figure 33). It is evident, that Caco-2 cells not exposed to IL-22 (Figure 33, left column) appear to be highly organized monolayers of cuboidal epithelial cells, whereas epithelia that have been exposed to IL-22 are a lot less organised and have formed multilayers (Figure 33, middle and right column). This is likely a consequence of epithelial junction remodelling, loss of epithelial cell polarity, increased cell motility and likely also cell proliferation, in line with what has been reported previously in similar experimental settings (Wang et al., 2017; Delbue et al., 2021). With prior exposure to Lab4 CM, the epithelium appears more organised, showing fewer of these changes typically

associated with inflammation, and in some areas mirroring the simple, cuboidal epithelial cell phenotype seen in controls (Figure 33, +Lab4 CM). Thus, there might be a protective effect from probiotic application prior to IL-22 insult, which is consistent with the observed reduction in barrier function loss compared to DMEM control (Figure 31C). Exposure to ethanol killed bacteria does not apparently exert a protective effect, at least not to the same extent (Figure 33, +Lab4 ET).

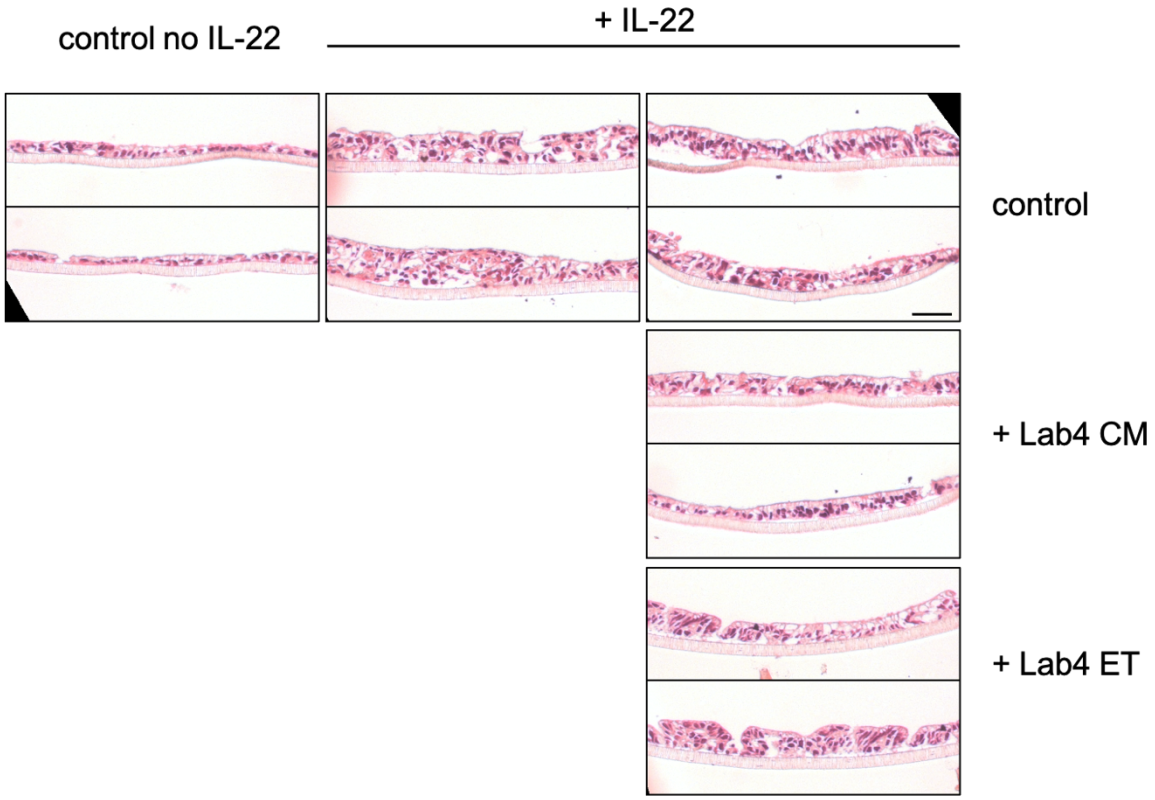

Figure 33 H&E stained sections of Caco-2 epithelia on day 30 with and without probiotic and IL-22 treatment reveal a protective effect of probiotic conditioned medium application. *Caco-2 cells were seeded onto human collagen type IV-coated transwells at a density of 0.4 x 10^5 cells/well and grown for 30 days (see Figure 31). Left column: control without IL-22 exposure. Middle column: control with 3 day IL-22 exposure (d18-d21) followed by 9 days of recovery. Right column: mock treatment control, Lab4 CM or Lab4 ET probiotic treatment for 2 days (d16-d18) prior to 3 day IL-22 exposure (d18-d21) followed by 9 days of recovery. Epithelia were fixed in paraformaldehyde, paraffin embedded, sectioned and stained with H&E. Two representative bright field images are shown for each experimental group. Bar = 50μm.*

To understand the impact of the presence of a mucus layer on the protective effect of probiotic application, a similar set of experiments was conducted with the mixed model (Figure 31 D-F). In line with earlier experiments (Figure 30), the magnitude of change in TEER in response to IL-22 was considerably smaller compared to the Caco-2 only model (15% versus 35% reduction), and in contrast to the Caco-2 only model, no

apparent effect on barrier integrity in response to probiotic pre-treatment could be observed for either of the two fractions (Figure 31F). The fact that neither probiotic application itself (d18) nor the subsequent insult (d21) showed an alteration in TEER between the experimental groups suggests that the mucus layer has a stabilising effect on the epithelium. Further support for this is born out of the histological analysis at the end of the experiment. H&E staining of sections of the mixed cell model on day 30 (Figure 34) shows a more complex epithelium with interspersed islands of mucus producing cells (Figure 34, left column), but also that IL-22 disruption of epithelial architecture is modest (Figure 34, middle & right column) compared to what was previously observed in the Caco-2 only model (Figure 33). No profound changes in epithelial morphology were evident for the experimental groups pre-treated with probiotics (Figure 34, right column).

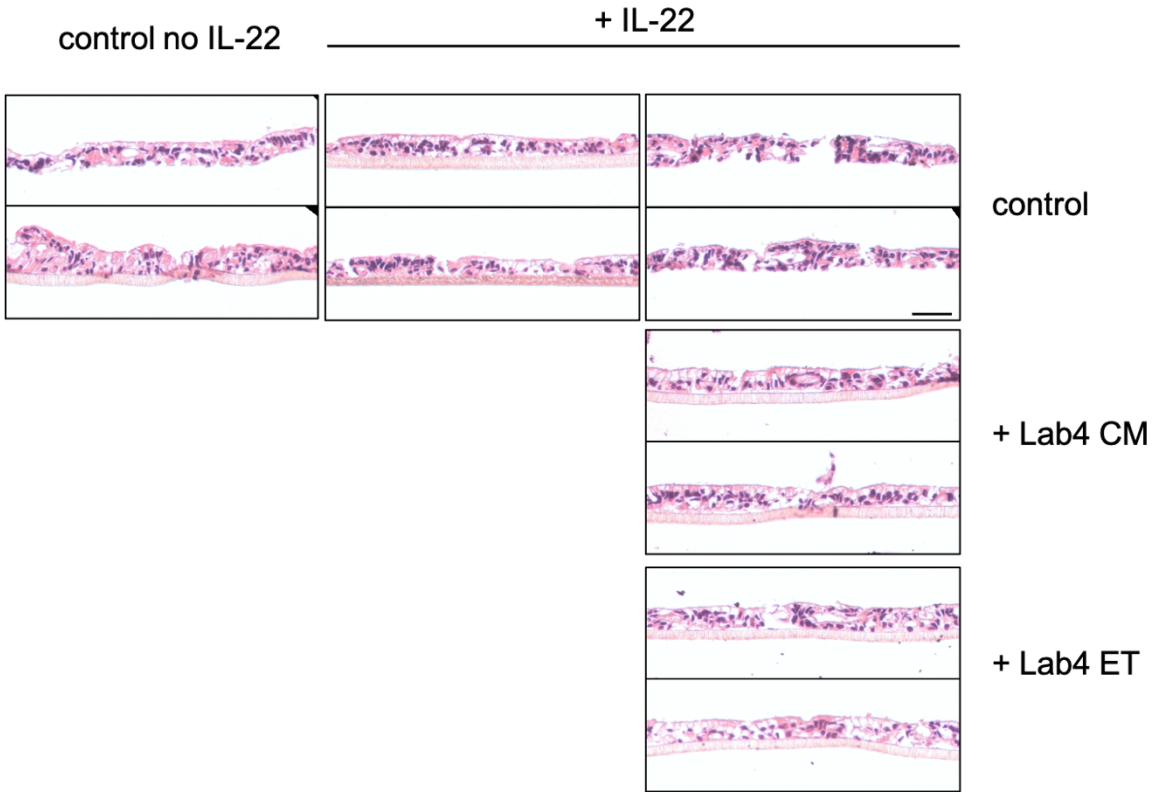

Figure 34 H&E stained sections of mixed epithelia on day 30 with and without probiotic and IL-22 treatment show that presence of mucus producing cells protects epithelia from IL-22 disruption*. A 9:1 mixture of Caco-2 and HT29-MTX cells were seeded onto collagen type IV-coated transwells at a density of 0.4 x 10^5 cells/well and grown for 30 days. Left column: control without IL-22 exposure. Middle column: control with 3 day IL-22 exposure (d18-d21) followed by 9 days recovery. Right column: mock treatment control, Lab4 CM or Lab4 ET probiotic treatment for 2 days (d16-d18) prior to 3 day IL-22 exposure (d18-d21), followed by 9 days recovery. Epithelia were fixed in paraformaldehyde, paraffin embedded, sectioned and stained with H&E. Two representative bright field images are shown for each experimental group. Bar = 50μm.*

Taken together, this suggests that the mucus layer alters the course of epithelial responses to both stabilising and destabilizing signals. This is in line with the literature (Sugimoto et al., 2008; Johansson et al., 2011), but also highlights the importance of taking the mucus layer into consideration when modelling intestinal responses.

As we wanted to look at the morphology of the epithelia at different critical points of these experiments, we repeated these experiments, fixing epithelia at different time points as follows: day 16 (control group), day 18 after probiotics treatment (control and Lab4 CM group) and day 21, after probiotics treatment and IL-22 disruption (control and Lab4 CM group). The fixed membranes were paraffin embedded, sectioned, and stained for H&E, cubilin, villin-1 and MUC-5AC (for mixed model only).

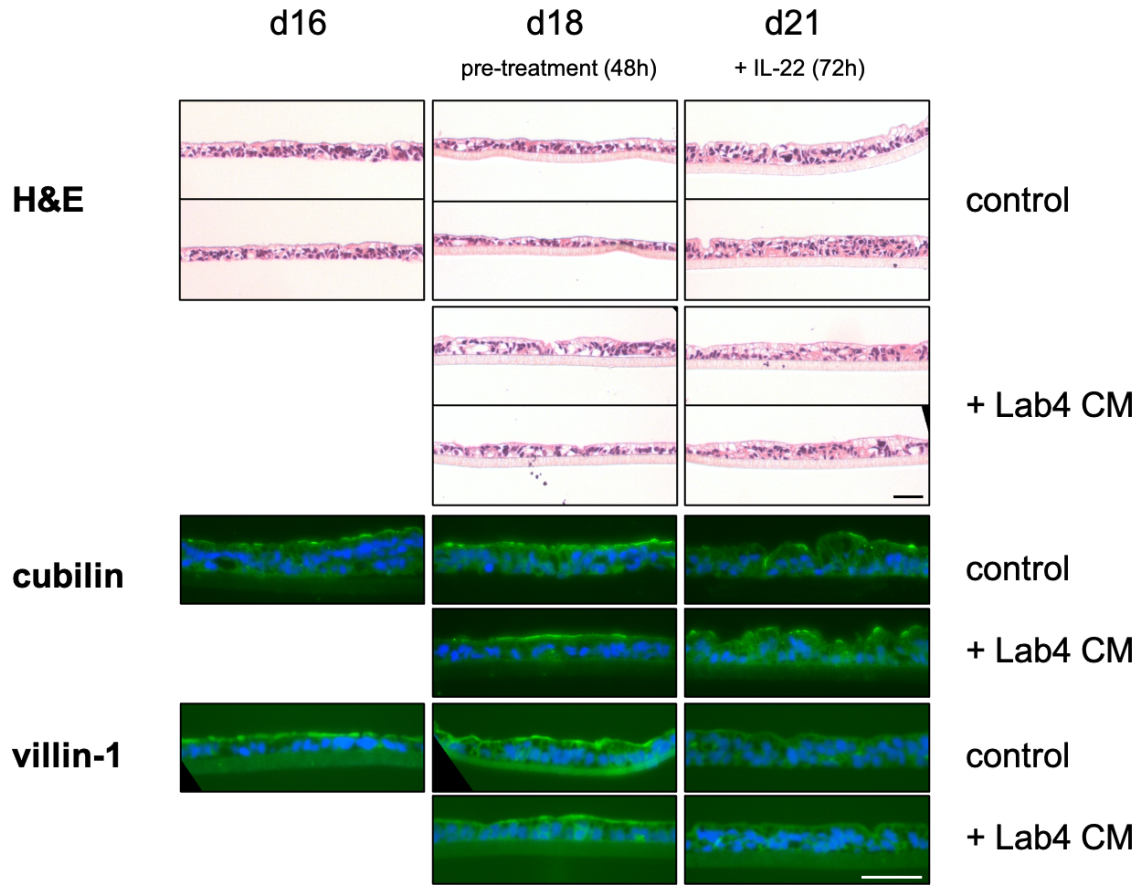

Figure 35 Immunostaining of Caco-2 epithelium for brush border markers cubilin and villin-1 before and after probiotic and IL-22 treatment. *Caco-2 cells were seeded (0.4 x 10^5 cells/well) onto human collagen type IV-coated PET transwells and grown to day 16 (left column). Middle column shows epithelia on day 18 after 2 days exposure to either control medium or probiotics (Lab4 CM), and right column, epithelia on day 21 after a subsequent 3 days exposure to IL-22. At the indicated day, epithelia were fixed in paraformaldehyde, paraffin embedded, sectioned and stained with H&E (two representative bright field images are shown for each experimental group) or immunolabeled with antibodies to cubilin or villin-1 and AlexaFluor 488 conjugated secondary antibodies (sections were counterstained with DAPI to reveal nuclei). Bars = 50μm.*

Figure 35 shows the result for the Caco-2 only model. H&E staining shows again how after 3 days of IL-22 exposure, the control epithelia are disorganised and hyperplastic on day 21, and this 'inflammatory' state appears not to resolve (Figure 33) despite improvement in barrier function (Figure 31C). In contrast, epithelia pre-treated with Lab4 CM appear less proliferative and with far better preservation of normal architecture following IL-22 stimulation (Figure 35, +Lab4 CM). Staining for the apical brush border markers cubilin and villin-1 show, that the cells are polarized on day 16 prior to the treatment, and this remains unaltered on day 18, following probiotic application (Figure 35). However, after the IL-22 insult, cubilin staining is patchy in both control and Lab4 CM treated epithelia, suggesting that receptor expression is reduced and cell polarity at least partially lost. Staining for villin-1 confirms that IL-22 has affected the cell phenotype, as staining for this actin cytoskeleton regulator is drastically reduced by day 21 compared to day 18, both for control and for Lab4 CM treated epithelia. This is in line with the literature. Villin-1 is known to be subject to proteolysis in the context of gut infection and inflammation, and villin-1 expression in intestinal epithelial cells is reduced in IBD, which is characterized by recurring inflammation and associated lesions (Klunder et al., 2016).

Figure 36 shows the analysis of the epithelium for the mixed cell model. No overt changes in the architecture of the epithelium could be observed following either probiotic treatment or IL-22 stimulation (Figure 36, H&E), consistent with the previous end-of-experiment analysis (Figure 34). Despite there being a mucus layer (Figure 36, d16 MUC-5AC), IL-22 stimulation appears to have affected epithelial polarization. Cubilin as well as villin-1 staining are reduced after IL-22 exposure (Figure 36), although not to the extent seen in the Caco-2 only model (Figure 35). Note, that strong villin-1 staining is still present in crypt like structures on day 21, indicating a degree of preservation of normal epithelial architecture. MUC-5AC staining did not reveal any overt qualitative differences in mucus producing cell islands.

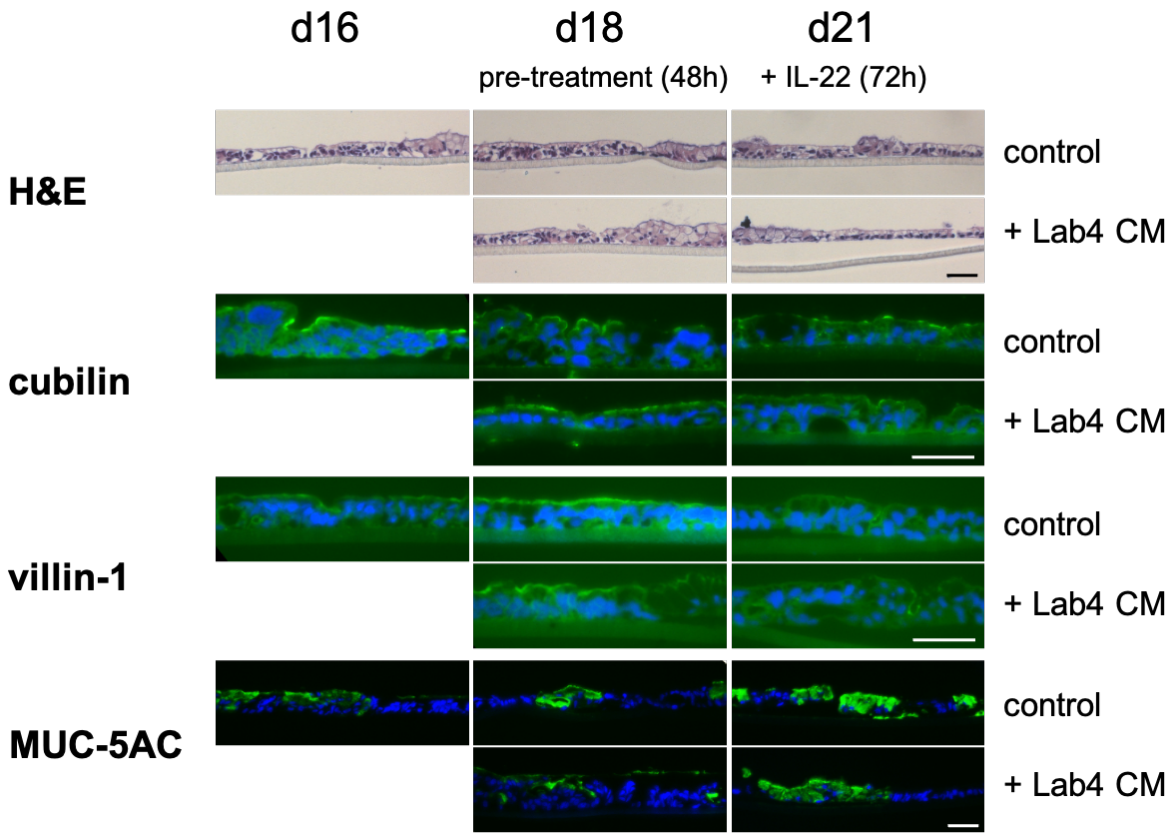

Figure 36 Immunostaining of mixed epithelium for brush border markers cubilin and villin-1 and mucus marker MUC-5AC before and after probiotic and IL-22 treatment. *A 9:1 mixture of Caco-2 and HT29-MTX cells were seeded (0.4 x 10^5 cells/well) onto human collagen type IV-coated PET transwells and grown to day 16 (left column). Middle column shows epithelia on day 18 after 2 days exposure to either control medium or probiotics (Lab4 CM), and right column epithelia on day 21 after a subsequent 3 days exposure to IL-22. At the indicated day, epithelia were fixed in paraformaldehyde, paraffin embedded, sectioned and stained with H&E (two representative bright field images are shown for each experimental group) or immunolabeled with antibodies to cubilin, villin-1 or MUC-5AC and AlexaFluor 488 conjugated secondary antibodies (sections were counterstained with DAPI to reveal nuclei). Bars = 50μm.*

3.3.2. Probiotic application after IL-22 insult

We also wanted to assess whether probiotics have an effect on the recovery of IL-22 disrupted epithelium. Therefore, in a second set of experiments, we applied probiotics immediately following the IL-22 insult to understand whether this could alter the course of epithelial barrier re-establishment (Figure 37). For this, mature epithelia were generated as before, with TEER measurements taken before every media change to monitor barrier establishment. On day 18, we disrupted the epithelia by adding IL-22 (10ng/ml) both apically and basolaterally for 3 days with a media change halfway through. On day 21, we applied the probiotic treatment to the apical side only for 2

days, with matching DMEM on the basolateral side. After that we put the cells back into supplemented DMEM to let them recover for an additional 7 days.

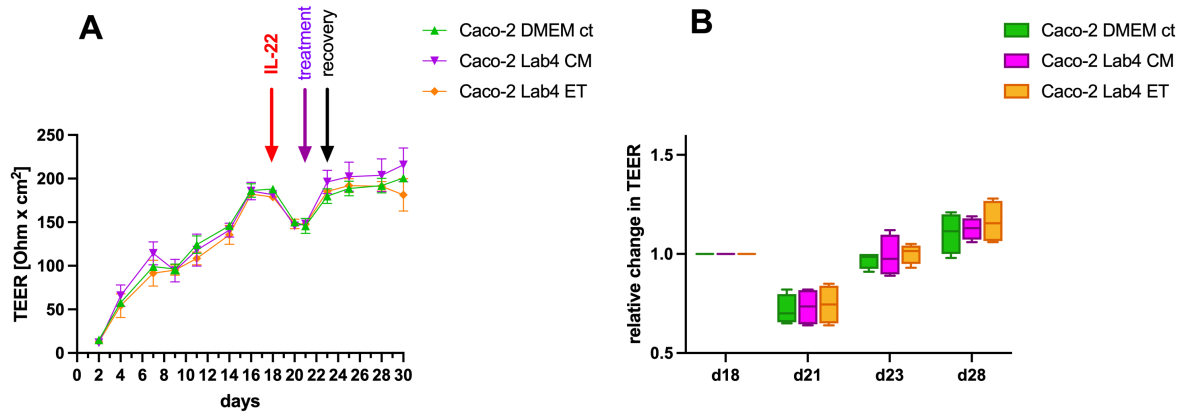

Figure 37 TEER measurements of epithelia undergoing probiotic treatment after IL-22 disruption. *Caco-2 cells were seeded on collagen IV-coated transwells and epithelia developed as before. Panel A shows TEER measurements of one representative experiment with IL-22 stimulation on day 18 for 3 days, followed by Lab4 CM or Lab4 ET probiotic or mock treatment for 2 days as indicated, and finally recovery for 7 days thereafter. Two independent experiments were conducted, and panel B shows the summary data of these at critical points as follows: day 21 – IL-22 stimulated, day 23 – probiotic or mock treated, and day 28 – following recovery period. For each transwell, TEER is given relative to its value at day 18 at which point treatment regimen was started. Averaged data is shown in box and whisker format with minimum and maximum indicated.*

TEER measurements for Caco-2 cell epithelial model (Figure 37B) or mixed cell model (data not shown) did not show any clear indication for a difference between controls and Lab4 probiotic treated cells. We also investigated the architecture of epithelia in H&E stained sections from day 30 (at the end of the experiment) to compare whether we can see any differences between the treatment groups (Figure 38 and 39). As in previous experiments, IL-22 was shown to promote a hyperplastic state in the epithelium, with patches of proliferative and disorganized epithelium interspersed into areas of near normal appearing epithelium. This was not substantially altered by probiotic application in either the Caco-2 only or the mixed cell model, and no clear differences were evident between the different treatment groups at the end of the recovery period.

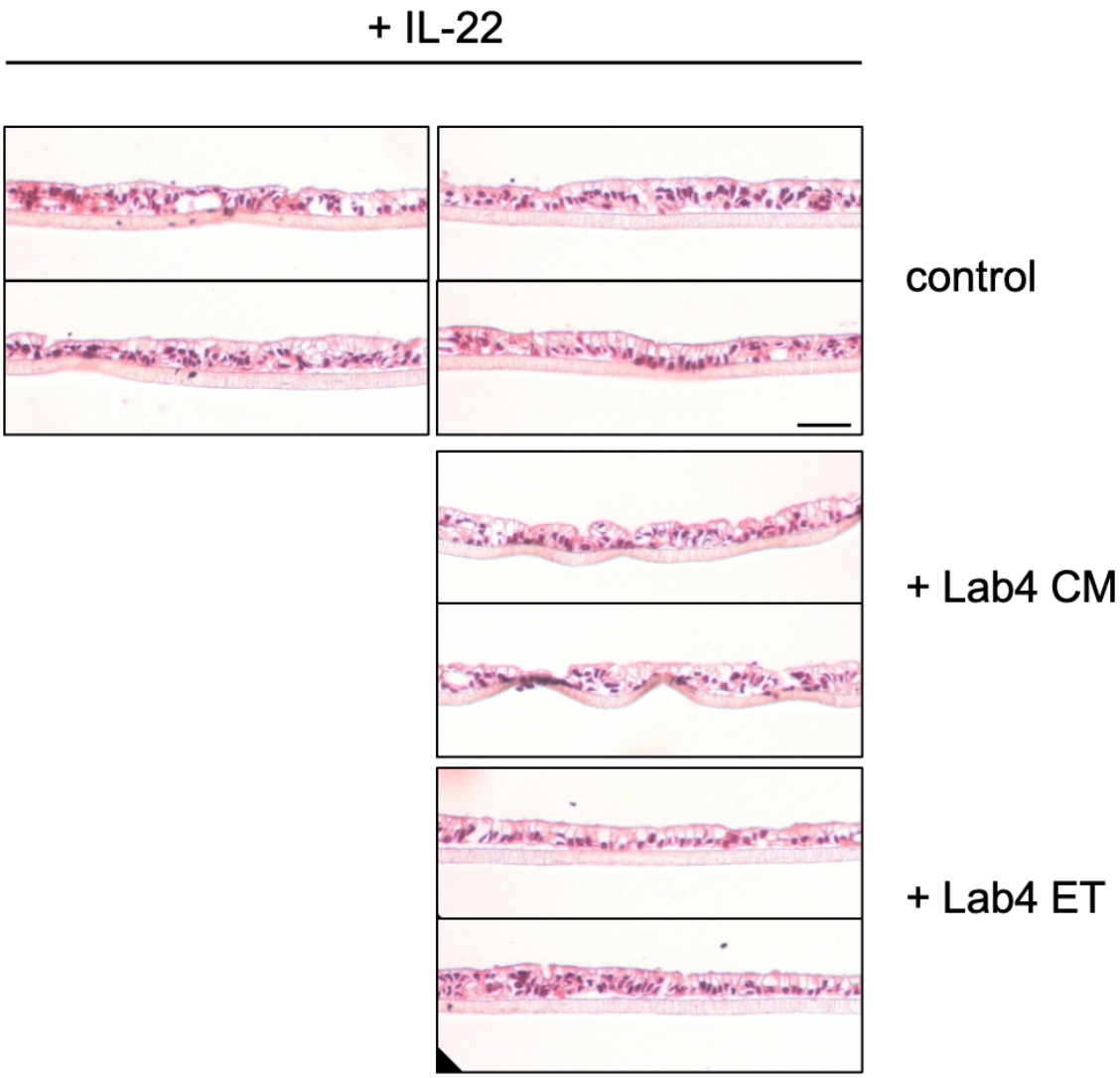

Figure 38 H&E stained sections of Caco-2 epithelia on day 30 after disruption by IL-22 and subsequent probiotic treatment. *Caco-2 cells were seeded onto human collagen type IV-coated transwells at a density of 0.4 x 10^5 cells/well and grown for 30 days (see Figure 37). Left column: control with 3 day IL-22 exposure (d18-d21), followed by 9 days recovery. Right column: mock treatment control and Lab4 CM or ET probiotic treatment for 2 days (d21-d23) directly after 3 day IL-22 exposure and subsequent 7 days recovery. Epithelia were fixed in paraformaldehyde, paraffin embedded, sectioned and stained with H&E. Two representative bright field images are shown for each experimental group. Bar = 50μm*

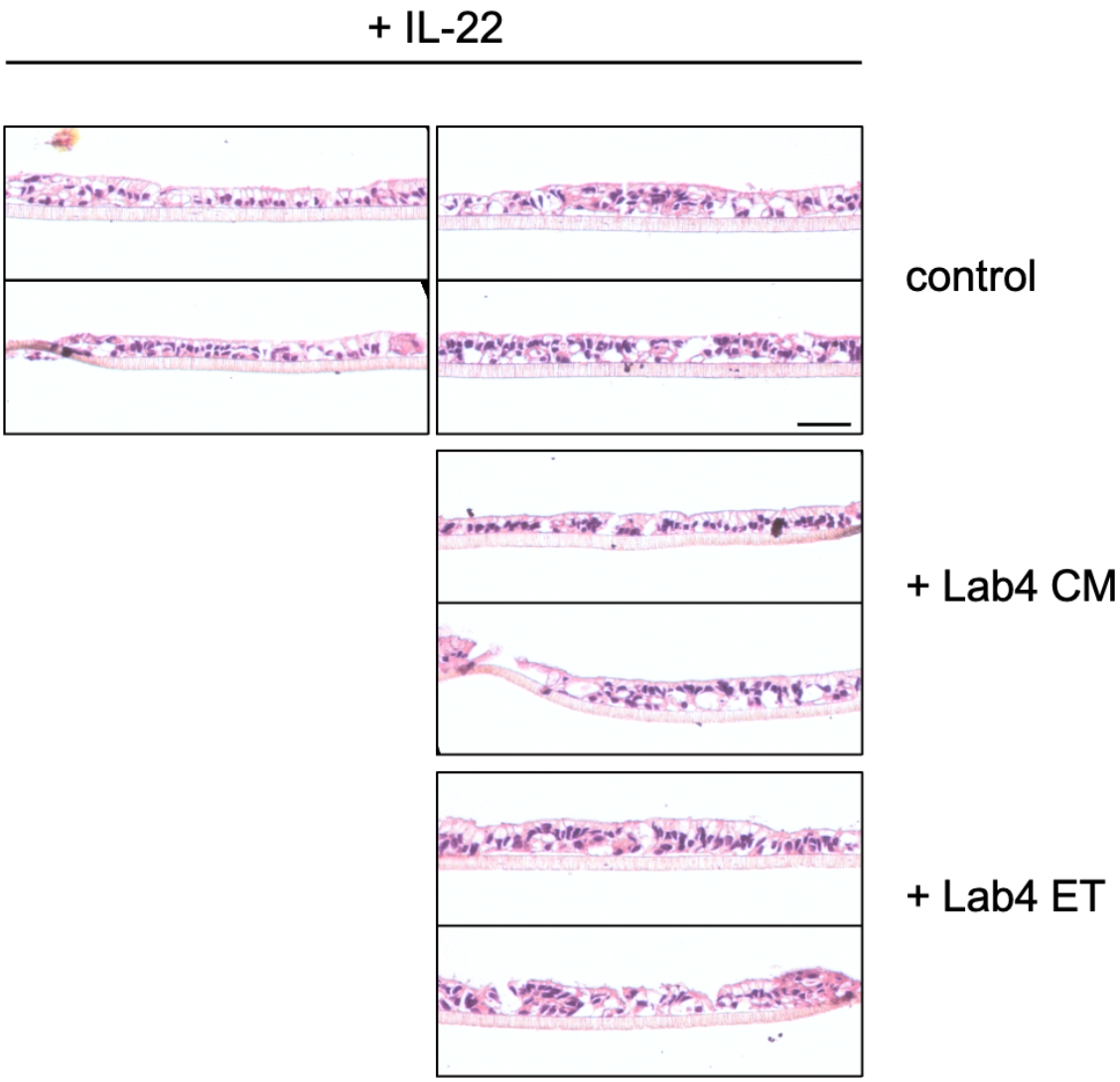

Figure 39 H&E stained sections of mixed cell epithelia on day 30 after disruption by IL-22 and subsequent probiotic treatment. *A 9:1 mixture of Caco-2 and HT29-MTX cells were seeded onto collagen type IV-coated transwells at a density of 0.4 x 10^5 cells/well and grown for 30 days. Left column: control with 3 day IL-22 exposure (d18-d21) and 9 days recovery. Right column: mock treated control and Lab4 CM or ET probiotic treatment for 2 days (d21-d23) directly after 3 day IL-22 exposure and subsequent 7 days recovery. Epithelia were fixed in paraformaldehyde, paraffin embedded, sectioned and stained with H&E. Two representative bright field images are shown for each experimental group. Bar = 50μm*

3.4. IL-22 MEDIATED EPITHELIAL RESPONSES

As the results in the preceding section demonstrated that pre-treatment of the epithelium with Lab4 CM modulated the subsequent response to IL-22, understanding the mechanism underpinning this finding became the focus of the ongoing work. As already discussed in section 3.2, IL-22 signalling has profound effects on the intestinal epithelium (Sonnenberg et al., 2011; Delbue et al., 2021), and does not just affect the

enterocytes, but also the mucus producing cells. It has also been shown that HT29 cells, which are used in my mixed model express IL-22 receptor (Zheng et al., 2008). IL-22 triggers a host of distinct responses, which can be broadly grouped into host defense, tissue protection, inflammation and tissue repair. Firstly, IL-22-induced STAT3 signalling mediates induction of the acute phase response (CXCL1, SAA1/2), alongside proliferation, and protection from cell death (Liang et al., 2010; Sano et al., 2015). Secondly, it triggers expression of effector molecules (β-defensins, REGβIII and REGγIII) of innate immunity (Zheng et al., 2008), and thirdly, secretion of pro-inflammatory and pro-angiogenic mediators, such as IL-6, IL-8, TNFα. Furthermore, IL-22 also directly regulates mucin expression (e.g. MUC3) and hence, contributes to formation of the protective mucus layer covering the cells lining the intestine (Lang and Pelaseyed, 2022). However, IL-22 does not only induce mediators of immunity and inflammation, but has profound effects on the epithelium itself through a complex reprogramming of epithelial cells that alters tight junction structure (Wang et al., 2017) and induces enzymes, that are involved in cell migration and tissue remodelling (e.g. matrix metalloprotease-1 and -3), resulting in a loss of cell polarity, increase motility and potentially epithelial-mesenchymal cell transition (Delbue et al., 2021), the later being characterized by expression of the transcription factors SNAI1 and SNAI2 (Delbue et al., 2021).

We decided, therefore, to decipher which aspects of the IL-22 mediated response are modulated by probiotic treatment as a first step towards gaining a mechanistic understanding. We selected representative genes within the above outlined broad categories and set out to investigate whether their expression is altered in response to treatment with probiotics (either conditioned medium harvested from live bacteria or ethanol killed bacteria). The selection of gene products was as follows:

1. mediators of inflammation - TNFα, IL-6, S100A8

2. acute phase response - SAA1/2

3. anti-microbial peptides - REGγIII

4. mucus layer synthesis – MUC-3A

5. state of adherence junctions - claudin 2

6. epithelial-mesenchymal transition – SNAI2

Primers were designed and tested, as described in Section 2.9.3. TNFα and SNAI2 have previously been investigated by our group, and the respective gene expression assays were already optimized for use. For an initial test of the newly designed primers, RNA isolated from an appropriate transwell sample (day 19 control with IL-22 exposure) was reverse-transcribed and used to set up test PCR reactions with the new primer sets. The resulting PCR products were analysed by running in a 1% agarose gel containing ethidium bromide (Figure 40). SAA1/2, claudin 2, SOCS3 and MUC-3A yielded a band of expected size, whereas S100A8 and REGγIII did not. This could be because the primer pair was either not efficiently amplifying the correct product or due to the fact that the gene of interest was not expressed under the conditions analysed. There was unfortunately no time to investigate this further due to my project coming to an end, and we had therefore to leave those 2 assays out of our further investigation.

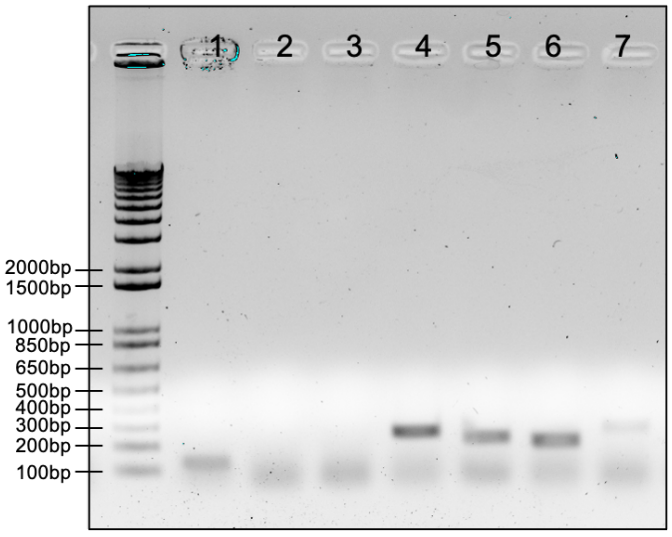

Figure 40 Agarose-gel analysis of PCR reactions for target genes from IL-22 stimulated Caco-2 cells. *RNA was isolated from Caco-2 only epithelium following 24h stimulation with IL-22 (transwell, day 19) and reverse transcribed. PCR was conducted over 50 cycles with indicated primer sets and products separated in 1% agarose gel calibrated with 1kb ladder (ethidium bromide stained) from left to right: 1kb ladder, (1) h36B4 [129bp; housekeeping gene], (2) S100A8 [126bp], (3) REGγIII [243bp], (4) claudin 2 [245bp], (5) SAA1/2 [219bp], (6) SOCS3 [202bp], (7) MUC-3A [269bp].*

3.4.1. CHANGES IN EXPRESSION OF INFLAMMATORY MEDIATORS

IL-22 can act on intestinal epithelial cells either luminally or basolaterally (Wang et al., 2017). As the IL-22 receptors reside predominantly at the basolateral side in a polarized epithelium (Sonnenberg et al., 2011; Onyiah and Colgan, 2016), we would expect to see different magnitudes of response depending on whether the IL-22 stimulus is applied luminally or basolaterally. Nevertheless, as either situation may present itself physiologically, we decided to carry out the following experiments in two ways: i. epithelia were grown in collagen IV-coated wells of 24-well plates and subsequently stimulated with IL-22, representing a scenario of stimulation from the apical side only, and ii. epithelia grown on transwells were stimulated both apically and basolaterally with IL-22 following our standard protocol. RNA was isolated on day 16 (mature epithelium), following treatment with probiotics (day 18), as well as after an additional 24h stimulation with IL-22 (day 19). QPCR reactions for genes of interest were set up according to Section 2.9.2. using either TaqMan (TNFα) or SybrGreen (all others) methods, and results expressed as fold change using the $\Delta\Delta$Ct method, whereby the respective $2^{-\Delta\Delta Ct}$ value for each treatment condition was calculated in relation to the day 16 control. h36B4 was used as the housekeeping gene for normalization, based on its well established robust constitutive expression (Wagener et al., 2001).

Figure 41 shows the QPCR results for the inflammatory cytokine TNFα (top row) and acute response protein serum amyloid SAA 1/2 (bottom row). The 2 graphs on the left show the gene expression changes for Caco-2 only (A,E) and mixed cell (B,F) epithelia on transwells, respectively, where IL-22 stimulation was applied from the top and bottom of the epithelia. The 2 graphs on the right show the results for Caco-2 only (C,G) and mixed cell (D,H) epithelia grown on plates, where IL-22 was only applied apically and is not expected to have direct access to the IL-22 receptors that are located at the basolateral side of the polarized epithelia.

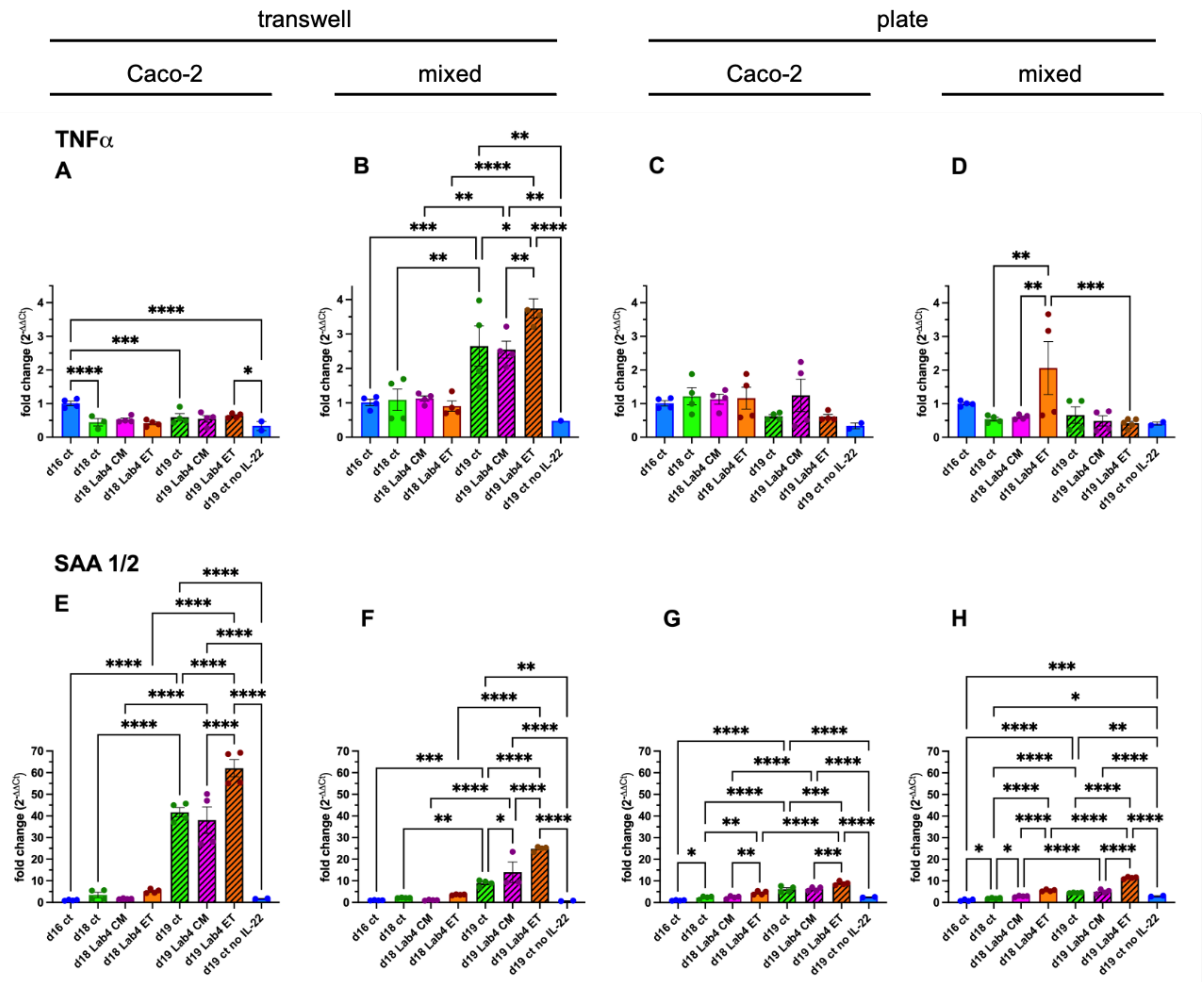

Figure 41 QPCR analysis for inflammatory mediators*. Caco-2 cell (A,C,E,G) or mixed cell (B,D,F,G) epithelia were established in transwells (A,B,E,F) or 24-well plates (C,D,F,G) over a 16 day period. Epithelia were then treated with probiotics (Lab4 CM or Lab4 ET) for 48h or left untreated (ct), followed by stimulation with IL-22 for 24h. RNA was isolated from epithelia before (d16) and after (d18) probiotic treatment, and following stimulation with IL-22 (d19), and mRNA transcripts for TNFα and SAA1/2 were quantified by QPCR. Data is expressed as fold change in relation to the day 16 control and was calculated using the ΔΔCt method. Top row: TNFα ; Bottom row: SAA1/2 ; left to right: Caco-2 transwells, Mixed model transwells; Caco-2 plate; Mixed model plate. Statistical analysis was done using one-way Anova with Fisher's LSD as post-hoc test; based on 2 independent experiments with duplicates.*

Low levels of TNFα mRNA were detectable, but no obvious change in response to treatments was observed for TNFα expression for cells grown on plates (top stimulation only) in either Caco-2 or the mixed model (Figure 41C,D), nor for transwells (dual stimulation) in our Caco-2 model (Figure 41A). In the mixed model, on the other hand, a robust response to IL-22 stimulation (~ 2.5-fold upregulation) could be observed for cells grown on transwells, when stimulated both apically and basolaterally (Figure 41B). The respective response may be greater in the ET treated cells compared to the other groups.

For SAA1/2, we observed a very robust induction by IL-22 in all groups as expected (Figure 41, bottom row). The response was much greater in transwells (dual stimulation) (Figure 41E,F) than on plates (apical stimulation only) (Figure 41G,H). We can conclude from this, that the primary driver of SAA1/2 induction was the basolateral stimulation. Furthermore, the response in Caco-2 only cells was of much greater magnitude (~20-fold increase) (Figure 41E), compared to the mixed model (~7-fold increase) (Figure 41F). Treatment with conditioned probiotic media (Lab4 CM) did not appear to be different from controls, but treatment with ethanol killed probiotic bacteria (Lab4 ET) enhanced the IL-22 response in all cases by almost 2-fold (Figure 41E-H). Interestingly, ET treatment itself prior to the IL-22 insult increased the SAA1/2 expression about 2-fold also (Figure 41E-H, d18). This might be suggestive of activation of a pathway other than STAT3, possibly toll-like receptors, which acts synergistically to STAT3 signalling.

Taken together, the data confirms that basolateral IL-22 has an overriding role in driving the immune defense response. The response is unaltered by pre-treatment with Lab4 bacteria-derived metabolites (Lab4 CM), but enhanced after exposure to ethanol killed bacteria (Lab4 ET). Importantly, it also revealed differences in the pattern of pro-inflammatory signals between Caco-2 epithelia (SAA1/2 induction only) and mixed cell epithelia (SAA1/2 induction of lower magnitude, TNFα induction) which would have a bearing on the nature of the immune response.

3.4.2. CHANGES IN EXPRESSION OF MARKERS CHARACTERISING EPITHELIAL PHENOTYPE / RESPONSES

Figure 42 shows the results for the transcription factor SNAI2 (top row), the tight junction protein claudin 2 (middle) and the mucus layer component MUC-3A (bottom row), markers which provide insights on barrier function and the state of the epithelium itself. Again, the two figures to the left represent the results from transwells (A,B,E-H), where IL-22 stimulation was done apically and basolaterally. For SNAI2, this experiment was also performed on cells grown on plates with only apical IL-22 stimulation (Figure 42C,D).

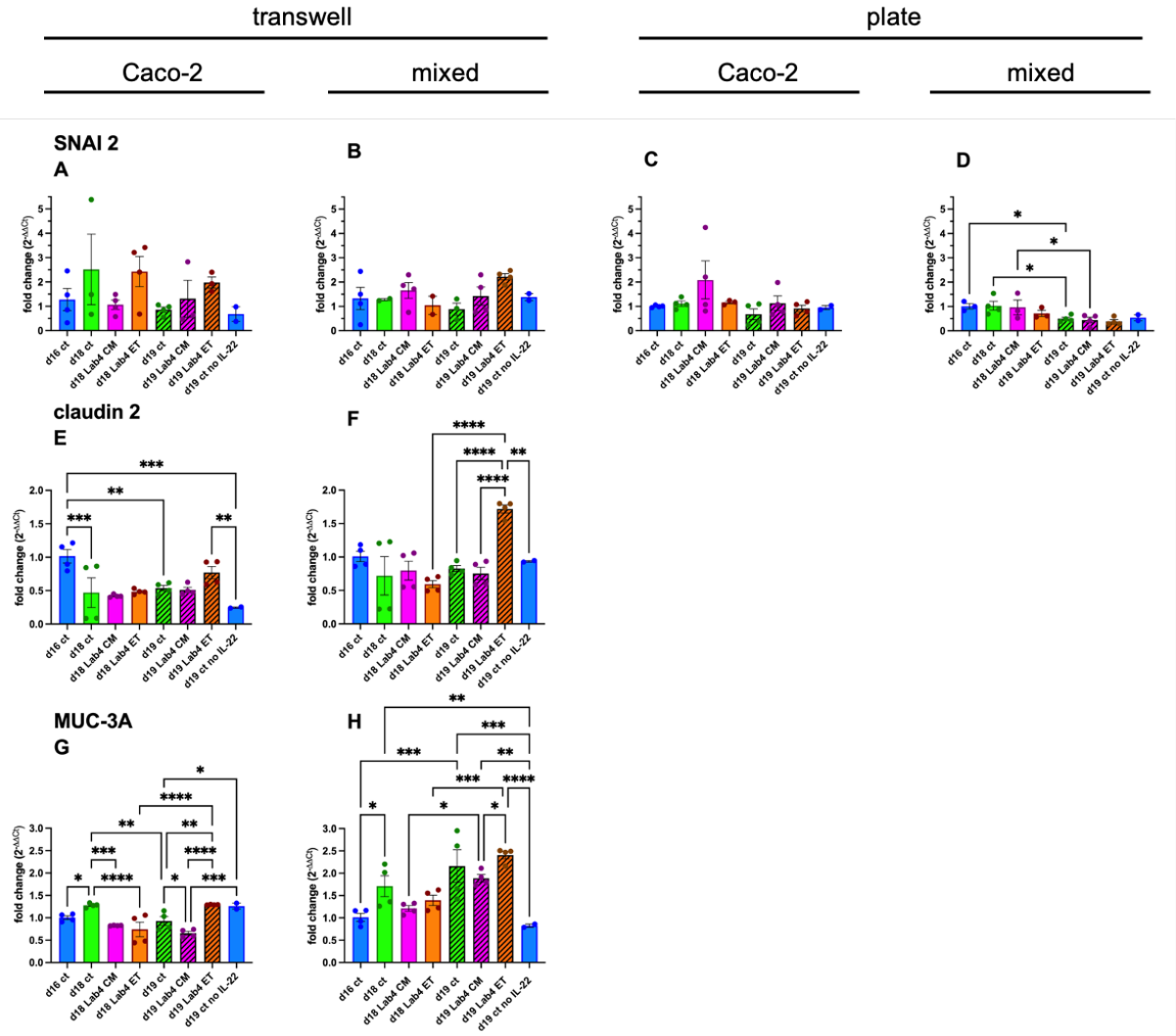

Figure 42 QPCR analysis for markers characterising epithelial phenotype. *Caco-2 cell (A,C,E,G) or mixed cell (B,D,F,H) epithelia were established in transwells (A,B,E,F,G,H) or 24-well plates (C,D) over a 16 day period. Epithelia were then treated with probiotics (Lab4 CM or Lab4 ET) for 48h or left untreated (ct), followed by stimulation with IL-22 for 24h. RNA was isolated from epithelia before (d16) and after (d18) probiotic treatment, and following stimulation with IL-22 (d19), and mRNA transcripts for SNAI2, claudin 2 and MUC-3A were quantified by QPCR. Data is expressed as fold change in relation to the day 16 control and was calculated using the ΔΔCt method. Top row: SNAI2; Middle row: claudin 2; Bottom row: MUC3A; left to right: Caco-2 transwells, Mixed model transwells; Caco-2 plate; Mixed model plate. Statistical analysis was done using one-way Anova with Fisher's LSD as post-hoc test; based on 2 independent experiments with duplicates.*

Epithelial-mesenchymal transition of cells is typically driven by Notch signalling-mediated SNAI2 activation. In an experimental setting similar to ours, IL-22 stimulation has recently been reported to upregulate SNAI2 and drive epithelial-mesenchymal transition (Delbue et al., 2021). We did not observe any responses considered biologically relevant in regards to SNAI2 expression with top only IL-22 application (Figure 42C,D). For cells grown on transwells, there was an apparent small induction of SNAI2 expression in response to IL-22 in the Lab4 ET pretreated group (~1.5-2-

fold; not statistically significant due to variability) (Figure 42A,B), but no changes in expression were observed for any of the other conditions analysed. However, given the variability in some of the data, further experiments would have to be conducted to substantiate this finding.

IL-22 induced upregulation of claudin 2 expression has been linked to increased epithelial permeability (Wang et al., 2017). Figure 42 (middle row) shows the results of our analysis of claudin 2 expression in epithelia grown on transwells. Interestingly, the expression of claudin 2 is upregulated (~2-fold) in both the Caco-2 and the mixed cell model after IL-22 stimulation for the Lab4 ET treatment group only (Figure 42E,F). This suggests that the respective probiotic treatment synergistically affects IL-22 mediated STAT3 signalling, in line with our previous observation (see Figure 41). This notion is further confirmed by enhanced SOCS3 expression in Lab4 ET treated samples (Figure 47). Note also, that in our models, IL-22 did not alter claudin 2 expression in either control or Lab4 CM treated samples, nor did the probiotic treatment themselves impact on claudin 2 expression.

Finally, Figure 42 (bottom row) shows the expression of the mucin MUC-3A which is produced by enterocytes. The difficulty in analysing expression of specific mucins lays in their extensive sequence similarity. Nevertheless, a recent report showed that although derived from the *MUC3* gene that is part of the *MUC3-MUC12-MUC17* gene cluster, isoform (MUC-3A) selective expression data can be obtained (Lang and Pelaseyed, 2022), and a modified version of this approach was used here. Overall, the changes in MUC-3A expression in our experimental models were modest. For mixed cell transwells, a small induction (~1.5-fold) with IL-22 stimulation could be observed for probiotic treated and untreated groups (Figure 42H), but no similar response was seen in Caco-2 only transwells, although expression was marginally higher in the Lab4 ET treated group (Figure 42G).

Although a number of important observations were made in these studies analysing marker expression, none of the findings directly provided an explanation or “read-out” for the biological activity linked previously to the Lab4 CM fraction. To address this, we decided to turn out attention to the intracellular signalling events following IL-22 receptor activation.

3.5. Impact of Probiotics on intracellular signalling mediated by IL-22

Activation of IL-22 receptor (IL22Rα1/IL10Rβ) by its ligand can lead to signalling through different intracellular pathways: the core pathway being the STAT3 signalling pathway. However, it can also signal via the MAPK (ERK1/2) pathway or the AKT-mTOR pathway in some cellular contexts. Previous experiments with intestinal epithelial cells in a similar set-up to the one used here have shown, that IL-22 is not activating AKT (Delbue et al., 2021). I, therefore, focussed my investigation on whether STAT3 or ERK1/2 activation is altered by probiotic treatment.

We therefore set up cultures in both transwells and plates as before to extract proteins for IL-22 signalling analysis (see Section 2.10.1.). Caco-2 cells or a 9:1 mixture of Caco-2 and HT29-MTX cells were seeded onto collagen IV-coated inserts or wells, respectively, and grown to day 16, with TEER measurements performed in transwell cultures before every medium change to confirm that epithelia reached the desired state of maturity. On day 16, half the wells were treated with the Lab4 CM probiotic fraction, with the other half receiving matched control medium for 2 days. On day 18, IL-22 was added to all wells as previously described (both apically and basolaterally for transwells), and the cells were extracted at various time points as follows: 0h (no IL-22), 15min, 30min, 1h, 4h, 8h, and 24h. The protein concentration in the extracts was determined using the BCA assay, and a set amount of protein was separated in a 4-20% Tris-glycine SDS-PAGE gel and subsequently transferred to a nitrocellulose membrane. The membrane was probed sequentially with antibodies against pSTAT3, STAT3, and GAPDH as a loading control.

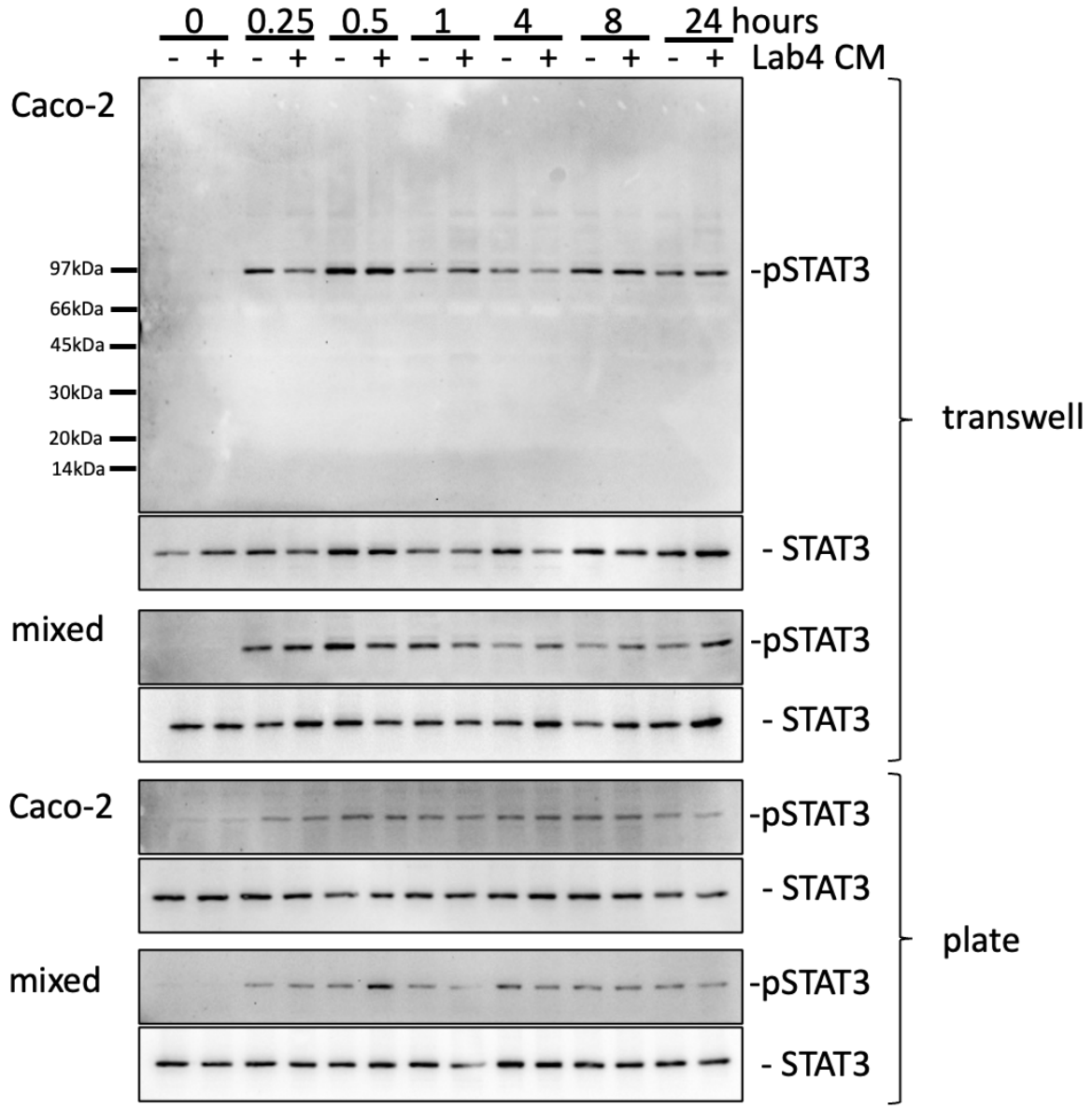

Figure 45 Western blotting for pSTAT3 in Caco-2 and mixed epithelia grown on either transwells or on plates confirms STAT pathway activation by IL-22. *Caco-2 cell or mixed cell epithelia were established in transwells or 24-well plates over a 16 day period. Epithelia were then treated with probiotics (+Lab4 CM) for 48h or left untreated (-Lab4 CM), followed by stimulation with IL-22 for 0, 0.25, 0.5, 1, 4, 8 or 24h. Protein was extracted from epithelia following stimulation with IL-22, and an equal amount separated in 4-20% SDS-PAGE gels. Western blots were probed with specific antibodies for pTyr^{705}STAT3 and STAT3. Picture shows a representative immunoblot for each experimental condition, with the top membrane shown in full to demonstrate specificity. For loading control see Appendix E.*

The immunoblots showed a single band of expected size (86kDa) for pSTAT3/STAT3 (Figure 45). IL-22 induced rapid phosphorylation of STAT3 at Tyr^{705} first detected at 15min in our experiment and peaking around 30min, and STAT3 remained phosphorylated for the duration of the stimulation period under all conditions investigated. In order to further dissect whether differences in the level of STAT3

activation were present, Western blots from multiple experiments (n=2) were analysed by densitometry. Figure 46 shows the extracted quantitative data as a plot of relative degree of STAT3 phosphorylation versus time of IL-22 stimulation, with left panel showing the comparison between mock treatment control and Lab4 probiotics treatment (Lab4 CM). The panel on the right shows the mock treated cells as a bar graph, with appropriate statistical evaluation. Panels A and B show results from cells grown on transwells, where IL-22 treatment was applied on both apex and basolaterally, and panels C and D the results from cells grown on plates with apical IL-22 stimulation. Once again, it is obvious, that the magnitude of the response is far greater in cells where IL-22 stimulation was applied on the basolateral side (Figure 46A,B). Nevertheless, in all cases we can see that the highest degree of STAT3 phosphorylation was at 30min of IL-22 exposure (Figure 46, compare A,B with C,D), surprisingly indicating that timing of activation is unaltered, perhaps indicating that IL-22 is recognized by receptors present at the apical surface, and not after translocation to the basolateral compartment. No differences in either timing or magnitude of STAT3 activation were observed between control and probiotic treated cells in the Caco-2 model (Figure 46A,C). The activation of STAT3 in Lab4 CM-treated cells was significantly lower in magnitude in the mixed cell transwell model at 15 and 30min (Figure 46B; $p=0.0002$), but no differences were seen between probiotic treated and untreated mixed cell epithelia following apical IL-22 stimulation (Figure 46D).

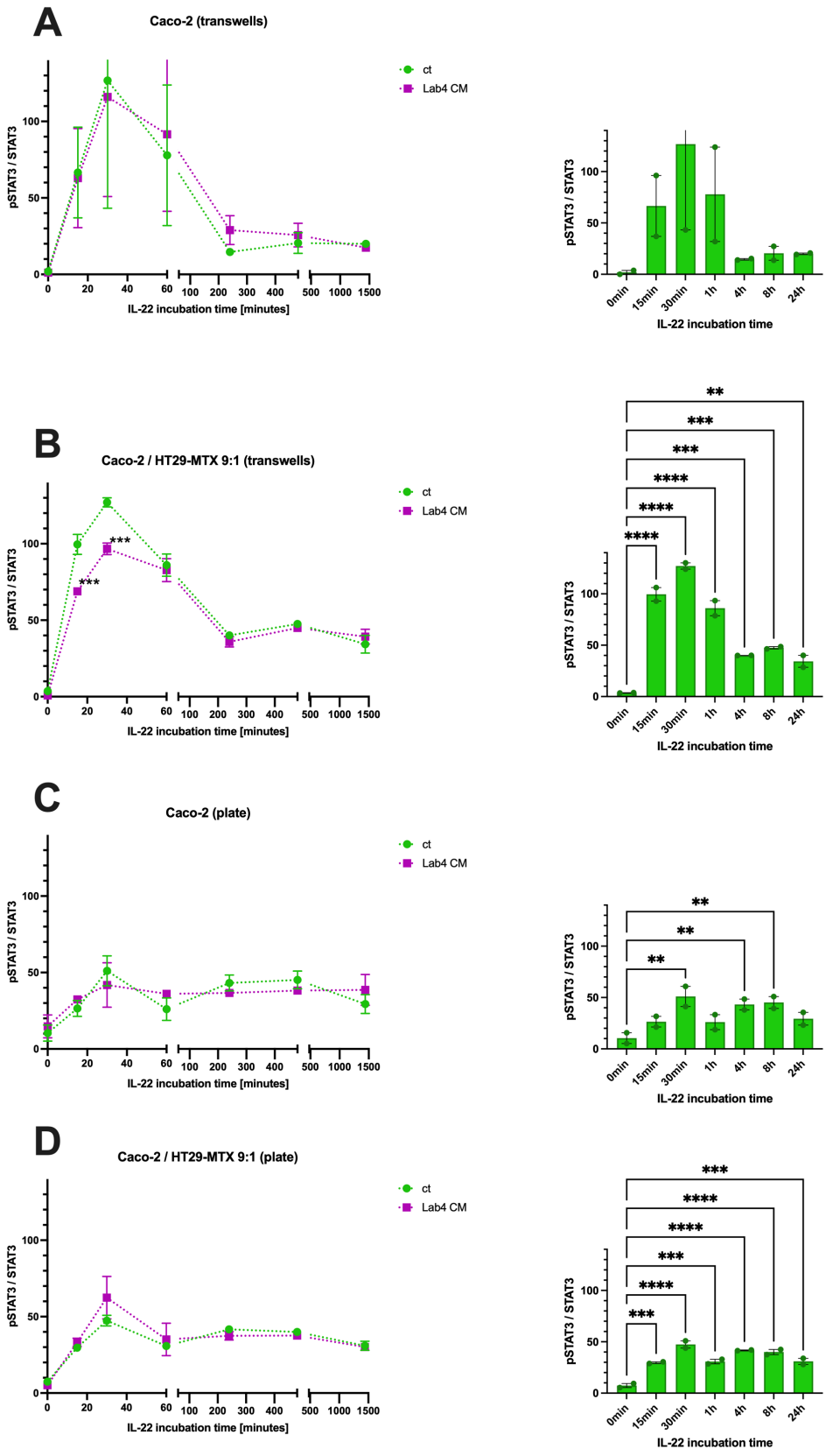

Figure 46 Analysis of STAT3 activation status in Caco-2 (A,B) and mixed (B,D) epithelia grown on either transwells (A,B) or on plates (C,D) following IL-22 stimulation*. Data from Western blots of two independent experiments (see Figure 45) was quantified using densitometry. Data was analysed for significant differences using two-way ANOVA with Fisher's LSD as post-hoc test (left panel), or one-way Anova with Fisher's LSD as post-hoc test (right panel).*

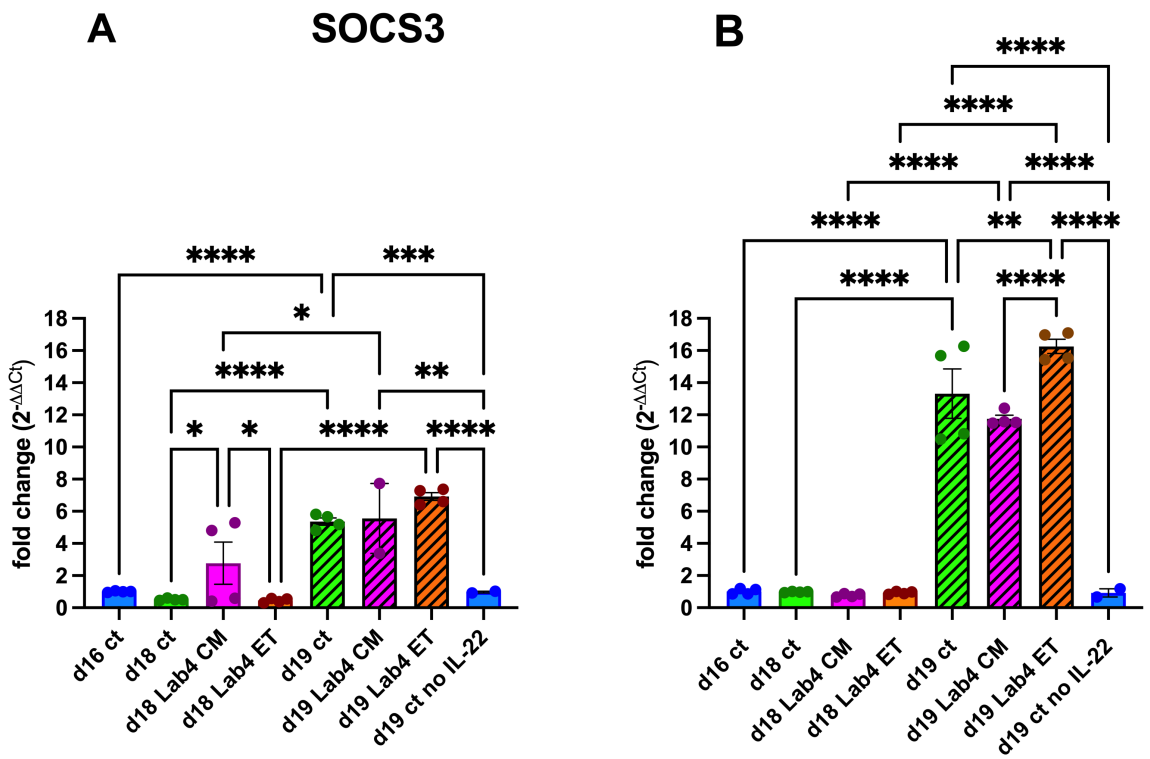

Figure 47 QPCR for SOCS3 expression in Caco-2 and mixed cell epithelia grown on transwells revealed enhanced JAK-STAT3 signalling in response to Lab4 ET pre-treatment. *Caco-2 cell (A) or mixed cell (B) epithelia were established in transwells over a 16 day period. Epithelia were then treated with probiotics (Lab4 CM or Lab4 ET) for 48h or left untreated (ct), followed by stimulation with IL-22 for 24h. RNA was isolated from epithelia before (d16) and after (d18) probiotic treatment, and following stimulation with IL-22 (d19), and mRNA transcripts for SOCS3 were quantified by QPCR. Data is expressed as fold change in relation to the day 16 control and was calculated using the ΔΔCt method. Results were evaluated for significance of differences between experimental groups, as relevant, using one-way Anova with Fisher's LSD as post-hoc test.*

Tight control of the JAK-STAT pathway is necessary to avoid the detrimental consequences of a pathological overstimulation. The suppressor of cytokine signalling-3 (SOCS3) is a feedback inhibitor of the JAK-STAT3 pathway that acts by preventing Janus kinase (JAK) activation or mediating degradation of the cytokine receptor through ubiquitination (Gao et al., 2018). Activation of IL10-family cytokine receptors drives rapid upregulation of SOCS3 which is part of the mechanism for termination of signalling. We therefore investigated SOCS3 expression in our transwell models using QPCR as a second approach to monitoring IL-22 receptor activation. Figure 47 shows a robust SOCS3 induction by IL-22 as expected, with stronger response in mixed cell epithelia (B) compared to Caco-2 only epithelia (A). This is consistent with differences we have seen in target gene expression (Figure 42). Once again, exposure of epithelia to ethanol killed bacteria (Lab4 ET) prior to the IL-22 insult appears to affect the SOCS3 response, i.e. increasing it by about 1.4-fold. Again, this

correlated with changes seen in target gene expression (Figure 42) and also enhanced induction of pro-inflammatory mediators (Figure 41), suggesting that these differences may relate to veracity of JAK-STAT3 pathway activation. No consistent effect on JAK-STAT3 signalling could be detected for Lab4 CM application to epithelia prior to IL-22 stimulation (Figure 47). However, given the comparably large variability in the respective data for Caco-2 only epithelia, repeating this experiment would be necessary to unequivocally clarify this point, but this was not possible within the time constraints of this project.

JAK-STAT3 signalling plays a central role in mediating intestinal cell responses to IL-22. Nevertheless, recent studies have identified that not STAT3, but only ERK1/2 signalling drives proliferation in response to IL-22, for example in human colonic epithelial cells (Moniruzzuman et al., 2019). p90RSK (ribosomal S6 family kinase) and c-Jun appear to be the downstream transcriptional mediators responsible for ERK1/2-dependent IL-22 mediated cell proliferation (Moniruzzuman et al., 2019). Firstly, p90RSK is known to be a downstream effector of MAP kinases and has a critical role in cell survival by regulating cell cycle checkpoints. Secondly, activation of c-Jun links to AP-1, a dimeric transcription factor known to regulate cell proliferation through inhibition of p16 and p21 and induction of cyclin D1. Histological analysis of our models stimulated with IL-22 provided clear evidence for a proliferative response by the epithelial cells (Figure 33 and 34). It was therefore imperative to consider the possible contribution of ERK1/2-mediated signalling to the biological responses seen in our models. Western blotting for the active 42/44kDa form of the kinase (pERK1/2), phosphorylated in activation loop (Thr^{202}/Tyr^{204}), was conducted on the extracts previously generated for analysis of STAT signalling. This revealed a complex and context dependent pattern of ERK activation (Figure 48). Firstly, the delayed induction of ERK activation previously reported (Delbue et al., 2021) was seen in epithelia on plate wells (apical stimulation only), but not those on transwells (Figure 48; Figure 49, compare C,D with A,B). Maximal activation in apically stimulated cells was seen in the 4h and 8h time points, in line with the literature (Delbue et al., 2021), and this pattern of activation was not altered through pre-treatment with probiotic (Lab4 CM) prior to IL-22 stimulation (Figure 49C,D). For transwells (apical and basolateral stimulation), peak ERK activation coincided with STAT3 signalling at 15-30min, but was of lesser

magnitude compared to epithelia with only apical stimulation (Figure 48, Figure 49A,B). Importantly, in epithelia on transwells, pre-treatment with Lab4 CM profoundly altered the pattern of ERK activation (Figure 49A,B). Not only was this apparent ERK induction of greater magnitude compared to controls, but it was also delayed. Interestingly, the timing of ERK activation differed between Caco-2 only (8-24h) and mixed cell (1-4h) epithelia (Figure 49A,B), and this finding may explain why Lab4 pre-treatment improved epithelial barrier function in Caco-2 only epithelia (Figure 31C) but not in mixed cell epithelia (Figure 31F).

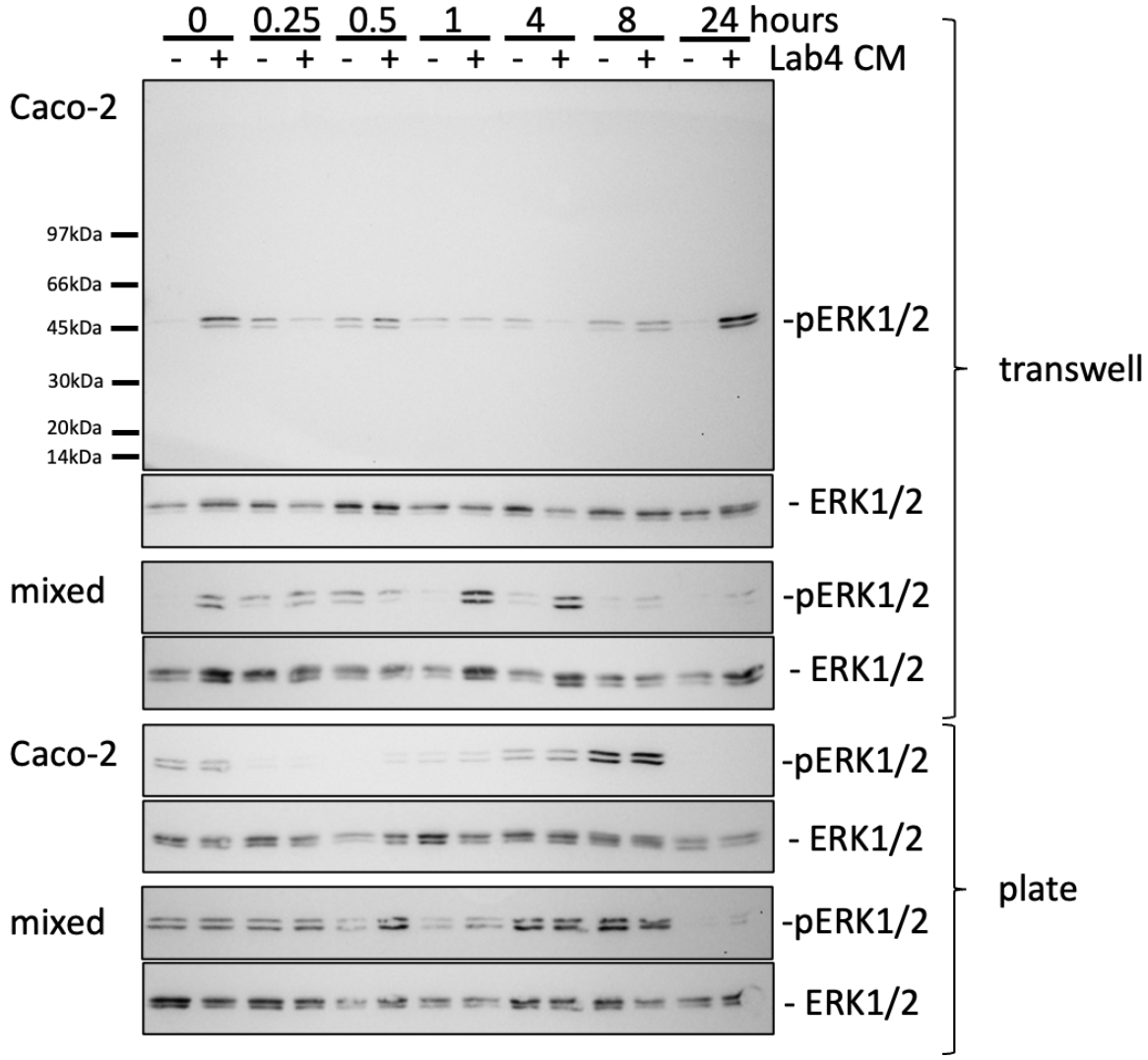

Figure 48 Western blotting for pERK1/2 in Caco-2 and mixed epithelia grown on either transwells or on plates reveals a context dependent pattern of IL-22-mediated MAPK signalling that is altered by probiotic application. *Caco-2 cell or mixed cell epithelia were established in transwells or 24-well plates over a 16 day period. Epithelia were then treated with probiotics (+Lab4 CM) for 48h or left untreated (-Lab4 CM), followed by stimulation with IL-22, and an equal amount separated in 4-20% SDS-PAGE gels. Western blots were probed with specific antibodies for pThr^{202}/Tyr^{204}ERK1/2 and ERK1/2. Picture shows a representative immunoblot for each experimental condition, with the top membrane shown in full to demonstrate specificity. For loading control see Appendix F.*

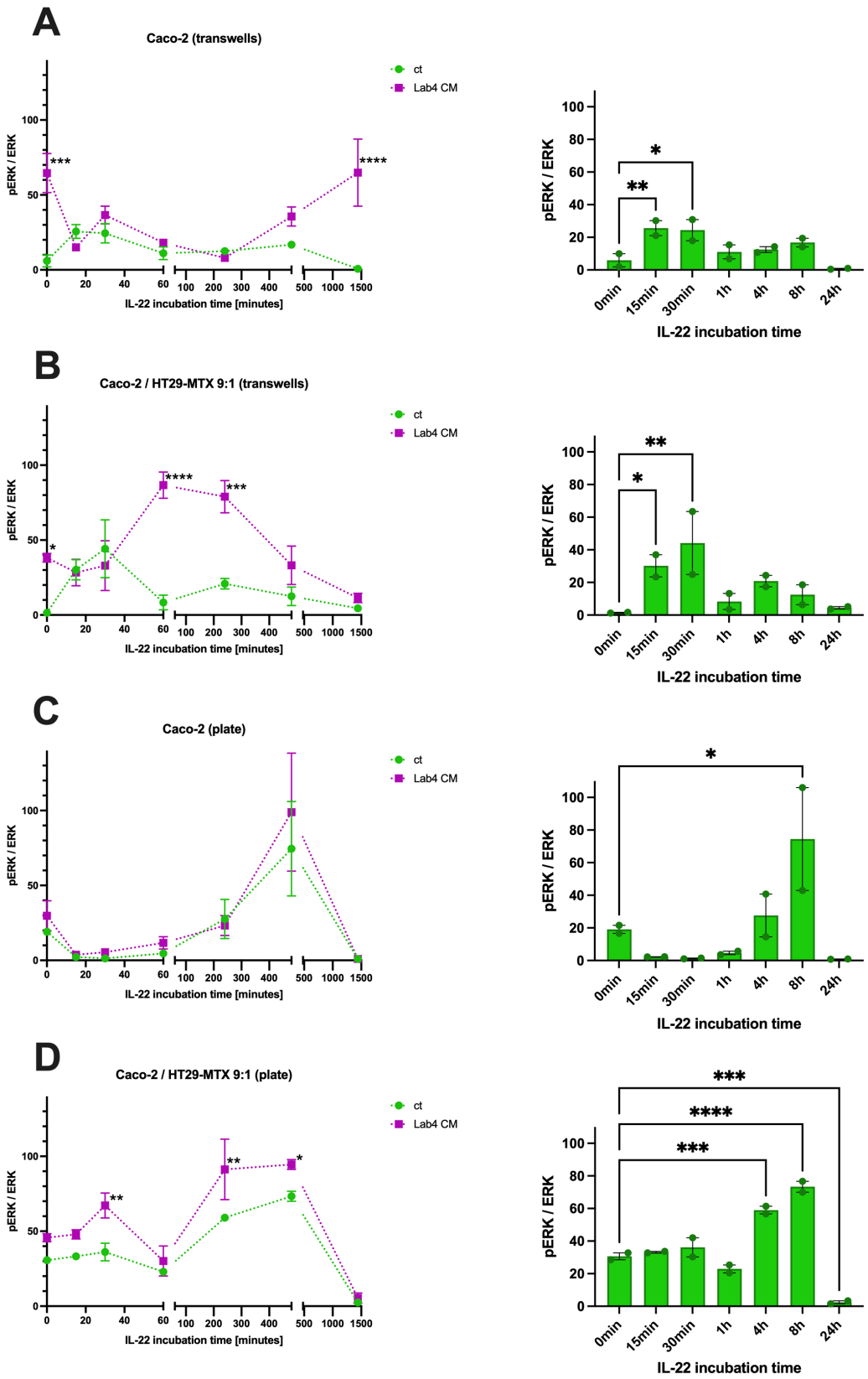

Figure 49 Analysis of ERK1/2 activation status in Caco-2 (A,B) and mixed (B,D) epithelia grown on either transwells (A,B) or on plates (C,D) following IL-22 stimulation. *Data from Western blots of two independent experiments (see Figure 48) was quantified using densitometry. Data was analysed for significant differences using two-way ANOVA with Fisher's LSD as post-hoc test (left panel), or one-way Anova with Fisher's LSD as post-hoc test (right panel).*

4. DISCUSSION

A substantial body of evidence from empirical observations, and importantly also placebo-controlled clinical trials, has provided strong evidence for a beneficial effect of probiotics on gut lining and patient quality of life, in both health and disease states, as outlined in the Introduction Section. Less clear are the molecular mechanisms through which specific probiotic formulations exert such effects. Here, we set out to investigate one such product, Lab4 produced by Cultech Ltd. Specifically, to address this gap and as a step towards gaining a mechanistic understanding of the determinant factors for efficacy of this product, this KESS project was designed with two central aims: Firstly, to investigate whether a beneficial effect of the probiotic formulation on the intestinal lining could be demonstrated in a well-controlled *in vitro* model. This was based on the hypothesis, that observed health benefits in clinical studies (Williams et al., 2009; Pugh et al., 2019; Mullish et al., 2023) related to improved barrier integrity. And secondly, to identify potential molecular mechanisms promoting improved epithelial cell functionality and enable the respective gains in barrier function of the gut lining.

The key discoveries of this work are that: 1. Metabolites derived from live bacteria (Lab4 CM), but not the devitalised probiotic bacteria themselves (Lab4 ET), exert a beneficial effect on epithelial barrier integrity. 2. Exposure of the epithelium to these metabolites had a protective effect to a subsequent inflammatory stimulus (IL-22), and moderated the extend of barrier disruption and epithelial hyperproliferation. 3. The presence of mucus producing cells profoundly altered the epithelial responses to the inflammatory insult, establishing distinct patterns of proinflammatory signalling with consequences on barrier functionality. 4. The probiotic metabolite-induced protective effect on epithelial barrier function correlates with altered MAPK, but not altered JAK-STAT3 signalling in enterocytes. Taken together, these findings have provided important insights on probiotic actions on a mechanistic level, that significantly advance our current understanding. We are, for the first time, able to propose a mechanism, that could satisfactorily explain the observations in terms of effect of probiotic (Lab4) on intestinal barrier function. Short-chain fatty acids (SCFA) are some

of the most abundant gut microbiota derived metabolites (reaching mM levels in gut lumen), are a major product of bacterial fermentation of dietary fiber, and are produced in abundance by strains of *Bifidobacterium* and *Lactobacillus* (Koh et al., 2016). SCFAs can exert a variety of effects on host physiology, including modulation of epithelial and immune responses, and impact on cross-talk with the enteric nervous system (Koh et al., 2016; Torres-Fuentes et al., 2017). A detailed discussion of the molecular interplay is outside of the scope of this document, but a schematic is included as Figure 50 to aid the reader, and the reader is referred to the review by Jayasimhan and Marino (2021) for detailed discussion.

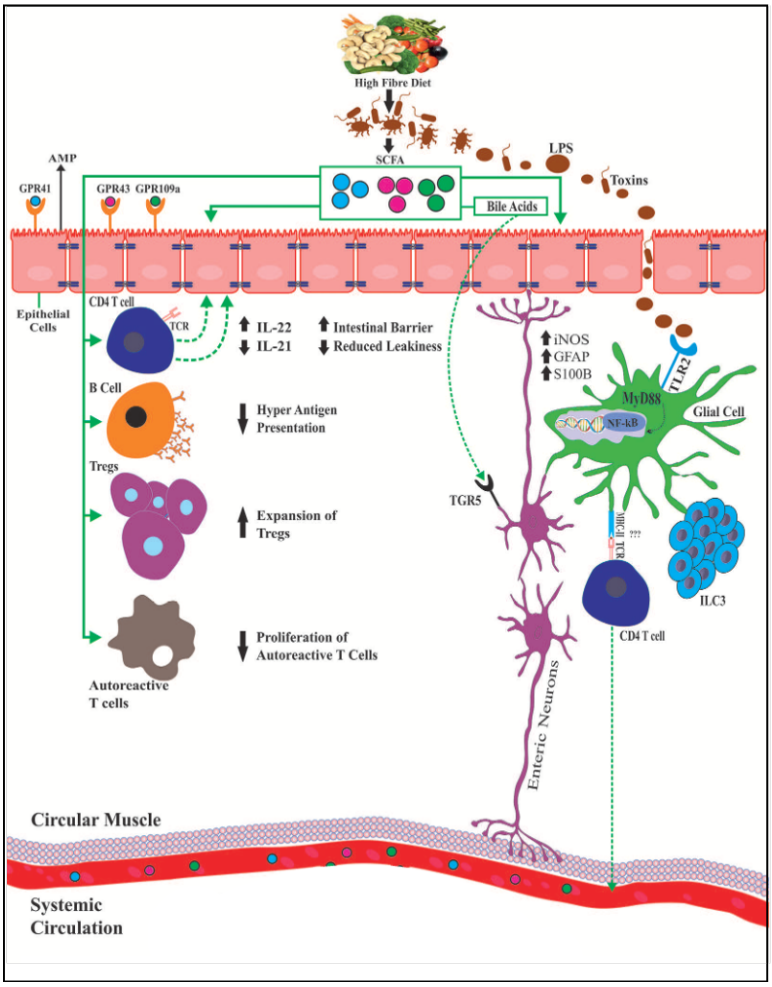

Figure 50 Diet and gut microbiota through the production of SCFAs exert anti-inflammatory effects. *SCFAs control the activity of multiple immune cell types, as well as the enteric glial cells and neurons. GPR41 (also known as free fatty acid receptor [FFAR]3), GPR43 (FFAR2), and GPR109 (nicotinic acid receptor) are G-protein-coupled receptors activated by SCFA ligands (acetate, propionate, and butyrate). SCFAs promote IL-22 production in a subset of CD4⁺ T cells or by supporting ILC3 cells, the major producers of IL-22, and reduce production of pro-inflammatory cytokines such as IL-21 to suppress effector functions of the adaptive immune system. Activation of GPCRs (GPR41 and GPR43) on enteroendocrine cells of the intestinal epithelium and Toll-like receptor (TLR) signalling (e.g. TLR2 and TLR4) maintains subsets of enteric neurons, resulting in changes in gut motility, conversion of primary bile acids into secondary bile acids, which activate TGRS expressed by enteroendocrine cells, enteric neurons, and others. (Adapted from Jayasimhan and Marino, 2021)*

SCFAs play a key role in promoting intestinal barrier integrity, including mucus production, and have a suppressive role on gut inflammation (Dalile et al., 2019). Butyrate or dietary fiber supplementation is protective in murine colitis models (Marcia et al., 2015). SCFAs also modulate GPCR signalling, that controls gut-brain interactions. For example, certain SCFAs can attenuate intracellular Ca^{2+} mobilization by ghrelin binding to growth hormone secretagogue receptor (GSHR)-1a (Torres-Fuentes, 2019). Biochemical cooperation of butyrate and IL-22 on Caco-2 cell responses has also recently been reported (Bachman et al., 2017). Although we did not see corresponding enhanced STAT3 activation or SOCS3 induction in our model, this is likely explained by the difference in the experimental setting (simplistic monolayer culture was used in these previous studies). Nevertheless, the sustained impact on signalling following pre-treatment with probiotic, as well as the alterations in the pattern of protein phosphorylation in intracellular signalling cascades reported to be mediated by SCFAs, are consistent with the changes we have seen in our Caco-2 epithelium model (Torres-Fuentes, 2019). Essentially, signalling via the ERK1/2 pathway in response to a stimulus (in our case IL-22) is dramatically altered following exposure to probiotic conditioned media (likely harbouring SCFAs), in line with what has previously been reported for alternative ligand-receptor systems. Mitogens induce a biphasic activation of ERK1 and ERK2, with a rapid initial burst around 10min, followed by a second wave of sustained activity of up to 6h (Mebratu and Tesfaigzi, 2009). For cell division, ERK1/2 activation must be sustained until late G1 phase of the cell cycle to transition into S-phase. Changes in this second wave of ERK activation in response to probiotic metabolites in our model may therefore explain the observed differences in epithelial responses.

Although we were unable to formally test this hypothesis, that SCFA exert this effect due to the limited time available for this project, the experimental systems we established provide the necessary tools to do so in the future. Interestingly, a very recent study employing a T84 cell organoid model demonstrated that butyrate indeed has a synergistic effect on IL-22 mediated mucus production (MUC13), and expression of certain antimicrobial peptides, and counteracts IL-22 induced barrier disruption (as monitored through claudin 2 expression and TEER) (Patnaude et al., 2021), in line with our observations and interpretation.

To this end, our project developed model systems of varying complexity, based on established cell lines, that have the intrinsic ability to adopt a mature enterocyte and mucus producing cell phenotype (Chanteret et al., 1988; Hilgendorf et al., 1999). Despite the potential drawbacks associated with the use of transformed cells, these constitute extensively validated cellular models, that provide an unlimited and reproducible cell source for studies. Clearly, findings will need to be verified with primary cells to ascertain, that any responses observed, are consistent with those of normal cells. Particular attention has been paid to ensure, that the employed models faithfully reproduce a well-developed epithelial lining. Histological analysis and immunostaining for brush border markers was employed in combination with TEER to verify consistent development of a mature epithelium across all experiments. We believe, that this is a strength of this work, and guarantees validity of our discoveries.

A number of aspects deserve further attention. Basson et al. (1996) investigated the effect of matrix proteins on intestinal epithelial differentiation. Caco-2 cells were grown either on uncoated, collagen type I or collagen type IV coated surfaces (collagen type I was of human origin, whereas collagen type IV was purified from mouse). They found that the activity of each brush border enzyme they analysed was higher in cells grown on collagen type IV than in cells grown on collagen type I or on plastic. Spreading and motility, on the other hand, was highest in Caco-2 cells grown on collagen type I, consistent with this substratum providing cues of injury repair, rather than supporting a mature cell phenotype (Fiedler et al., 2008). Collagen type IV, on the other hand, has been reported to support maintenance and proliferation of $Lg5^{+}$ intestinal epithelial stem cells (Tong et al., 2018). This is likely facilitated by engagement of distinct receptors as discussed in Khoshnoodi et al., 2008. Most studies in the field use uncoated or collagen I coated transwells, either of which we believe, provides inappropriate cues for cells. In support of this, Schreider and colleagues (2002) found, that Caco-2 cells grown on murine collagen IV coated transwells formed domes, a sign of maturity (Chantret et al., 1988), 2 days earlier than cells grown on uncoated transwells. All our experiments employed an *in situ* fibrillized preparation of human collagen type IV as substratum, which is likely to be the most appropriate ECM environment for the cells. This may be the reason for the epithelia reaching a mature

polarized phenotype far earlier than in some previous studies (Chantret et al., 1988; Le Ferrec et al., 2001; Sambuy et al., 2004).

In our models, we have shown that a 3 day IL-22 challenge caused disruption in epithelial integrity (significant reduction in TEER). Treatment with metabolites from probiotics for 48h prior to the IL-22 challenge had a protective effect on Caco-2 epithelia. Interestingly, Guo et al. (2017) showed, that treatment of Caco-2 cells with either *Bifidobacterium-* or *Lactobacillus acidophilus*-conditioned media (in the absence of an inflammatory challenge) produced a sustained increase in TEER, with a maximum at 4h, before returning to levels in the control over a two-day period. This suggests, that the effect of probiotic metabolites on cells, although sustained as discussed above, is time sensitive. Within the confines of this project, it was not possible to execute a time course for probiotic application, but in light of the data by Guo and colleagues, it appears important to revisit this point and analyse shorter probiotic metabolite exposure times prior to the IL-22 challenge. This should be investigated alongside SCFA dose-dependence to obtain a more realistic delineation of true effect size.

5. REFERENCES

Abreu, M.T. (2012). Toll-like receptor signalling in the intestinal epithelium: how bacterial recognition shapes intestinal function. *Nature Reviews Immunology* **10**(2): 131-144

Bachmann, M., Meissner, C., Pfeilschifter, J., and Mühl, H. (2016). Cooperation between the bacterial-derived short-chain fatty acid butyrate and interleukin-22 detected in human Caco-2 colon epithelial/carcinoma cells. *BioFactors* **43**(2): 283-292

Barker, N., van Es, J.H., Kuipers, J., Kujala, P., van den Born, M., Cozijnsen, M., Haegebarth, A., Korving, J., Begthel, H., Peters, P.J., and Clevers, H. (2007). Identification of stem cells in small intestine and colon by marker gene Lgr5. *Nature* **449**(7165): 1003-1007

Basson, M.D., Modlin, I.M., and Madri, J.A. (1992). Human Enterocyte (Caco-2) Migration Is Modulated In Vitro by Extracellular Matrix Composition and Epidermal Growth Factor. The *Journal of Clinical Investigation* **90**(1):15-23

Basson, M.D., Turowski, G., and Emenaker, N.J. (1996). Regulation of Human (Caco-2) Intestinal Epithelial Cell Differentiation by Extracellular Matrix Proteins. *Experimental Cell Research* **225**(2): 301-305

Behrens, I., Stenberg, P., Artursson, P., and Kissel, T. (2001). Transport of lipophilic drug molecules in a new mucus-secreting cell culture model based on HT29-MTX cells. *Pharmaceutical Research* **18**(8): 1138-1145

Bevins, C.L., and Salzman, N.H. (2011). Paneth cells, antimicrobial peptides and maintenance of intetstinal homeostasis. *Nature Reviews Microbiology* **9**: 356-368

Bron, P.A., Kleerebezem, M., Brummer, R-J., Cani, P.D., Mercenier, A., MacDonald, T.T., Garcia-Ródenas, C.L., and Wells, J.M. (2017). Can probiotics modulate human disease by impacting intestinal barrier function? *British Journal of Nutrition* **117**: 93-107

Cereijido, M., Contreras, R.G., Flores-Benítez, D., Flores-Maldonado, C., Larre, I., Ruiz, A., and Shoshani, L. (2007). New Diseases Derived or Associated with the Tight Junction. *Archives of Medical Research* **38**(5): 465-478

Chang, J.E., Buechler, M.B., Gressier, E., Turley, S.J., and Carrol, M.C. (2019). Mechanosensing by Peyer's patch stroma regulates lymphocyte migration and mucosal antibody responses. *Nature Immunology* **20**(11): 1506-1516

Chantret, I., Barbat, A., Dussaulx, E., Brattain, M.G., and Zweibaum, A. (1988). Epithelial Polarity, Villin Expression, and Enterocytic Differentiation of Cultured Human Colon Carcinoma Cells: A Survey of Twenty Cell Lines. *Cancer Research* **48**: 1936-1942

Cheng, H., and Leblond, C.P. (1974). Origin, differentiation and renewal of the four main epithelial cell types in the mouse small intestine. I. Columnar cell. *The American Journal of Anatomy* **141**(4): 461-479

Creff, J., Malaquin, L., and Besson, A. (2021). In vitro models of intestinal epithelium: Toward bioengineered systems. *Journal of Tissue Engineering* **12**: 1-16

Dalile, B., Van Oudenhove, L., Vevliet, B., and Vebeke, K. (2019). The role of short-chain fatty acids in microbiota-gut-brain communication. *Nature Reviews. Gastroenterology & Hepatology* **16**(8): 461-478

Delbue, D., Lebenheim, L., Cardoso-Silva, D., Dony, V., Krug, S.M., Richter, J.F., Manna, S., Muñoz, M., Wolk, K., Heldt, C., Heimesaat, M.M., Sabat, R., Siegmund, B., and Schumann, M. (2021). Reprogramming Interstinal Epithelial Cell Polarity by Interleukin-22. *Frontiers in Medicine* **8** (656047): 1-15

Dudakov, J.A., Hanash, A.M., and van den Brink, M.R.M. (2015). Interleukin-22: Immunobiology and Pathology. *Annual Review of Immunology* **33**: 747-785

Fanucci, A., Cerro, P., and Fanucci, E. (1988). Normal small-bowel measurements by enteroclysis. *Scandinavian Journal of Gastroenterology* **23**: 574-576

Fedi, A., Vitale, C., Ponschin, G., Ayehunie, S., and Fato, M. (2021). *In vitro* models replicating the human intestinal epithelium for absorption and metabolism studies: A systematic review. *Journal of Controlled Release* **335**: 247-268

Ferraretto, A., Bottani, M., De Luca, P., Cornaghi, L., Arnaboldi, F., Maggioni, M., Fiorilli, A., and Donetti, E. (2018). Morphofunctional properties of a differentiated Caco2/HT-29 co-culture as an *in vitro* model of human intestinal epithelium. *Bioscience Reports* **38** (2): BSR20171497

Ferruzza, S., Rossi, C., Scarino, M.L., and Sambuy, Y. (2012). A protocol for in situ enzyme assays to assess the differentiation of human intestinal Caco-2 cells. *Toxicology in Vitro* **26**: 1247-1251

Fiedler, L.R., Schönherr, E., Waddington, R., Niland, S., Seidler, D.G., Aeschlimann, D., and Eble, J.A. (2008). Decorin regulates endothelial cell motility on collagen I through activation of insulin-like growth factor I receptor and modulation of alpha2beta1 integrin activity. *The Journal of Biological Chemistry* **283**(25): 17406-17415

Ford, A.C., Quigley, E.M.M., Lacy, B.E., Lembo, A.J., Saito, Y.A., Schiller, L.R., Soffer, E.E., Spiegel, B.M.R., and Moayyedi, P. (2014). Efficacy of prebiotics, probiotics, and synbiotics in irritable bowel syndrome and chronic idiopathic constipation: systematic review and meta-analysis. *American Journal of Gastroenterology* **109**(10): 1547-1561

Forgue-Lafitte, M.E., Fabiani, B., Levy, P.P., Maurin, N., Fléjou, J.F., and Bara, J. (2007). Abnormal Expression of M1/MUC5AC mucin in distal colon of patients with diverticulitis, ulcerative colitis and cancer. *International Journal of Cancer* **121**: 1543-1549

Gao, Y., Zhao, H., Wang, P., Wang, J., and Zou, L. (2018). The roles of SOCS3 and STAT3 in bacterial infection and inflammatory diseases. *Scandinavian Journal of Immunology* **88**(6): e12727

Guo, S., Gillingham, T., guo, Y., Meng, D., Zhu, W., Walker, W.A., and Ganguli, K. (2017). Secretions of *Bifidobacterium infantis* and *Lactobacillus acidophilus* Protect Intestinal Epithelial Barrier Function. *Journal of Pediatric Gastroenterology and Nutrition* **64**(3): 404-412

Hasnain, S.Z., Evans, C.M., Roy, M., Gallagher, A.L., Kindrachuk, K.N., Barron, L., Dickey, B.F., Wilson, M.S., Wynn, T.A., Grencis, R.K., and Thornton, D.J. (2011). Muc5ac: a critical component mediating the rejection of enteric nematodes. *The Journal of Experimental Medicine* **208** (5): 893-900

Helander,H.F., and Fändriks, L. (2014). Surface area of the digestive tract – revisited. *Scandinavian Journal of Gastroenterology* **49**: 681-689

Hilgendorf, C., Spahn-Langguth, H., Regårdh, C.G., Lipka, E., Amidon, G.L., and Langguth, P. (2000). Caco-2 versus Caco-2/HT29-MTX Co-cultured Cell Lines: Permeabilities Via Diffusion, Inside- and Outside-Directed Carrier-Mediated Transport. *Journal of Pharmaceutical Sciences* **89** (1): 63-75

Hill, C., Guarner, F., Reid, G., Gibson, G.R., Merenstein, D.J., Pot, B., Morelli, L., Canani, R.B., Flint, H.J., Salminen, S., Calder, P.C., and Sanders, M.E. (2014). The Intestinal Scientific Association for Probiotics and Prebiotics consensus statement on the scope and appropriate use of the term probiotic. *Nature Reviews Gastroenterology & Hepatology* **11**: 506-514

Hungin, A.P.S., Mitchell, C.R., Whorwell, P., Mulligan, C., Cole, O., Agréus, L., Fracasso, P., Lionis, C., Mendive, J., Philippart de Foy, J.-M., Seifert, B., Wensaas, K.-A., Winchester, C., and de Wit, N. (2018). Systematic review: probiotics in the management of lower gastrointestinal symptoms – an updated evidence-based international consensus. *Alimentary Pharmacology & Therapeutics* **47**(8): 1054-1070

Jayasimhan, A., and Mariño, E. (2019). Dietary SCFAs, IL-22, and GFAP: The Three Musketeers in the Gut-Neuro-Immune Network in Type I Diabetes. *Frontiers in Immunology* **10**: 2429

Johansson, M.E.W., Holmén-Larsson, J.M., and Hansson, G.C. (2011). The two mucin layers of colon are organized by the MUC2 mucin, whereas the outer layer is a legislator of host – microbial interactions. *Proceedings of the National Academy of Sciences of the United States of America* **108** (Suppl 1): 4659-65

Kermanizadeh, A., Ude, V., Johnston, H., and Stone, V. (2018). Culture and characterisation of mono and multi-cellular models of the gastrointestinal system. *PATROLS Advanced Tools for NanoSafety Testing* **SOP Handbook**: 4101

Khoshnoodi, J., Pedchenko, V., and Hudson, B.G. (2008). Mammalian collagen IV. *Microscopy Research and Technique* **71**(5):357-370

Klunder, L.J., Faber, K.N., Dijkstra, G., Van IJzendoorn, S.C.D. (2016). Mechanisms of Cell Polarity-controlled Epithelial Homeostasis and Immunity in the Intestine. *Cold Springer Harbor Perspectives in Biology* **9**: a027888

Knoop, K.A., and Newberry, R.D. (2018). Goblet cells: multifaceted players in immunity at mucosal surfaces. *Mucoscal Immunology* **11**: 1551-1557

Koh, A., De Vadder, F., Kovatcheva-Datchary, P., and Bäckhed, F. (2016). From Dietary Fiber to Host Physiology: Short-Chain Fatty Acids as Key Bacterial Metabolites. *Cell* **165**(6): 1332-1345

Lang, T, and Pelaseyed, T. (2022). Discovery of a *MUC3B* gene reconstructs the membrane mucin gene cluster on human chromosome 7. *PLoS One* **17**(10): e0275671

Le Ferrec, E., Chesne, C., Artusson, P., Brayden, D., Fabre, G., Gires, P., Guillou, F., Rousset, M., Rubas, W., and Scarino, M.L. (2001). In vitro models of the intestinal barrier: The report and recommendations of ECVAM Workshop 46. European Centre for the Validation of Alternative Methods. *Alternatives to Laboratory Animals* **29**(6): 649-668

Lea, T. (2015a). Epithelial Cell Models; General Introduction. *In:* The Impact of Food Bioactives on Health, Verhoeckx, K., Cotter, P., López-Expósito, I., Kleiveland, C., Lea, T., Mackie, A., Requena, T., Swiatecka, D., and Wichers, H., eds. *Springer International Publishing AG Switzerland* **Chapter 9**: 95-102

Lea, T. (2015b). Caco-2 Cell Line. *In:* The Impact of Food Bioactives on Health, Verhoeckx, K., Cotter, P., López-Expósito, I., Kleiveland, C., Lea, T., Mackie, A., Requena, T., Swiatecka, D., and Wichers, H., eds. *Springer International Publishing AG Switzerland* **Chapter 10**: 103-111

Leffler, D.A., Kelly, C.P., Green, P.H.R., Fedorak, R.N., DiMarino, A., Perrow, W., Rasmussen, H., Wang, C., Bercik, P., Bachir, N.M., and Murray, J.A. (2015). Larazotide acetate for fersistant symptoms of celiac disease despite a gluten-free diet: a randomized controlled trial. *Gastroenterology* **148**(7): 1311-1319

Lesuffleur, T., Barbat, A., Dussaulx, E., and Zweibaum, A. (1990). Growth adaptation to methotrexate of HT-29 human colon carcinoma cells is associated with their ability to differentiate into columnar absorptive and mucus-secreting cells. *Cancer Research* **50**(19): 6334-6343

Leupold, T, and Wirtz, S. (2022). ILCs – Crucial Players in Enteric Infectious Diseases. *International Journal of Molecular Sciences* **23**: 14200

Liang, S.C., Nickerson-Nutter, C., Pittman, D.D., Carrier, Y., Goodwin, D.G., Shields, K.M., Lambert, A.J., Schelling, S.H., Medley, Q.G., Ma, H.L., Collins, M., Dunussi-Joannopoulos, K., and Fouser, L.A. (2010) Il-22 Induces an Acute-Phase Response. *The Journal of Immunology* **185**(9): 5531-5538

Lindblom, A., Quadt, N., Marsh, T., Aeschlimann, D., Mörgelin, M., Mann, K., and Paulsson, M. (1999). The intrinsic factor-vitamin B12 receptor, cubilin, is assembled into trimers via a coiled-coil alpha-helix. *The Journal of Biological Chemistry* **274**(10): 6374-6380

Lindemans, C.A., Calafiore, M., Mertelsmann, A.M., O'Connor, M.H., Dudakov, J.A., Jenq, R.R., Velardi, E., Young, L.F., Smith, O.M., Lawrence, G., Ivanov, J.A., Fu, Y.Y., Takashima, S., Hua, G., Martin, M.L., O'Rourke, K.P., Lo, Y.H., Mokryn, M., Romera-Hernandez, M., Cupedo, Y., Dow, L., Nieuwenhuis, E.E., Shroyer, N.F., Lio, C., Kolesnick, R., van den Brink, M.R.M., and Hanash, A.M. (2015). Interleukin-22 promotes intestinal-stem-cell-mediated epithelial regeneration. *Nature* **528**(7583): 560-564

Mahler G.J., Shuler, M.L., and Glahn, R.P. (2009). Characterization of Caco-2 and HT29-MTX cocultures in an *in vitro* digestion/cell culture model used to predict iron bioavailablility. *Journal of Nutritional Biochemistry* **20**: 494-502

Marcia, L., Tan, J., Vieira, A.T., Leach, K., Stanley, D., Luong, S., Maruya, M., McKenzie, C.I., Hijikata, A., Wong, C., Binge, L., Thorburn, A.N., Chevalier, N., Ang, C., Marino, E., Robert, R., Offermanns, S., Teixeira, M.M., Moore, R.J., Flavell, R.A., Fagarasan, S., and Mackay, C.R. (2015). Metabolite-sensing receptors GPR43 and GPR109A facilitate dietary fibre-induced gut homeostasis through regulation of the inflammasome. *Nature Communications* **6**: 6734

Martínez-Maqueda, D., Miralles, B., and Recio, I. (2015). HT29 Cell Line. *In:* The Impact of Food Bioactives on Health, Verhoeckx, K., Cotter, P., López-Expósito, I., Kleiveland, C., Lea, T., Mackie, A., Requena, T., Swiatecka, D., and Wichers, H., eds. *Springer International Publishing AG Switzerland* **Chapter 11**: 113-124

McFarland, L.V. (2021). Efficacy of Single-Strain Probiotics Versus Multi-Strain Mixtures: Systematic Review of Strain and Disease Specificity. *Digestive Diseases and Sciences* **66**(3): 694-704

Mebratu, Y., and Tesfaigzi, Y. (2009). How ERK1/2 activation controls cell proliferation and cell death: is subcellular localization the answer? *Cell Cycle* **8**(8): 1168-1175

Michael, D.R., Davies, T.S., Moss, J.W.E., Lama Calvente, D., Ramji, D.P., Marchesi, J.R.., Pechlivanis, A., Plummer, S.F., and Hughes, T.R. (2017). The anti-cholesterolaemic effect of a consortium of probiotics: An acute study in C57BL/6J mice. *Scientific Reports* **7**(1): 2883

Moniruzzuman, M.D., Wang, R., Jeet, V., McGuckin, M.A., and Hasnain, S.Z. (2019). Interleukin (IL)-22 from IL-20 Subfamily of Cytokines Induces Colonic Epithelial Cell Proliferation Predominantly through ERK1/2 Pathway. *International Journal of Molecular Sciences* **20**(14): 3468

Morán-Ramos, S., Tovar, A.R., and Torres, N. (2012). Diet: Friend or Foe of Enteroendocrine Cells: How It Interacts with Enteroendocrine Cells. *Advanced Nutrition* **3**: 8-20

Mullish, B.H., Michael, D.R., Webberley, T.S., John, D., Ramanathan, G., Plummer, S.F., Wang, D., and Marchesi, J.R. (2023). The gastrointestinal status of healthy adults: a *post hoc* assessment of the impact of three distinct probiotics. *Beneficial Microbes* [doi: 10.3920/BM2022.0092]

Natoli, M., Leoni, B.D., D'Agnano, I., D'Onofrio, M., Brandi, R., Arisi, I., Zucco, F., and Felsani, A. (2011). Cell Growing Density Affects the Structural and Functional Properties of Caco-2 Differentiated Monolayer. *Journal of Cellular Physiology* **226**: 1531-1543

Onyiah, J.C., and Colgan, S.P. (2016). Cytokine responses and epithelial function in the intestinal mucosa. *Cellular and Molecular Life Sciences* **73**: 4203-4212

Pagnini, C., Saeed, R., Bamias, G., Arseneau, K.O., Pizarro, T.T., and Cominelli, F. (2010). Probiotics promote gut health trough stimulation of epithelial innate immunity. *Proceedings of the National Academy of Science of the United States of America* **107**(1): 454-459

Parks, O.B., Pociask, D.A., Hodzic, Z., Kolls, J.K., and Good, M. (2016). Interleukin-22 Signalling in the Regulation of Intestinal Health and Disease. *Frontiers in Cell and Developmental Biology* **3**: 85

Patnaude, L., Mayo, M., Mario, R., Wu, X., Knight, H., Creamer, K., Wilson, K., Pivorunas, V., Karman, J., Phillips, L., Dunstan, R., Kamath, R.V., McRae, B., and Terrillon, S. (2021). Mechanisms and regulation of IL-22-mediated intestinal epithelial homeostasis and repair. *Life Sciences* **271**: 119195

Pereira, C., Costa, J., Sarmento, B., and Araújo, F. (2016) Cell-based in vitro models for intestinal permeability studies. *In:* Concepts and Models for Drug Permeability Studies. *Elsiever* **Chapter 3.3.**: 57-81

Pinto, M., Robine-Leon, S., Appay, M.D., Kedinger, M., Triadou, N., Dussaulx, E., Lacroix, B., Simon-Assmann, P., Haffen, K., Fogh, J., and Zweibaum, A. (1983). Enterocyte-like Differentiation and Polarization of the Human Colon Carcinoma Cell Line Caco-2 in Culture. *Biologie Cellulaire* **47**: 323-330

Pugh, J.N., Sparks, A.S., Doran, D.A., Fleming, S.C., Langan-Evans, C., Kirk, B., Fearn, R., Morton, J.P., and Close, G.L. (2019). Four weeks of probiotic supplementation reduces GI symptoms during a marathon race. *European Journal of Applied Physiology* **119**: 1491-1501

Rao, M., and Gershon, M.D. (2016). The bowel and beyond: the enteric nervous system in neurological disorders. *Nature reviews. Gastroenterology & Hepatology* **13**(9): 517-528

Raygan, F., Rezavandi, Z., Bahmani, F., Ostadmohammadi, V., Mansournia, M.A., Tajabadi-Ebrahimi, M., Borzabadi, S., and Asemi, Z. (2018). The effects of probiotic supplementation on metabolic status in type 2 diabetic patients with coronary heart disease. *Diabetology & Metabolic Syndrome* **10**:51

Ruiz, L., Margolles, A., and Sánchez, B., (2013). Bile resistance mechanisms in *Lactobacillus* and *Bifidobacterium*. *Frontiers in Microbiology* **4**: 396

Sambuy, Y., De Angelis, I., Ranaldi, G., Scaino, M.L., Stammati, A., and Zucco, F. (2005). The Caco-2 cell line as a model of the intestinal barrier: influence of cell and culture-related factors on Caco-2 cell functional characteristics. *Cell Biology and Toxicology* **21**: 1-26

Sanders, M.E. Merenstein, D.J., Reid, G., Gibson, G.R., and Rastall, R.A. (2019). Probiotics and prebiotics in intestinal health and disease: from biology to the clinic. *Nature Reviews Gastroenterology & Hepatology* **16**: 605-616

Sano, T., Huang, W., Hall, J.A., Yang, Y., Chen, A., Gavzy, S.J., Lee, J.Y., Ziel, J.W., Miraldi, E.R., Domingos, A.I., Bonneau, R., and Littman, D.R. (2015). An IL-23R/IL-22 Circuit Regulates Epithelium Serum Amyloid A to Promote Local Effector Th17 Responses. *Cell* **163**: 381-393

Sawa, S., Lochner, M., Stoh-Takayama, N., Dulauroy, S., Bérard, M., Kleinschek, M., Cua, D., Di Santo, J.P., and Eberl, G. (2011). RORγt+ innate lymphoid cells regulate intestinal homeostasis by integrating negative signals from the symbiotic microbiota. *Nature Immunology* **12**(4): 320-326

Schreider, C., Peignon, G., Thenet, S., Chambaz, J., and Pinçon-Raymond, M. (2002). Integrin-mediated functional polarization of Caco-2 cells through E-cadherin-actin complexes. *Journal of Cell Science* **115**: 543-552

Sekiguchi, R., and Yamada, K.M. (2018). Basement membranes in development and disease. *Current Topics in Developmental Biology* **130**: 143-191

Sharkey, K.A., and Mawe, G.M. (2023). The enteric nervous system. *Physiological Reviews* **103**(2): 1487-1564

Shimizu, M. (2010). Interaction between Food Substances and the Intestinal Epithelium. *Bioscience, Biotechnology, and Biochemistry* **74**(2): 232-241

Shin, W., and Kim, H.J. (2022). 3D in vitro morphogenesis of human intestinal epithelium in a gut-on-a-chip or a hybrid chip with a cell culture insert. *Nature Protocols* **17**: 910-939

Sonnenberg, G.F., Fouser, L.A., and Artis, D. (2010). Functional Biology of the IL-22-IL-22R Pathway in Regulating Immunity and Inflammation at Barrier Surfaces. *Advances in Immunology* **107**: 1-29

Sonnenberg, G.F., Fouser, L.A., and Artis, D. (2011). Border patrol: regulation of immunity, inflammation and tissue homeostasis at barrier surfaces by IL-22. *Nature Immunology* **12**(5): 383-390

Srinivasan, B., Koll, A.R., Esch, M.B., Abaci, H.E., Shuler, M.L., and Hickman, J.J. (2015). TEER measurement techniques for in vitro barrier model systems. *Journal of Laboratory Automation* **20**: 107-126

Staudacher, H.M., Lomer, M.C.E., Farquharson, F.M., Louis, P., Fava, F., Franciosi, E., Scholz, M., Tuohy, K.M., Lindsay, J.O., Irving, P.M., and Whelan, K. (2017). A Diet Low in FODMAPs Reduces Symptoms in Patients With Irritable Bowel Syndrome and A Probiotic Restores Bifidobacterium Species: A Randomized Controlled Trial. *Gastroenterology* **153**: 936-947

Stephens, P., Grenard, P., Aeschlimann, P., Langley, M., Blain, E., Errington, R., Kipling, D., Thomas, D., and Aeschlimann, D. (2004). Crosslinking and G-protein functions of transglutaminase 2 contribute differentially to fibroblast wound healing responses. *Journal of Cell Science* **117**(Pt15): 3389-3403

Sugimoto, K., Ogawa, A., Mizoguchi, E., Shimomura, Y., Andoh, A., Bhan, A.K., Blumberg, R.S., Cavier, R.J., and Mizoguchi, A. (2008). IL-22 ameliorates intestinal inflammation in a mouse model of ulcerative colitis. *The Journal of Clinical Investigation* **118**(2): 534-544

Talbot, J., Hahn, P., Kroehling, L., Nguyen, H., Li, D., and Littman, D.R. (2020). Feeding-dependent VIP neuron-ILC3 circuit regulates the intestinal barrier. *Nature* **579**(7800): 575-580

Tong, Z., Martyn, K., Yang, A., Yin, X., Mead, B.E., Joshi, N., Sherman, N.E., Langer, R.S., and Karp, J.M. (2018). Towards a Defined ECM and Small Molecule Based Monolayer Culture System for the Expansion of Mouse and Human Intestinal Stem Cells. *Biomaterials* **154**: 60-73

Torres-Fuentes, C., Schellekens, H., Dinan, T.G., and Cryan, J.F. (2017). The microbiota-gut-brain axis in obesity. *The Lancet Gastroenterology & Hepatology* **2**(10): 747-756

Torres-Fuentes, C., Golubeva, A.V., Zhdanov, A.V., Wallace, S., Arboleya, S., Papkivsky, D.B., El Aidy, S., Ross, P., Roy, B.L., Stanton, C., Dinan, T.G., Cryan, J.F., and Schellekens, H. (2019). Short-chain fatty acids and microbiota metabolites attenuate ghrelin receptor signaling. *FASEB Journal* **33**(12): 13436-13559

Tracey, H., Coates, N., Hulme, E., John, D., Michael, D.R., and Plummer, S.F. (2023). Insights into the enumeration of mixtures of probiotic bacteria by flow cytometry. *BMC Microbiology* **23**(1): 48

Trainer, D.L., Kline, T., McCabe, F.L., Faucette, L.F., Feild, J., Chaikin, M., Anzano, M., Rieman, D., Hoffstein, S., Li, D.J., Gennaro, D., Buscarion, C., Lynch, M., Poste, G., and Greig, R. (1988). Biological characterization and oncogene expression in human colorectal carcinoma cell lines. *International Journal of Cancer* **41**(2): 287-296

Vivier, H., Ross, E.J., and Cassisi, J.E. (2020). Classification of gastrointestinal symptom patterns in young adults. *BMC Gastroenterology* **20**: 326

Wang, L., Guo, M.J., Gao, Q., Yang, J.F., Yang, L., Pang, X.L., and Jiang, X.J. (2018a). The effects of probiotics on total cholesterol: A meta-analysis of randomized controlled trials. *Medicine* **97**(5): 9679.

Wang, Y., Mumm, J.B., Herbst, R., Kolbeck, R., and Wang, Y. (2017). IL-22 Increases Permeability of Intestinal Epithelial Tight Junctions by Enhancing Claudin-2 Expression. *The Journal of Immunology* **199**: 000-000

Wang., Y., Kim, R., Hinman, S.S., Zwarycz, B., Magness, S.T., and Allbritton, N.L. (2018b). Bioengineered Systems and Designer Matrices That Recapitulate the Intestinal Stem Cell Niche. *Cellular and Molecular Gastroenterology and Hepatology* **5**: 440-453

Williams, E.A., Stimpson, J., Wang, D., Plummer, S., Garaiova, I., Barker, M.E. and Corfe, B.M. (2009). Clinical trial: a multistrain probiotic preparation significantly reduces symptoms of irritable bowel syndrome in a double-blind placebo-controlled study. *Alimentary Pharmacology and Therapeutics* **29**: 97-103

Zheng, Y., Valdez, P.A., Danilenko, D.M., Hu, Y., Sa, S.M., Gong, Q., Abbas, A.R., Modrusan, Z., Ghilardi, N., de Sauvage, F.J., and Ouyang, W. (2008). Interleukin-22 mediates early host defense against attaching and effacing bacterial pathogens. *Nature Medicine* **14**(3): 282-289

Zierer, J., Jackson, M.A., Kastenmüller, G., Mangino, M., Long, T., Telenti, A., Mohney, R.P., Small, K.S., Bell, J.T., Steves, C.J., Valdes, A.M., Spector, T.D., and Menni, C. (2018). The fecal metabolome as a functional readout of the gut microbiome. *Nature Genetics* **50**: 790-795

6. APPENDIX

APPENDIX A – ZO-1 IMMUNOLABELING OF CACO-2 CELLS ON DIFFERENT SUBSTRATES

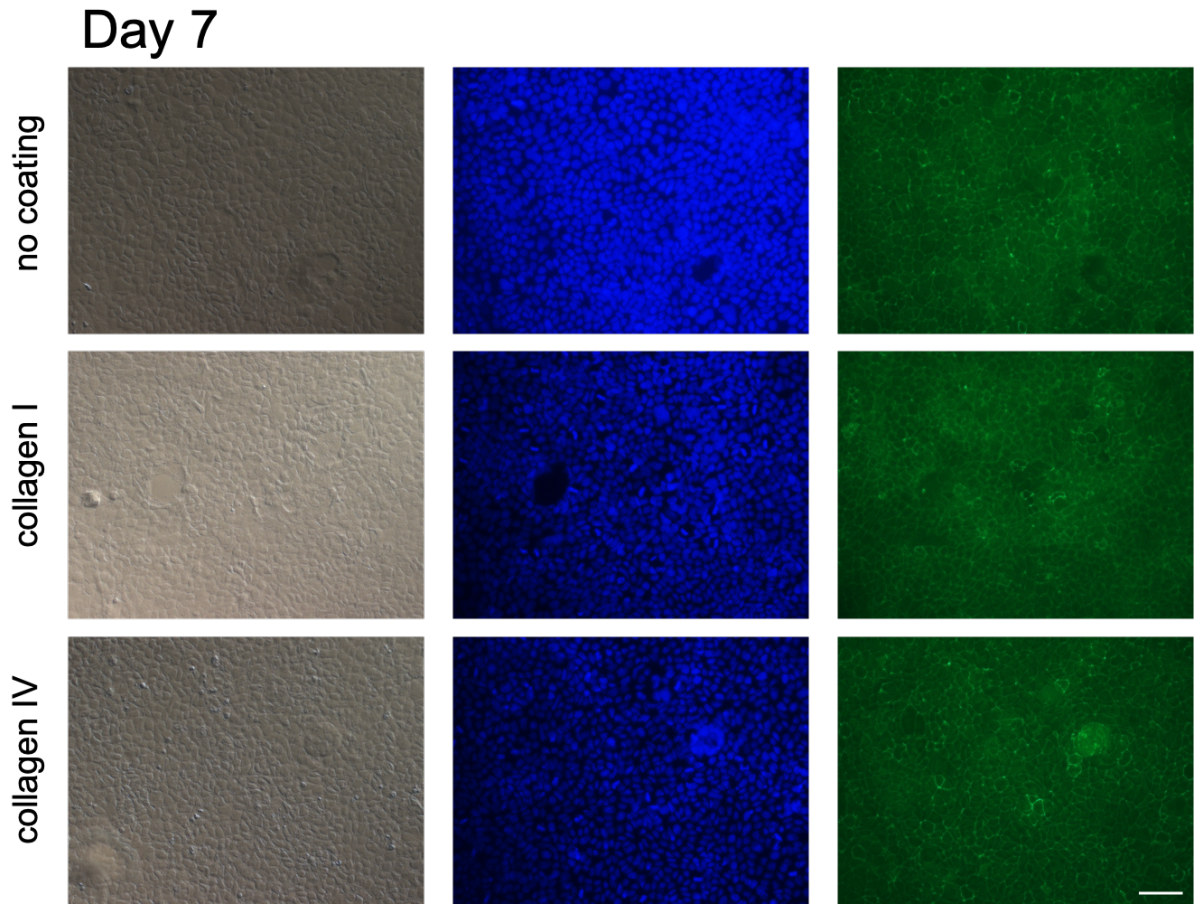

Appendix A 1 ZO-1 immunolabeling of Caco-2 cells on different substrates. *Caco-2 cells (1.2 x 10^5 cells/cm2) were seeded on uncoated chamber slides or following coating with 44ug/ml collagen type I or collagen type IV. On* ***day 7****, cells were fixed with paraformaldehyde, permeabilized and immunolabeled with polyclonal antibodies to ZO-1, Alexa Fluor 488 secondary antibodies (green), and counterstained with DAPI (blue). DIC images (left), as well as epifluorescence images for DAPI (middle) and ZO-1 (right) were captured, and are given to illustrate cell boundaries, nuclei and associated ZO-1 localization. Bar = 50μm*

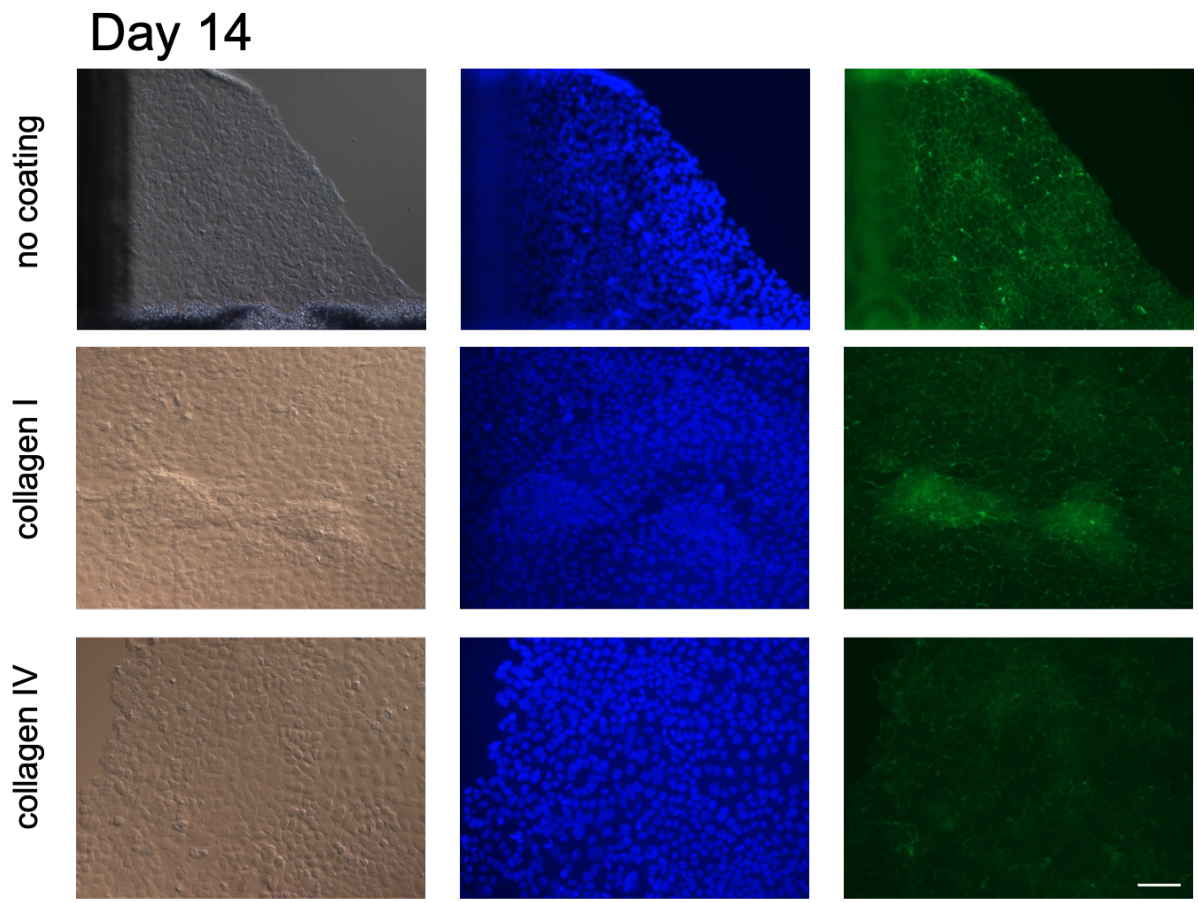

Appendix A 2 ZO-1 immunolabeling of Caco-2 cells on different substrates. *Caco-2 cells (1.2 x 10^5 cells/cm2) were seeded on uncoated chamber slides or following coating with 44ug/ml collagen type I or collagen type IV. On* ***day 14****, cells were fixed with paraformaldehyde, permeabilized and immunolabeled with polyclonal antibodies to ZO-1, Alexa Fluor 488 secondary antibodies (green), and counterstained with DAPI (blue). DIC images (left), as well as epifluorescence images for DAPI (middle) and ZO-1 (right) were captured, and are given to illustrate cell boundaries, nuclei and associated ZO-1 localization. Bar = 50μm*

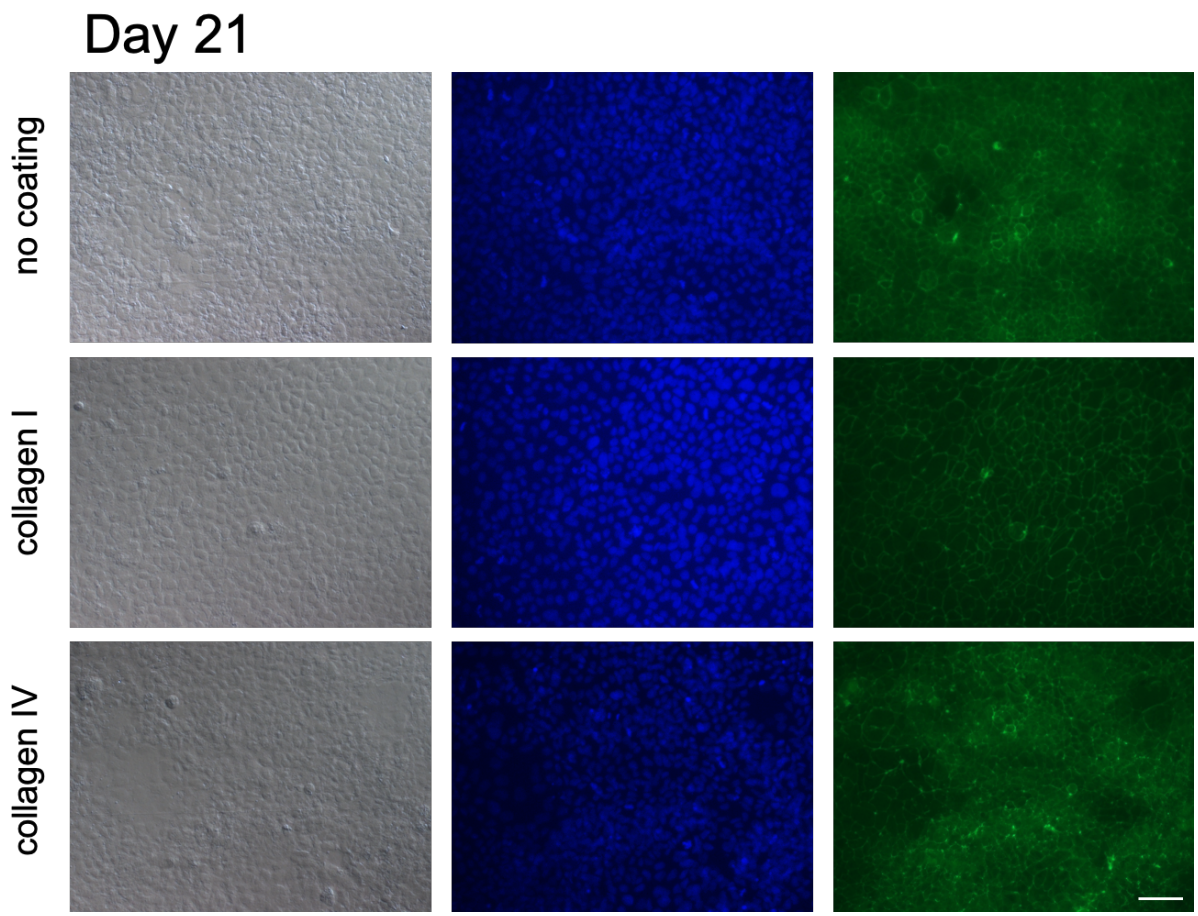

Appendix A 3 ZO-1 immunolabeling of Caco-2 cells on different substrates. *Caco-2 cells (1.2 x 10^5 cells/cm2) were seeded on uncoated chamber slides or following coating with 44ug/ml collagen type I or collagen type IV. On* ***day21****, cells were fixed with paraformaldehyde, permeabilized and immunolabeled with polyclonal antibodies to ZO-1, Alexa Fluor 488 secondary antibodies (green), and counterstained with DAPI (blue). DIC images (left), as well as epifluorescence images for DAPI (middle) and ZO-1 (right) were captured, and are given to illustrate cell boundaries, nuclei and associated ZO-1 localization. Bar = 50μm*

APPENDIX B – VILLIN-1 IMMUNOLABELING OF CACO-2 EPITHELIUM GROWN IN COLLAGEN IV-COATED TRANSWELLS FOR 30 DAYS

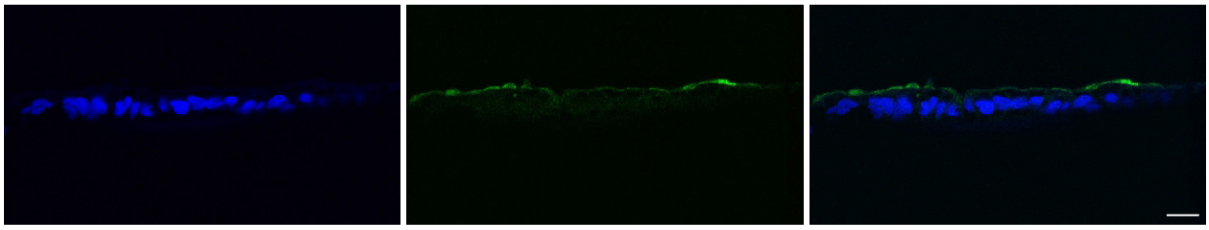

Appendix B Optical section acquired by confocal microscopy. *Caco-2 epithelium grown in collagen IV-coated transwell for 30 days and stained for villin-1 as described in Figure 20. Bar 20um*

APPENDIX C – ZO-1 IMMUNOLABELING OF CACO-2 EPITHELIUM GROWN ON COLLAGEN IV-COATED TRANSWELLS

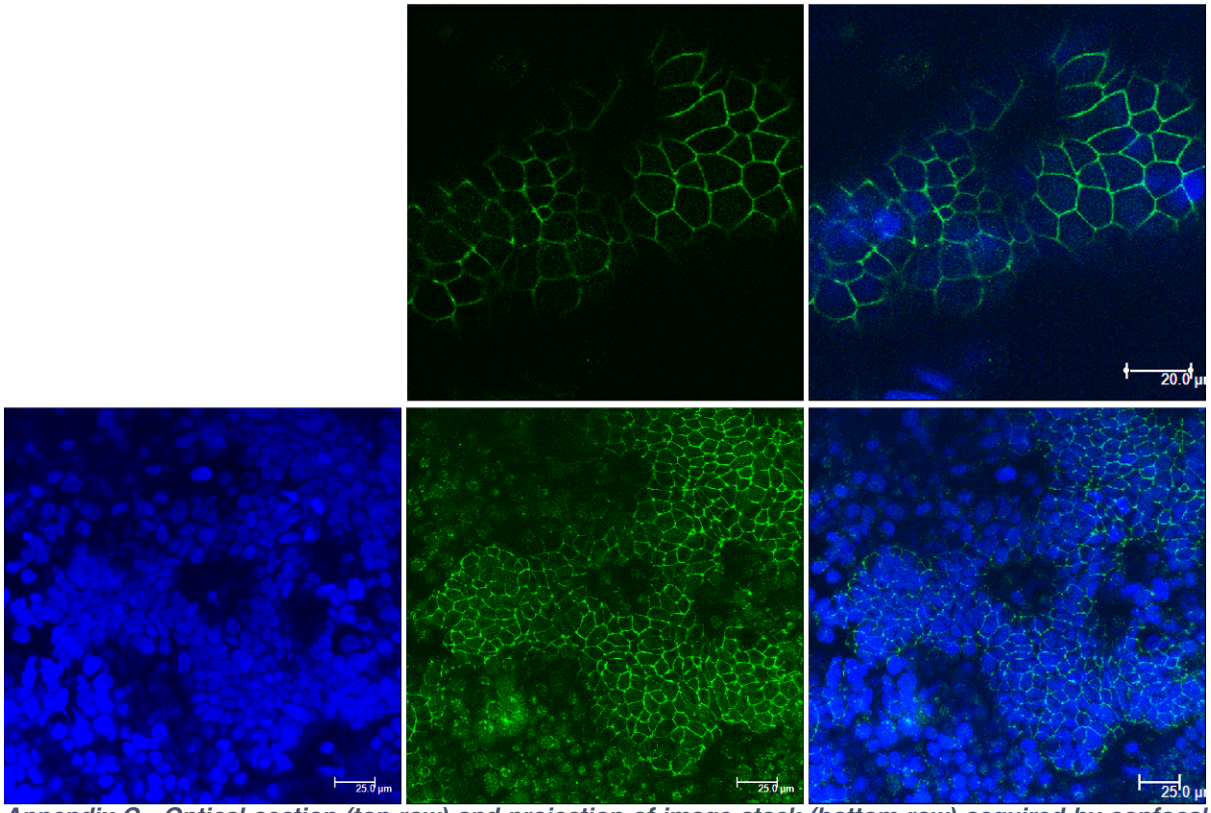

Appendix C Optical section (top row) and projection of image stack (bottom row) acquired by confocal microscopy. *Caco-2 cells (0.4 x 10^5 cells/well) were seeded on PET transwells following coating with 44ug/ml collagen type IV. On day 21, cells were fixed with paraformaldehyde, permeabilized and immunolabeled with polyclonal antibodies to ZO-1, Alexa Fluor 488 secondary antibodies (green), and counterstained with DAPI (blue). Top row: zoomed picture. Bar = 20μm. bottom row: merged z-stack pictures over 19.76μm. Bar = 25μm*

APPENDIX D – H&E STAINED SECTIONS OF EPITHELIA GROWN ON COLLAGEN IV-COATED TRANSWELLS WITH AND WITHOUT MUCUS PRODUCING CELLS

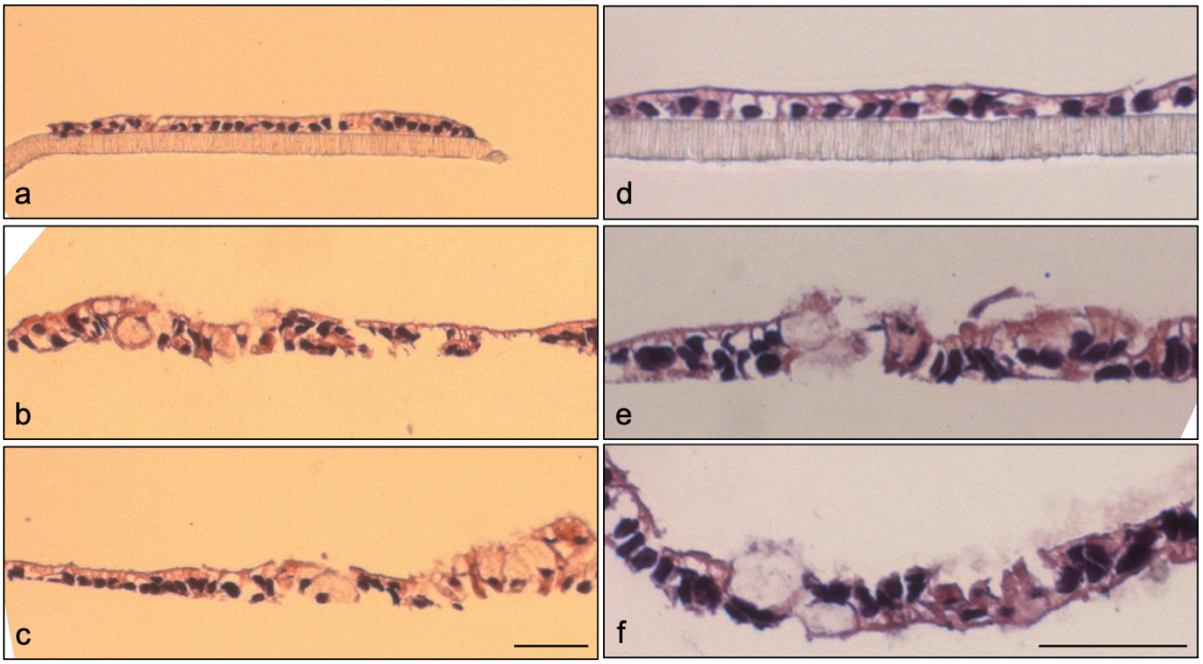

Appendix D H&E stained sections of epithelia grown on collagen type IV coated transwells with and without mucus producing cells on day 21. *Cells were seeded onto collagen type IV coated transwells at a density of 0.4 x 10^5 cells/well, either (a/d) Caco-2 only, (b/e) Caco-2 / HT29-MTX 9:1 mixture, or (c/f) Caco-2 / HT29-MTX 3:1 mixture, and grown for to 21 days. Cells were fixed, membranes cut out, paraffin embedded, cut into 4μm sections and H&E stained. (a/b/c) 20x magnification. (d/e/f) 40 x magnification. Bar = 50μm*

APPENDIX E – GAPDH LOADING CONTROL OF STAT 3 WESTERN BLOTS

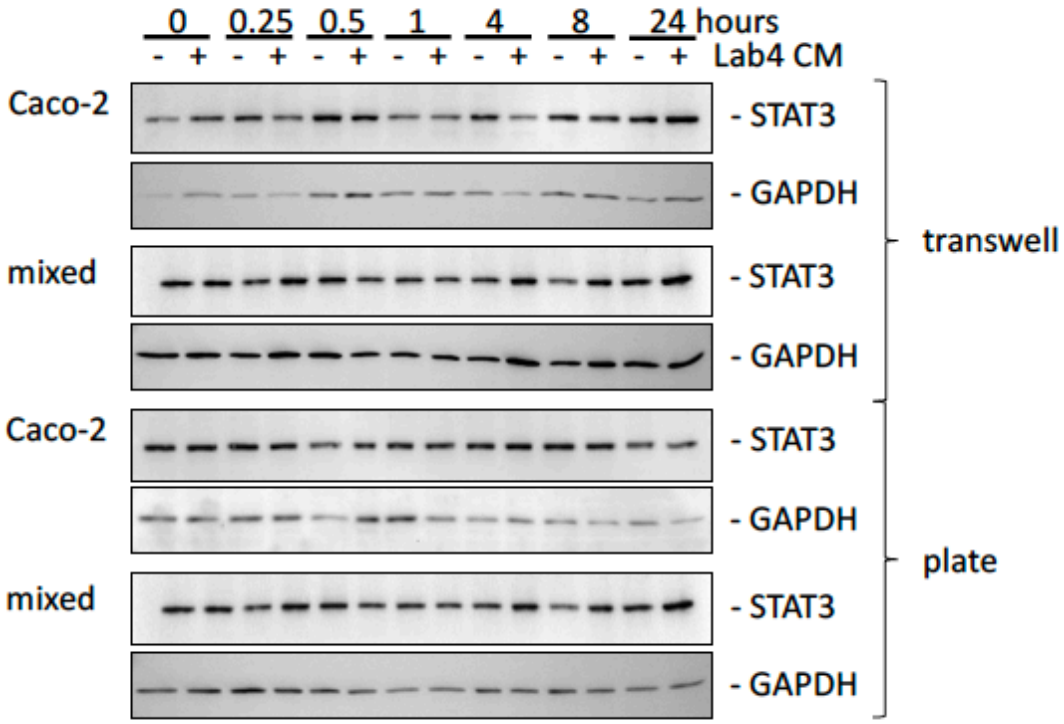

Appendix E Western blotting for pSTAT3 in Caco-2 and mixed epithelia grown on either transwells or on plates. *Caco-2 cell or mixed cell epithelia were established in transwells or 24-well plates over a 16 day period. Epithelia were then treated with probiotics (+Lab4 CM) for 48h or left untreated (-Lab4 CM), followed by stimulation with IL-22 for 0, 0.25, 0.5, 1, 4, 8 or 24h. Protein was extracted from epithelia following stimulation with IL-22, and an equal amount separated in 4-20% SDS-PAGE gels. Western blots were probed with specific antibodies for STAT3 and GAPDH. Picture shows a representative immunoblot for each experimental condition. This constitutes supplementary data and needs to be read in conjunction with Figure 45.*

APPENDIX F – GAPDH LOADING CONTROL OF MAPK WESTERN BLOTS

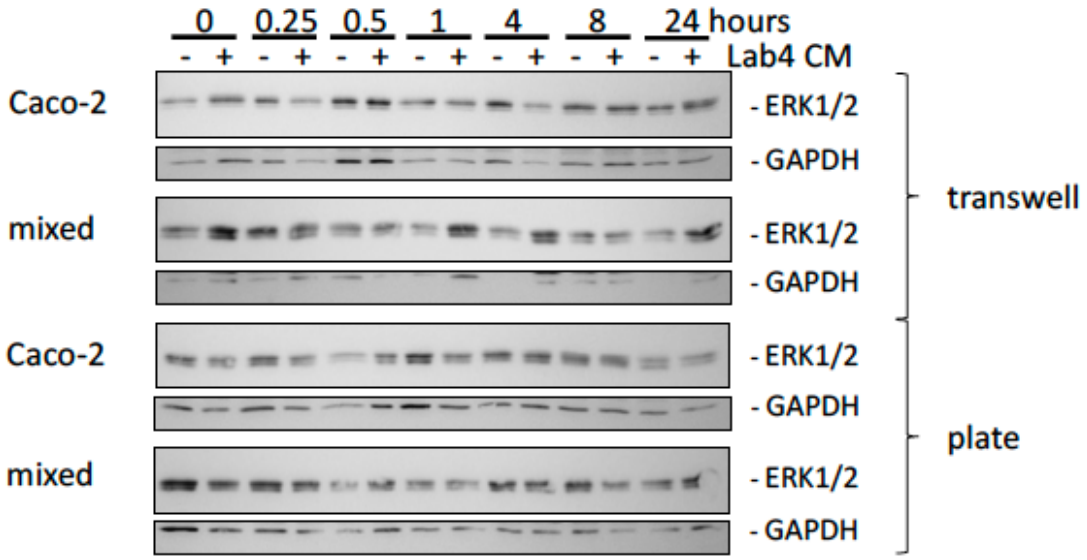

Appendix F Western blotting for pERK1/2 in Caco-2 and mixed epithelia grown on either transwells or on plates. *Caco-2 cell or mixed cell epithelia were established in transwells or 24-well plates over a 16 day period. Epithelia were then treated with probiotics (+Lab4 CM) for 48h or left untreated (-Lab4 CM), followed by stimulation with IL-22, and an equal amount separated in 4-20% SDS-PAGE gels. Western blots were probed with specific antibodies for ERK1/2 and GAPDH. Picture shows a representative immunoblot for each experimental condition. This constitutes supplementary data and needs to be read in conjunction with Figure 48.*